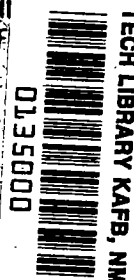


**NASA  
Technical  
Paper  
2125**

March 1983

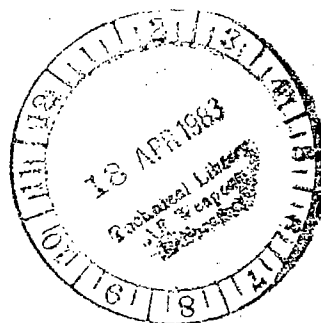
NASA  
TP  
2125  
c.1

LOAN COPY:  
AFWL TECHNICAL  
KIRTLAND AFB



# Experimental Study of Wing Leading-Edge Dev for Improved Maneuver Performance of a Supercritical Maneuvering Fighter Configuration

Michael J. Mann,  
Jarrett K. Huffman,  
Charles H. Fox, Jr.,  
and Richard L. Campbell



**NASA**



25th Anniversary  
1958-1983



# Experimental Study of Wing Leading-Edge Devices for Improved Maneuver Performance of a Supercritical Maneuvering Fighter Configuration

Michael J. Mann,  
Jarrett K. Huffman,  
Charles H. Fox, Jr.,  
and Richard L. Campbell  
*Langley Research Center  
Hampton, Virginia*



National Aeronautics  
and Space Administration

Scientific and Technical  
Information Branch

## SUMMARY

Wind-tunnel tests have been conducted to examine the use of wing leading-edge devices for improved subsonic and transonic maneuver performance. These devices were tested on a fighter configuration which utilized supercritical-wing technology. The configuration had a leading-edge sweep of  $45^\circ$  and an aspect ratio of 3.28. The tests were conducted at Mach numbers of 0.60 and 0.85 with angles of attack from  $-0.5^\circ$  to  $22^\circ$ . At both Mach numbers, sharp leading-edge flaps produced vortices which greatly altered the flow pattern on the wing and resulted in substantial reductions in drag at high lift. At a Mach number of 0.60, deflection of the flaps was effective for drag reduction. The effect of flap chord was much smaller than the effect of flap deflection. At a Mach number of 0.85, a large undeflected flap produced significant drag reduction. Underwing or pylon-type vortex generators also reduced drag at high lift. The vortex generators worked better at a Mach number of 0.60. The vortex generators gave the best overall results with zero toe-in angle and when mounted on either the outboard part of the wing or at both an outboard location and halfway out the semispan. Both the flaps and the vortex generators had a minor effect on the pitching moment. Fluorescent minitufts were found to be useful for flow visualization at transonic maneuver conditions.

## INTRODUCTION

Recent developments in the aerodynamic design of highly maneuverable combat aircraft include the application of supercritical-airfoil technology. This type of technology has been utilized on wings with moderate aspect ratios and leading-edge sweep angles to reduce the shock-induced flow separation at transonic maneuver conditions. For conditions approaching maximum lift, however, these wings still develop extensive regions of separated flow. This flow separation produces high levels of drag and usually results in wing buffeting and a general degradation of aerodynamic characteristics.

The present experimental study has examined the use of wing leading-edge devices to reduce the flow separation on the wing and, therefore, to lower the drag at maneuver conditions. The devices tested include sharp leading-edge flaps (SLEF) and underwing or pylon-type vortex generators (VG). These devices were used to enhance the subsonic and transonic maneuver capability of a supercritical maneuvering fighter. The tests were conducted in the Langley 7- by 10-Foot High-Speed Tunnel at Mach numbers of 0.60 and 0.85 and for lift coefficients up to about 1.

The current study has addressed only the application of leading-edge devices to the wing geometry required for maneuver conditions. It is recognized, of course, that some form of variable geometry would be required to provide the wing shapes for both the desired maneuver and cruise conditions. This type of variable geometry has not been examined in this study.

A study has also been made of the use of fluorescent minitufts for flow visualization at transonic maneuver conditions. The tufts were used to study the flow separation on a supercritical wing with and without vortex generators.

## SYMBOLS

All forces and moments are relative to the wind axes. The moments are referenced to a center-of-gravity location of 50.34 percent of the mean aerodynamic chord. (See fig. 1(a).) Force and moment coefficients are based on the geometry of the basic trapezoidal wing extended to the model center line. (See table I.) Dimensions are given in the International System of Units (SI) with the U.S. Customary Units in parentheses. The measurements and calculations were made in U.S. Customary Units.

b	wing span, cm (in.)
$C_D$	drag coefficient, $\frac{\text{Drag}}{qS}$
$C_L$	lift coefficient, $\frac{\text{Lift}}{qS}$
$C_m$	pitching-moment coefficient, $\frac{\text{Pitching moment}}{qS\bar{c}}$
$C_p$	pressure coefficient, $\frac{p_l - p}{q}$
c	local wing chord, cm (in.)
$\bar{c}$	mean aerodynamic chord, cm (in.)
M	free-stream Mach number
p	free-stream static pressure, $N/m^2$ (lbf/ft <sup>2</sup> )
$p_l$	local static pressure, $N/m^2$ (lbf/ft <sup>2</sup> )
q	free-stream dynamic pressure, $N/m^2$ (lbf/ft <sup>2</sup> )
S	wing reference area, m <sup>2</sup> (ft <sup>2</sup> )
x	local distance measured aft from wing leading edge, parallel to plane of symmetry, cm (in.)
y	spanwise distance from plane of symmetry, cm (in.)
$\alpha$	angle of attack, referenced to horizontal reference line in figure 1(a), deg
$\delta_f$	sharp leading-edge flap-deflection angle, positive with leading edge down (fig. 1(c)), deg
$\eta$	semispan location, $y/(b/2)$
$\phi$	vortex-generator toe-in angle, positive toward fuselage (fig. 1(e)), deg

Subscript:

i internal flow-through nacelle

## Abbreviations:

SLEF      sharp leading-edge flaps

VG        vortex generators

## APPARATUS AND TESTS

### Model Description

Drawings of the wind-tunnel model are shown in figure 1. Several photographs of the model are shown in figure 2, and the general geometric characteristics are given in table I. The configuration represents a highly maneuverable combat aircraft with a wing leading-edge sweep of  $45^\circ$  and an aspect ratio of 3.28. The model is a midwing configuration with the upper surface of the wing blended into the fuselage. (See fig. 1(b).) The wing-root incidence is approximately  $1^\circ$ , and there is approximately  $10^\circ$  of twist (washout) between the root and tip.

The sharp leading-edge flaps (SLEF) are an adaptation of the vortex-flap concept of Rao. (See ref. 1.) However, the intended purpose of the SLEF was to influence the flow over the entire chord length of the wing, in contrast to the purpose of reference 1 which was to increase the leading-edge thrust by means of a vortex situated on the flap itself.

The SLEF and the associated fences are shown in figures 1(c) and 1(d), respectively, and the SLEF geometric characteristics are given in table I. Two constant-chord SLEF configurations and a tapered SLEF were tested. The tapered SLEF was designed to account for the spanwise growth of the vortex in situations where the vortex happened to lie on the SLEF. The large fence was tested with the large SLEF, and the small fence was tested on the small and tapered SLEF. Certain SLEF geometries were tested with the fences removed.

The design of the vortex generators (VG) is based on the work of references 2 and 3. The geometric details and wing locations of the VG are given in figure 1(e) and table I.

Two supercritical wings have been used to assess the ability of these leading-edge devices to reduce subsonic and transonic maneuver drag. These wings are identified as configurations 1 and 2 of the SMF-2 (supercritical maneuvering fighter) wing and are completely described in reference 4. Both wings have identical planforms. Figure 1(f) gives a comparison of the airfoil sections for the two wings.

Configuration 1 was designed to reduce the shock-induced flow separation at a Mach number of 0.90 and a wing lift coefficient of 0.86. Configuration 1 developed strong shock waves and extensive flow separation at a Mach number of 0.85. Configuration 2 was designed both to reduce the shock-induced flow separation and the attendant maneuver drag penalties, which occurred on configuration 1 at a Mach number of 0.85, and to maintain the performance of configuration 1 at the higher transonic Mach numbers.

The tests for the current study involved two separate investigations in which the SLEF were tested on configuration 2 and the VG were tested on configuration 1.

## Tests and Corrections

The investigation was conducted in the Langley 7- by 10-Foot High-Speed Tunnel. This is a continuous-flow, single-return atmospheric tunnel with a closed, rectangular test section. A description of the tunnel is given in reference 5.

The tests were run at Mach numbers of 0.60 and 0.85. The Reynolds number, based on the wing mean aerodynamic chord, varied from  $2.5 \times 10^6$  at  $M = 0.60$  to  $3.0 \times 10^6$  at  $M = 0.85$ . The angle of attack was varied from  $-0.5^\circ$  to  $22^\circ$ .

Boundary-layer transition strips 0.32 cm (0.125 in.) wide were applied to the model. (See ref. 6.) No. 120 carborundum grains were applied 1 cm (0.4 in.) streamwise behind the leading edges of the wings and vertical tail. No. 100 grains were applied 2.8 cm (1.1 in.) behind the nose and 1 cm (0.4 in.) behind the inlet of the nacelle (outside only).

Aerodynamic forces and moments were measured by an internal six-component strain-gage balance. The angle of attack was measured by a pendulous, inertial, single-axis accelerometer (closed-loop type) mounted inside the model. The data have been corrected for blockage and lift interference by the methods of references 7 and 8, respectively. The force data have been corrected to a condition of free-stream static pressure over the fuselage base. The internal drag of the flow-through nacelle has been subtracted from the measured drag. The values of internal drag are given in table II. These values of  $C_{D,i}$  were measured for this fuselage with a similar wing geometry during a test in the Langley 8-Foot Transonic Pressure Tunnel. Linear interpolation of the values in table II was used for intermediate values of angle of attack and Mach number, and linear extrapolation was used for angles of attack above the range of the table.

The wing was instrumented with flush-surface static-pressure orifices. The orifices were distributed in streamwise rows over the upper-right and lower-left wing panels. The orifices were located at semispan stations of  $\eta = 0.30, 0.45, 0.80$ , and  $0.90$ . All surface pressures were recorded by the use of differential-pressure scanning valves mounted in the nose section of the model.

A study was made of the use of fluorescent minitufts to provide flow visualization at transonic high-lift conditions. (See refs. 9 and 10.) The minitufts were tested at a Mach number of 0.85 on the configuration-1 wing with and without the VG (where the VG were located at  $\eta = 0.50$  and  $0.75$  with  $\phi = 0^\circ$ ).

The tufts were made of very thin nylon monofilament material which had been treated so that it fluoresced when exposed to ultraviolet light. Monofilament diameters of approximately 0.0018 cm (0.0007 in.) and approximately 0.013 cm (0.005 in.) were tested. The monofilaments were laid chordwise across the wing at various span stations, and small drops of glue were placed on the monofilament at selected chordwise locations. After the glue had dried, the monofilaments were cut at the forward edges of the glue dots, which created an array of tufts on the upper surface of both wing panels. A water-soluble white glue was used which could be easily peeled off after the tests were completed. Therefore, the use of chemicals which might have dissolved the filler material used to build up parts of the wing geometry was avoided.

The tuft length was varied in order to study the effect of length on the flexibility required to respond to the local flow conditions. A length of 1 cm (0.4 in.) was used on the right wing, and a length of 1.5 cm (0.6 in.) was used on the left

wing. The spanwise spacing of the tufts was adjusted to avoid interference between the tufts or between the tufts and the pressure orifices.

## PRESENTATION OF RESULTS

The results of this study are presented in the following figures:

	Figure
Configuration-2 supercritical wing:	
Effect of fence on longitudinal aerodynamic characteristics at $M = 0.60$ . Small SLEF; $\delta_f = 20^\circ$ .....	3
Effect of SLEF deflection angle $\delta_f$ on longitudinal aerodynamic characteristics at $M = 0.60$ .....	4
Effect of SLEF chord length on longitudinal aerodynamic characteristics at $M = 0.60$ .....	5
Summary of longitudinal aerodynamic characteristics of constant-chord SLEF at $M = 0.60$ . $\delta_f = 20^\circ$ .....	6
Effect of SLEF chord length on the longitudinal aerodynamic characteristics at $M = 0.85$ . $\delta_f = 20^\circ$ .....	7
Longitudinal aerodynamic characteristics of SLEF with $\delta_f = 0^\circ$ at $M = 0.85$ .....	8
Effect of SLEF on wing upper- and lower-surface pressure coefficients .....	9
Oil-flow patterns at $M = 0.60$ with and without the small SLEF. $\delta_f = 20^\circ$ .....	10
Oil-flow patterns at $M = 0.85$ with and without the large SLEF. $\delta_f = 0^\circ$ ; fence off .....	11
Configuration-1 supercritical wing:	
Effect of VG toe-in angle on longitudinal aerodynamic characteristics at $M = 0.60$ . VG at $\eta = 0.50$ and $0.75$ .....	12
Effect of spanwise location and number of VG on longitudinal aerodynamic characteristics at $M = 0.60$ . $\phi = 5^\circ$ .....	13
Summary of longitudinal aerodynamic characteristics of VG with $\phi = 0^\circ$ at $M = 0.60$ . VG at $\eta = 0.50$ and $0.75$ .....	14
Effect of VG on longitudinal aerodynamic characteristics at $M = 0.85$ . VG at $\eta = 0.50$ and $0.75$ ; $\phi = 0^\circ$ .....	15
Effect of VG on wing upper- and lower-surface pressure coefficients. VG at $\eta = 0.50$ and $0.75$ ; $\phi = 0^\circ$ .....	16
Minituft patterns at $M = 0.85$ with and without VG. VG at $\eta = 0.50$ and $0.75$ ; $\phi = 0^\circ$ .....	17
Effect of minitufts on longitudinal aerodynamic characteristics at $M = 0.85$ .....	18

## DISCUSSION OF RESULTS

Supercritical attached-flow technology was used in reference 4 to improve the maneuver performance of the SMF-2 fighter. The purpose of the present study is to enhance further the maneuver performance of this fighter at subsonic and transonic speeds by the use of wing leading-edge devices. The leading-edge devices were intended to generate vortices which would favorably alter the flow pattern at high lift coefficients and result in less flow separation and a reduction in the drag. The concept, then, involves supercritical attached-flow technology, supplemented by

leading-edge or vortex devices, where the latter are intended to enhance the performance at maneuver conditions and to cause a negligible drag increase at moderate or low lift coefficients.

The leading-edge devices have been tested at Mach numbers of 0.60 and 0.85. A Mach number of 0.60 creates essentially a subsonic condition with supercritical flow confined to the wing leading edge at the higher lift coefficients tested. (The critical pressure coefficient based on wing leading-edge sweep angle is  $-1.596$ .) A Mach number of 0.85 creates a transonic condition with a large region of embedded supersonic flow and shock waves.

The sharp leading-edge flap (SLEF) has been tested on the configuration-2 supercritical wing (fig. 1(f)), and the vortex generator (VG) has been tested on the configuration-1 supercritical wing. The results for the SLEF will be discussed first.

#### SLEF Results

Aerodynamic characteristics at  $M = 0.60$ .— Figures 3 to 6 show the effect of the SLEF on the longitudinal aerodynamic characteristics at a Mach number of 0.60. Figure 3 shows the results for the small SLEF deflected to  $20^\circ$  with and without the fence. It can be seen that the effects of the fence are negligible at this Mach number and, therefore, it will be assumed that these effects can be ignored in comparisons of different flap geometries.

The effect of flap-deflection angle is shown in figure 4 for both the small and large flaps. All flap configurations, including zero-deflection angle, significantly reduce drag for lift coefficients above 0.8. As the flap-deflection angle is increased, the drag is progressively decreased. At a lift coefficient of 1.0, deflecting either flap to  $20^\circ$  reduces the drag coefficient by about 0.04 (400 counts). There is some drag penalty at low lift coefficients; however, it is expected that such a device could be retracted to eliminate this drag penalty. Figure 5 shows the effect of flap chord length for deflection angles of  $0^\circ$  and  $20^\circ$ . Changes in the flap chord have a relatively small effect on the drag at high lift coefficients. Figure 5(b) illustrates that the tapered SLEF does not have any advantage over the constant-chord SLEF. Figure 6 summarizes the results for the SLEF which produced the greatest drag reduction at a Mach number of 0.60 (a flap deflection of  $20^\circ$ ). For the sake of clarity and since the tapered SLEF did not show any advantage over the constant-chord SLEF, results are shown only for the large and the small constant-chord SLEF.

Figures 4 to 6 show that for a Mach number of 0.60, the effect of the SLEF on the pitching moment is small.

Oil-flow photographs and wing pressure distributions at  $M = 0.60$ .— Oil-flow photographs for a Mach number of 0.60 are shown in figure 10. The photographs show the effects of the small SLEF deflected to  $20^\circ$  with and without the fence. Results cover the angle-of-attack range from  $8.39^\circ$  to  $20.07^\circ$ . Selected wing pressure distributions which correspond to some of the same conditions are shown in figures 9(a) and 9(b).

At angles of attack of  $8.39^\circ$  and  $13.88^\circ$  (figs. 10(a) to 10(e)), the oil flows indicate that the flow is predominantly attached for all configurations and that there is a snag vortex coming from the inboard edge or "snag" of the SLEF. Only the

angle of attack of  $13.88^\circ$  corresponds to conditions where the SLEF produced any significant drag reduction ( $C_L \approx 0.84$ ).

As the angle of attack is increased to  $17.18^\circ$ , the plain wing (SLEF off) has a large region of separation at the tip; and at  $20.07^\circ$ , almost the entire upper surface is separated. (See figs. 10(f) and 10(i).) As shown in figure 6, these angles of attack correspond to values of the lift coefficient (near unity) where the SLEF produced significant reductions in drag. The oil-flow photographs in figures 10(f) to 10(j) show that the addition of the SLEF to the wing strongly alters the flow pattern at both angles of attack. The changes at these angles of attack are similar but more pronounced at  $20.07^\circ$ , where the flow seems to be divided into three regions. (See fig. 10(j).) The inboard region still exhibits the same separated character that occurred with the SLEF off. The middle region is a strip of rather chordwise flow which appears to be dominated by the snag vortex emanating from the inboard edge of the SLEF. This vortex is blocking the spanwise flow from the inboard region. The spanwise flow is so strong that the vortex is bent outward toward the wing tip. The flow in the outboard or tip region has also been altered by the presence of the SLEF. This region of the wing apparently has a forced separation at the sharp leading edge of the flap which is rolling up into a rotating-vortex type of flow. The pressure distributions of figures 9(a) and 9(b) provide some support for this explanation. As the angle of attack of the plain wing is increased from  $13.9^\circ$  to  $19.1^\circ$ , the flow at the wing tip becomes separated as indicated by the almost constant pressure distribution across the chord. However, with the SLEF attached, the wing tip has a broad low-pressure region at  $\eta = 0.90$  for an angle of attack of  $17.2^\circ$ . This low-pressure region is consistent with the presence of a rotating or vortex flow in the tip region.

In general, then, the oil-flow photographs and the wing pressure distributions for a Mach number of 0.60 indicate that the addition of the SLEF produces very significant changes in the flow at high angles of attack. These changes appear favorable and help to explain the improved drag characteristics at high lift when the SLEF is added to the wing.

Aerodynamic characteristics at  $M = 0.85$ .— The effect of the SLEF at a Mach number of 0.85 is shown in figures 7 and 8. Figure 8 shows the results for the large and the small SLEF with zero deflection. The large SLEF has the fence removed and the small SLEF has the fence attached. The large SLEF considerably improves the drag polar at the high lift coefficients. For example, at a lift coefficient of 1.0, the drag coefficient is reduced by about 0.04 (400 counts). With zero-deflection angle, the large SLEF causes only a small increase in drag at the low lift coefficients. The small SLEF produces no real benefit for any lift coefficient. When the SLEF are deflected to  $20^\circ$ , as shown in figure 7 (fences attached), neither the large nor the small SLEF produces a significant benefit within the range of these data.

Although sufficient force data were not obtained to identify clearly the effect of the fence at a Mach number of 0.85, the experimental results suggest that a large flap chord and zero deflection are preferable at a Mach number of 0.85. This contrasts with the results for a Mach number of 0.60 where some flap deflection was found to be beneficial and the effect of flap chord length was found to be negligible. At any rate, the large SLEF with zero deflection and with the fence removed produces sizable reductions in the drag at high lift for a Mach number of 0.85.

Figures 7 and 8 show that for a Mach number of 0.85, the effect of the SLEF on the pitching moment is small.

Oil-flow photographs and wing pressure distributions at  $M = 0.85$ . Oil-flow photographs and pressure distributions can again be used to obtain some understanding of the influence of the SLEF on the flow. Oil-flow photographs showing the effects of the best SLEF at a Mach number of 0.85 (large SLEF with zero deflection) are presented in figure 11, and pressure distributions which approximately correspond to some of the same conditions are shown in figures 9(c) and 9(d).

Figure 11 indicates that for an angle of attack of  $8.97^\circ$ , the flow on the upper surface of the wing is almost entirely attached. There is some evidence of a snag vortex emanating from the inboard edge of the SLEF.

As the angle of attack is increased to  $12.67^\circ$ , the oil-flow photographs (figs. 11(c) and 11(d)) and the pressure distributions (fig. 9(c)) define the location of a system of shock waves. On the inboard region of the wing there appears to be a forward and an aft shock wave which run out the span and merge into a single shock wave on the outboard region of the wing. These shock waves thus form a lambda pattern, and figures 11(c) and 11(d) show that the flow separates at the portion of this "lambda shock" which runs approximately parallel to the wing trailing edge. When the SLEF is added to the wing, the flow separation on the outboard region of the wing is reduced and, as seen in figure 8, this reduction corresponds with a reduction in drag ( $C_L \approx 0.9$ ). A reasonable explanation for the reduced flow separation is the presence of a separation bubble on the SLEF itself. It appears (fig. 11(d)) that the rotating flow in the separation bubble has scrubbed the oil from part of the SLEF and pooled the oil into a line running along the SLEF. This bubble would modify the effective wing leading-edge geometry and may, therefore, produce a favorable influence on the transonic-flow development over the outboard sections. The dominant influence for reduced separation, however, may be the presence of a series of streamwise vortices as indicated by the series of discrete lines running streamwise and ending in the wavy line along the boundary between the attached and separated flows. The differing motions of the rotating bubble flow and the mainstream flow would explain the development of a shear layer which would produce this series of streamwise vortices. (See ref. 11.) This phenomenon suggests the use of other means for the generation of a series of streamwise vortices which would not depend on the peculiar conditions required for a leading-edge separation bubble.

Figures 11(e) to 11(h) show the effects of the SLEF on the flow pattern at higher lift coefficients ( $C_L > 1$ ) where the SLEF produced even larger reductions in drag. The dominant effect of the SLEF on the surface flow is to generate a corridor of generally chordwise flow which emanates from the inboard edge of the SLEF. This chordwise flow appears to be the result of the snag vortex, which is already evident at an angle of attack of  $8.97^\circ$ . (See fig. 11(b).) At an angle of attack of  $14.83^\circ$  with the SLEF removed, the oil-flow pattern shows a shock wave extending across the inboard region of the wing to about  $\eta = 0.50$  with  $x/c$  varying from about 0.2 to 0.3. (See fig. 11(e).) It is interesting to note that when the SLEF is added to the wing (fig. 11(f)), the snag vortex appears to penetrate through the shock wave.

Figure 9(d) shows the effect of the SLEF on the wing pressure distribution for a lift coefficient of unity. The flow separation over the inboard region of the wing seems to have been somewhat reduced, as evidenced by the improved flow compression near the wing trailing edge.

## VG Results

Aerodynamic characteristics at  $M = 0.60$  and  $0.85$ .— Figures 12 to 14 show the effects of the vortex generators (VG) on the longitudinal aerodynamic characteristics of the configuration-1 supercritical wing at a Mach number of 0.60. Figure 12 shows the effect of VG toe-in angle  $\phi$ . The VG are mounted at  $\eta = 0.50$  and  $0.75$ . With the toe-in angle set at  $0^\circ$ , the VG produce a significant drag reduction at high lift coefficients (0.02 reduction in  $C_D$  at  $C_L = 0.96$ ), and there is almost no drag penalty at low lift coefficients. A toe-in angle of  $5^\circ$  produces only a modest additional amount of drag reduction, and there is some drag penalty at low lift coefficients. With the toe-in angle increased to  $10^\circ$ , the drag is higher than with zero toe-in.

Figure 13 illustrates the effect of spanwise location and the number of VG. Vortex generators placed at only  $\eta = 0.75$  reduce drag at high lift coefficients; however, when they are placed at both  $\eta = 0.50$  and  $0.75$ , they reduce drag even more at these high lift coefficients. Vortex generators placed inboard at only  $\eta = 0.50$  produce a drag penalty at some maneuver lift coefficients.

When considering the results over the entire range of lift coefficients, VG with a toe-in angle of  $0^\circ$  and located at both  $\eta = 0.50$  and  $0.75$  appear to be the best overall choice. For the sake of clarity, the results for only this VG arrangement and the plain wing (VG off) are repeated in figure 14. Figure 16(a) presents corresponding wing pressure distributions at lift coefficients close to unity. The VG appear to have reduced the flow separation near the wing tip.

Figure 15 shows the effects of the VG at a Mach number of 0.85. The VG are located at  $\eta = 0.50$  and  $0.75$  and have zero toe-in. There is some drag reduction for a small range of conditions at high lift, although the benefits are not as great as at a Mach number of 0.60. Corresponding wing pressure distributions for a Mach number of 0.85 are shown in figure 16(b) for a lift coefficient of about 0.9. The pressure distribution at  $\eta = 0.80$  indicates that the VG have reduced the flow separation at that span station.

At both Mach numbers, the VG have produced minor changes in the pitching moment. (See figs. 12 to 15.)

Both the SLEF and the VG have produced significant drag reductions at high lift coefficients. However, a comparison of the results for these leading-edge devices clearly shows that the SLEF produced much larger drag reductions on configuration 2 than the VG produced on configuration 1. (Compare figs. 6 and 8 with figs. 14 and 15.) When the VG (located at  $\eta = 0.50$  and  $0.75$  with  $\phi = 0^\circ$ ) were tested on configuration 2 (ref. 4), it was found that they did not produce any significant drag reduction in the Mach number range from 0.60 to 0.95.

Minituft flow-visualization studies.— Figure 17 presents some results obtained from the use of the fluorescent minitufts. The minitufts were used to study the effects of the VG on the flow pattern at a Mach number of 0.85 and for lift coefficients up to 0.9. When the minitufts were exposed to ultraviolet radiation, they became highly visible (fluorescent) and were easily photographed. Figures 17(a) and 17(b) are for a lift coefficient of about 0.6 and indicate that with the VG off there is an area of spanwise flow on the outboard region of the wing. This area of

spanwise flow appears to be a separation bubble at the foot of the shock wave. (See also the pressure distribution at  $\eta = 0.80$  in fig. 16(c).)<sup>1</sup> When the VG are added (figs. 16(c) and 17(b)), the separation is almost completely eliminated; however, for this lift coefficient, the reduced separation did not decrease the drag (fig. 15).

The tuft photographs in figures 17(c) and 17(d) and the pressure distributions in figure 16(b) are for a lift coefficient of about 0.9. Both types of data indicate that the VG reduce the flow separation, and figure 15 shows that the drag is thereby reduced (by about 0.02 in drag coefficient).

Monofilament material with a diameter of 0.0018 cm (0.0007 in.) was used to make the tufts for the tests on the plain wing. However, these tufts broke off in areas of the wing where there was extensive flow separation. (See fig. 17(c).) Apparently, the high degree of turbulence fatigued the monofilament material. Therefore, a diameter of 0.013 cm (0.005 in.) was used for runs with the VG attached. These tufts stayed on the wing much longer and still possessed adequate flexibility to respond to the flow.

As mentioned in the section entitled "Apparatus and Tests," tuft lengths of 1 cm (0.4 in.) and 1.5 cm (0.6 in.) were used on the right and left wings, respectively. (See fig. 17.) Both lengths displayed adequate flexibility.

The effect of the minitufts on the force data is shown in figure 18. The minitufts caused a significant drag reduction on the plain wing at high lift coefficients. Apparently, for these conditions, the minitufts were acting like a multitude of vortex generators. (See fig. 18(a).) With the VG attached to the wing (fig. 18(b)), the effect of the minitufts varied from no change in  $C_D$  to an increase in  $C_D$  of about 0.0030 (30 counts). The effect of the minitufts on the force data may be attributed to the size of the tufts or the size of the glue dots. Further studies are required; however, the present results indicate that it may be difficult to obtain force data and tuft flow-visualization data simultaneously at transonic maneuver conditions.

## CONCLUSIONS

Wind-tunnel tests have been conducted to examine the use of wing leading-edge devices for improved subsonic and transonic maneuver performance. These devices were tested on a fighter configuration which utilized supercritical-wing technology. The following conclusions are presented:

1. The sharp leading-edge flaps (SLEF) produced a system of vortices on the upper surface of the wing which greatly altered the flow pattern at subsonic and transonic maneuver conditions. The altered flow patterns resulted in substantially reduced drag.
2. At a Mach number of 0.60, increasing the flap-deflection angle reduced the drag. The influence of flap chord was much less than the influence of flap-deflection angle. At a Mach number of 0.85, the large flap chord with zero-deflection angle produced a significant drag reduction.

---

<sup>1</sup>All pressure data were obtained with tufts removed.

3. The SLEF had a minor effect on the pitching moment.
4. A fence attached to the inboard edge of the SLEF had a negligible effect at a Mach number of 0.60. The effect of the fence was not specifically determined at a Mach number of 0.85; however, the SLEF worked well without a fence at this Mach number.
5. The vortex generators (VG) reduced the drag at maneuver-lift conditions for Mach numbers of 0.60 and 0.85; however, the VG were more effective at a Mach number of 0.60.
6. The VG had a minor effect on the pitching moment.
7. At a Mach number of 0.60, setting the VG at a toe-in angle of 5° (toward the fuselage) produced a relatively small additional drag reduction relative to zero toe-in. A toe-in angle of 10° produced higher drag than zero toe-in.
8. Vortex generators located at only 75 percent of the semispan reduced drag at high lift for a Mach number of 0.60; VG located at both the 50- and 75-percent semispan stations resulted in a larger drag reduction. Vortex generators located at only the 50-percent semispan station increased drag at some high-lift conditions.
9. Fluorescent minitufts were used at transonic maneuver conditions to identify regions of flow separation. The tufts caused significant changes in the force data.

Langley Research Center  
National Aeronautics and Space Administration  
Hampton, VA 23665  
January 19, 1983

#### REFERENCES

1. Rao, Dhanvada M.: Leading-Edge 'Vortex Flaps' for Enhanced Subsonic Aerodynamics of Slender Wings. ICAS-80-13.5, Oct. 1980.
2. Johnson, Thomas D.; and Rao, Dhanvada M.: Experimental Study of Delta Wing Leading-Edge Devices for Drag Reduction at High Lift. NASA CR-165846, 1982.
3. Bartlett, Dennis W.; Harris, Charles D.; and Kelly, Thomas C.: Wind-Tunnel Development of Underwing Leading-Edge Vortex Generators on an NASA Supercritical-Wing Research Airplane Configuration. NASA TM X-2808, 1973.
4. Mann, Michael J.; Mercer, Charles E.; and Campbell, Richard L.: Supercritical Manuevering Fighter Configuration - Wind-Tunnel Investigation at Mach Numbers of 0.60 to 0.95. NASA TM-84513, 1982.
5. Fox, Charles H., Jr.; and Huffman, Jarrett K.: Calibration and Test Capabilities of the Langley 7- by 10-Foot High Speed Tunnel. NASA TM X-74027, 1977.
6. Braslow, Albert L.; and Knox, Eugene C.: Simplified Method for Determination of Critical Height of Distributed Roughness Particles for Boundary-Layer Transition at Mach Numbers From 0 to 5. NACA TN 4363, 1958.
7. Herriot, John G.: Blockage Corrections for Three-Dimensional-Flow Closed-Throat Wind Tunnels, With Consideration of the Effect of Compressibility. NACA Rep. 995, 1950. (Supersedes NACA RM A7B28.)
8. Garner, H. C.: Lift Interference on Three-Dimensional Wings. Subsonic Wind Tunnel Wall Corrections, H. C. Garner, ed., AGARDograph 109, Oct. 1966, pp. 75-217.
9. Crowder, J. P.; Hill, E. G.; and Pond, C. R.: Selected Wind Tunnel Testing Developments at the Boeing Aerodynamics Laboratory. A Collection of Technical Papers - AIAA 11th Aerodynamic Testing Conference, Mar. 1980, pp. 262-272. (Available as AIAA-80-0458.)
10. Crowder, James P.: Add Fluorescent Minitufts to the Aerodynamicist's Bag of Tricks. Astronaut. & Aeronaut., vol. 18, no. 11, Nov. 1980, pp. 54-56.
11. Peake, David J.; and Tobak, Murray; Three-Dimensional Interactions and Vortical Flows With Emphasis on High Speeds. AGARD-AG-252, 1980.

TABLE I.- GENERAL GEOMETRIC CHARACTERISTICS OF MODEL

## Wing (reference trapezoid extended to center line):

Sweepback of leading edge, deg	45
Sweepback of trailing edge, deg	11.90
Aspect ratio	3.28
Taper ratio	0.2142
Area, m <sup>2</sup> (ft <sup>2</sup> )	0.140 (1.504)
Span, cm (in.)	67.686 (26.648)
Mean aerodynamic chord, cm (in.)	23.518 (9.259)
Wing station of mean aerodynamic chord, cm (in.)	13.272 (5.225)
Fuselage station of 25-percent wing mean aerodynamic chord, cm (in.)	52.426 (20.640)
Root chord, cm (in.)	33.993 (13.383)
Tip chord, cm (in.)	7.282 (2.867)
Dihedral, deg	0
Twist (washout from root to tip), deg	10
Incidence (root), deg	1

## Vertical tail (exposed trapezoid):

Sweepback of leading edge, deg	61
Aspect ratio	0.856
Taper ratio	0.2854
Ratio of tail area to wing area	0.168
Span, cm (in.)	14.145 (5.569)
Root chord, cm (in.)	25.718 (10.125)
Tip chord, cm (in.)	7.341 (2.890)
Airfoil section	4-percent circular-arc biconvex

## Vortex generator (one of four):

Aspect ratio	0.778
Taper ratio	1
Area, cm <sup>2</sup> (in <sup>2</sup> )	4.06 (0.63)
Ratio of area of two vortex generators to wing semispan area	0.012
Span, cm (in.)	1.78 (0.70)
Root chord, cm (in.)	2.29 (0.90)
Tip chord, cm (in.)	2.29 (0.90)
Airfoil section (streamwise)	NACA 64A006

## Sharp leading-edge flaps (one of two):

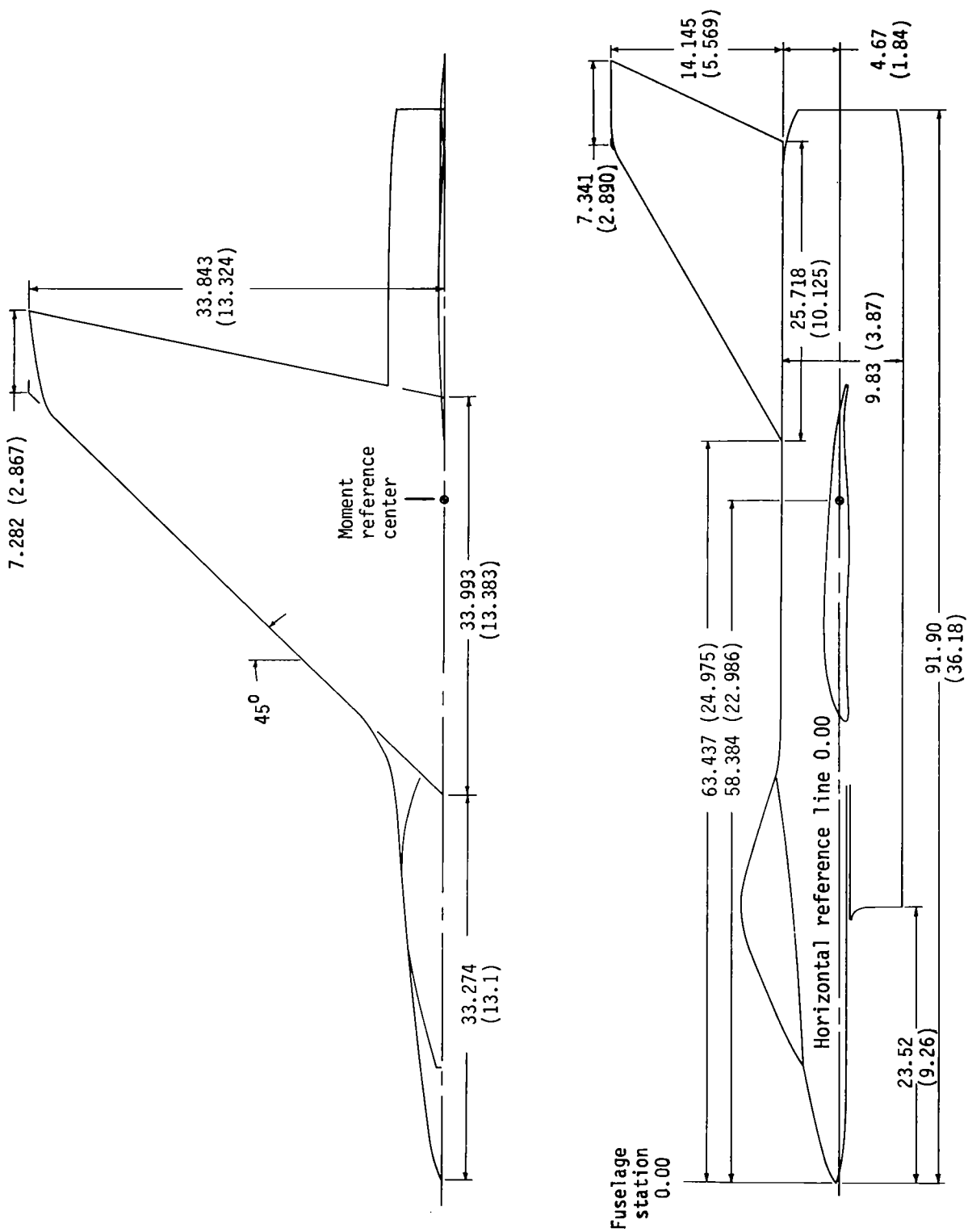
	Small	Tapered	Large
Ratio of flap area to wing semispan area	0.016	0.024	0.032
Span, cm (in.)	14.88 (5.86)	14.88 (5.86)	14.88 (5.86)
Root chord, cm (in.)	0.76 (0.3)	0.76 (0.3)	1.5 (0.6)
Tip chord, cm (in.)	0.76 (0.3)	1.5 (0.6)	1.5 (0.6)

## Fuselage:

Flow-through inlet area, cm <sup>2</sup> (in <sup>2</sup> )	23.019 (3.568)
Flow-through exit area, cm <sup>2</sup> (in <sup>2</sup> )	18.871 (2.925)
Base area, cm <sup>2</sup> (in <sup>2</sup> )	28.852 (4.472)

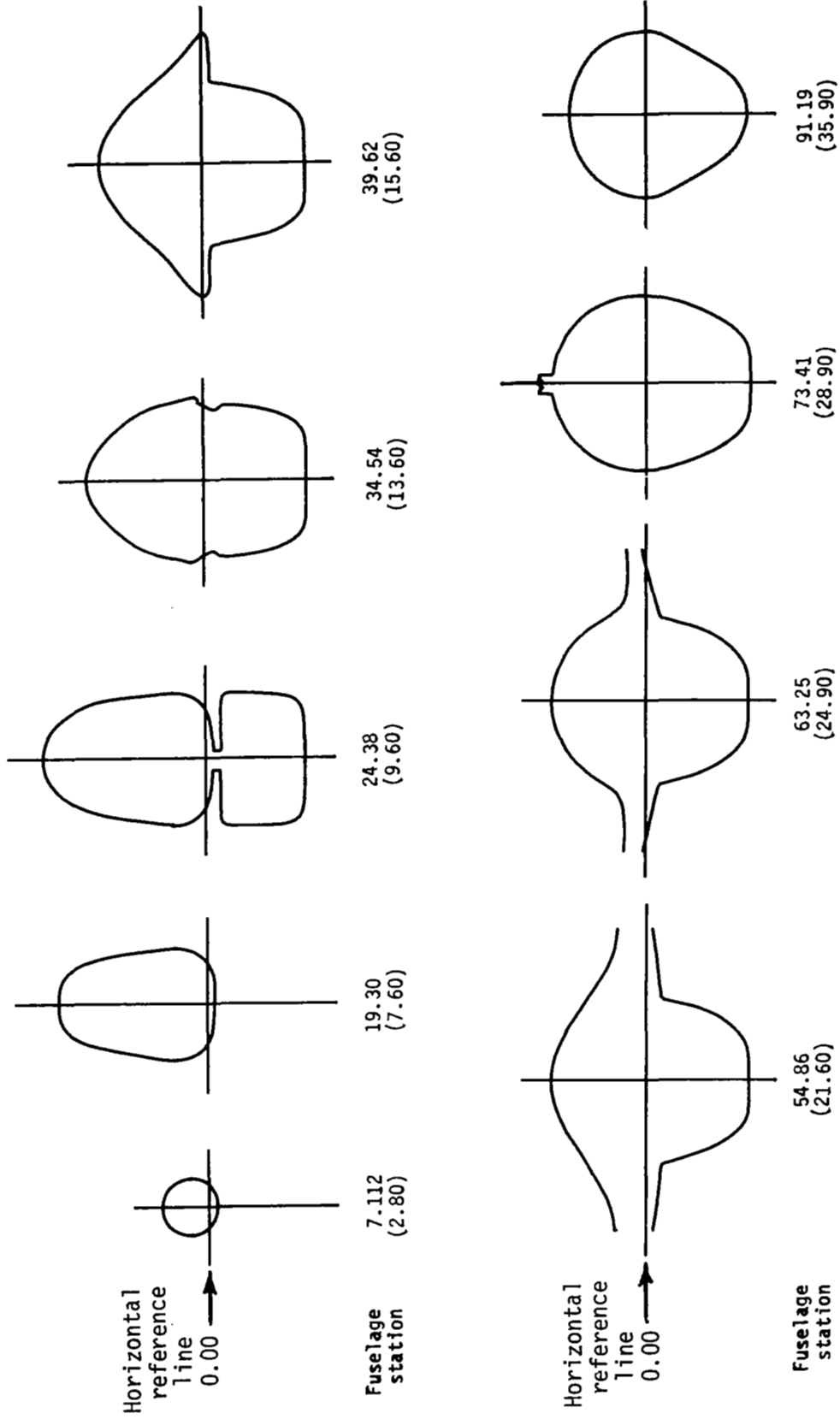
TABLE II.- INTERNAL DRAG CHARACTERISTICS

$\alpha$ , deg	Values of $C_{D,i}$ for -			
	M = 0.601	M = 0.800	M = 0.849	M = 0.899
-0.02	0.00242	0.00253	0.00258	0.00247
1.99	.00243	.00254	.00259	.00248
3.97	.00245	.00258	.00262	.00252
6.04	.00251	.00264	.00267	.00258
7.99	.00259	.00273	.00275	.00267
10.01	.00270	.00285	.00287	.00279
11.98	.00286	.00299	.00302	.00295
13.98	.00307	.00318	.00320	.00315



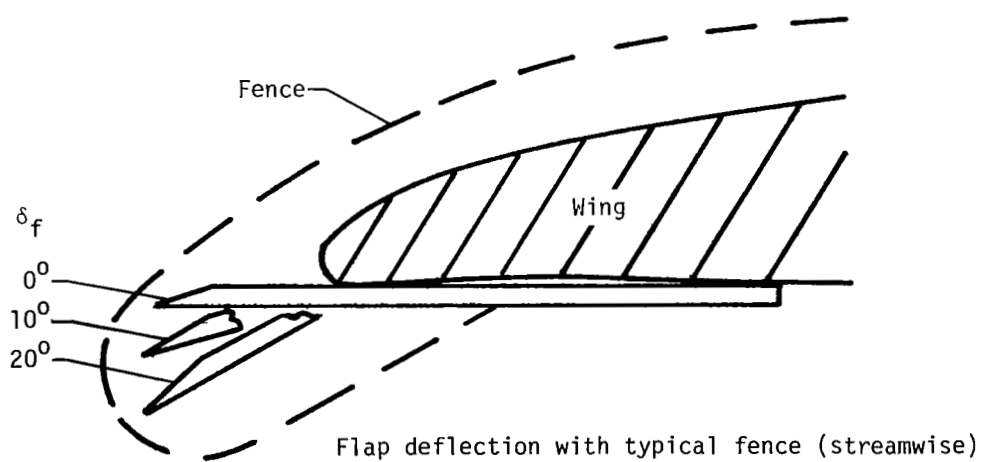
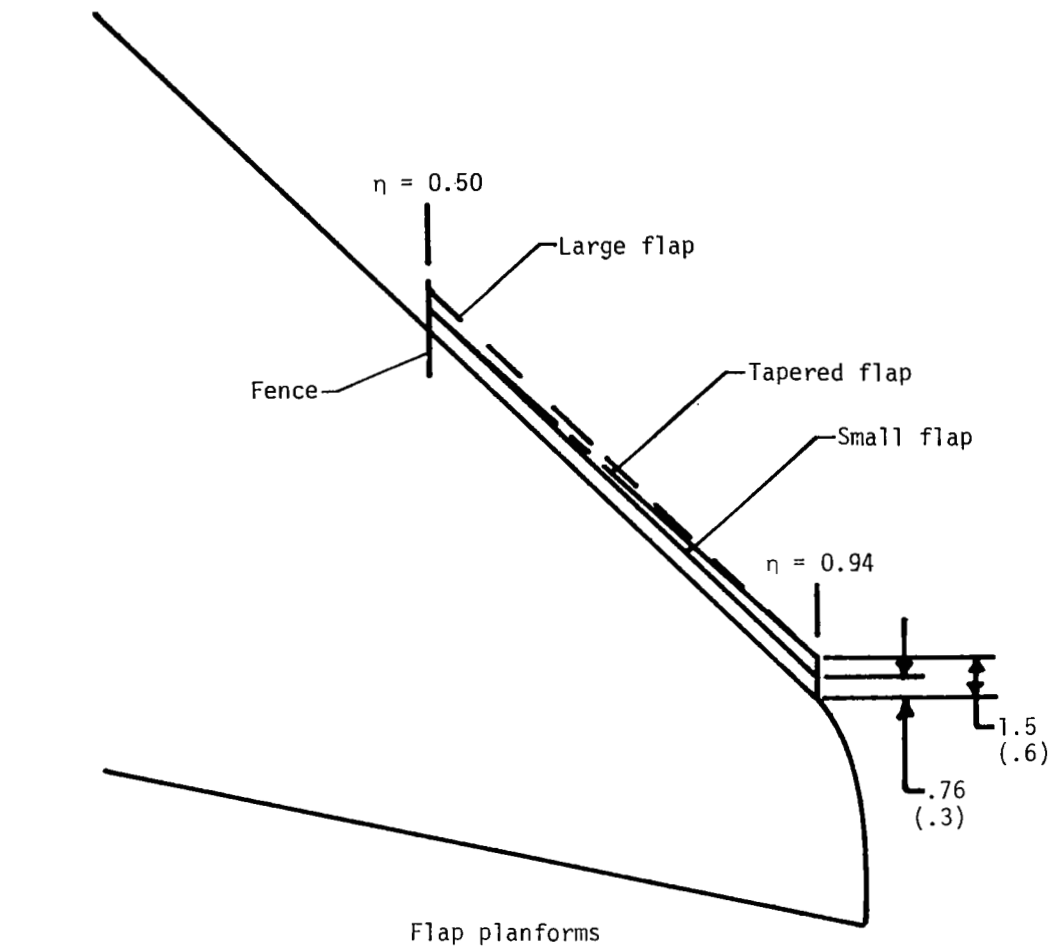
(a) General arrangement of model.

Figure 1.- Details of model geometry. Dimensions are given in centimeters (inches).



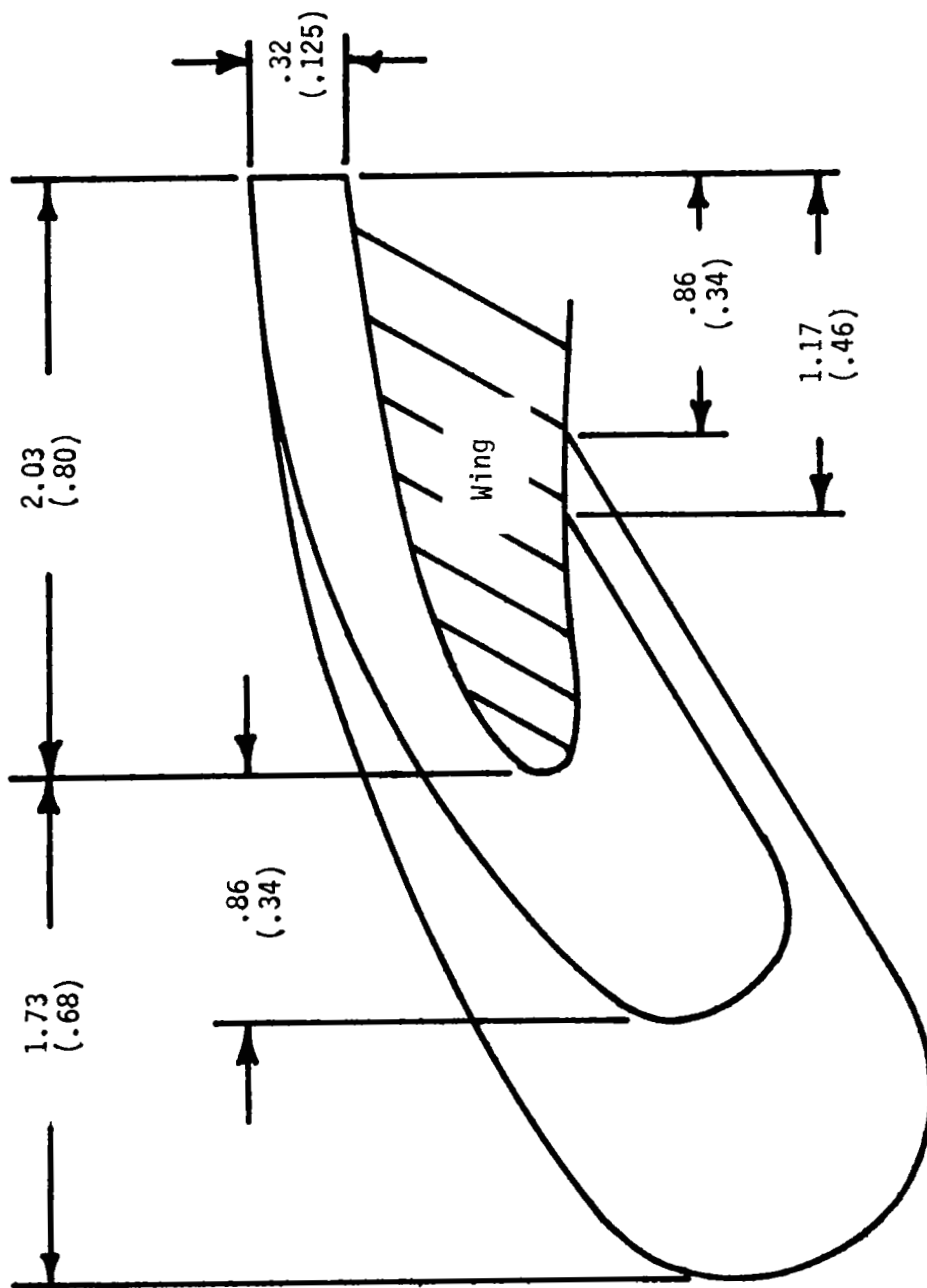
(b) Fuselage external contours.

Figure 1.- Continued.



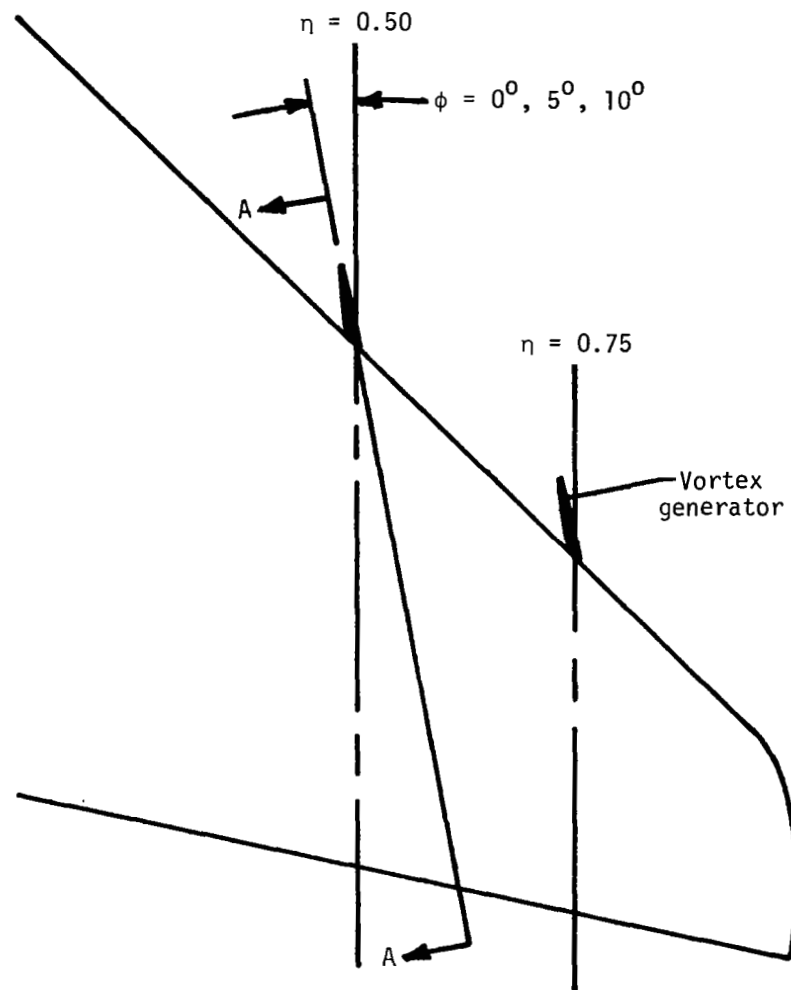
(c) Sharp leading-edge flaps.

Figure 1.- Continued.

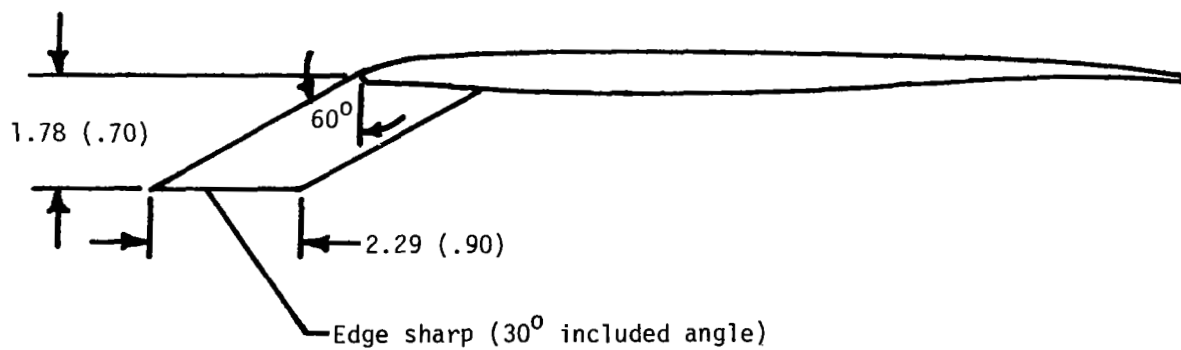


(d) Fences for sharp leading-edge flaps.

Figure 1.- Continued.



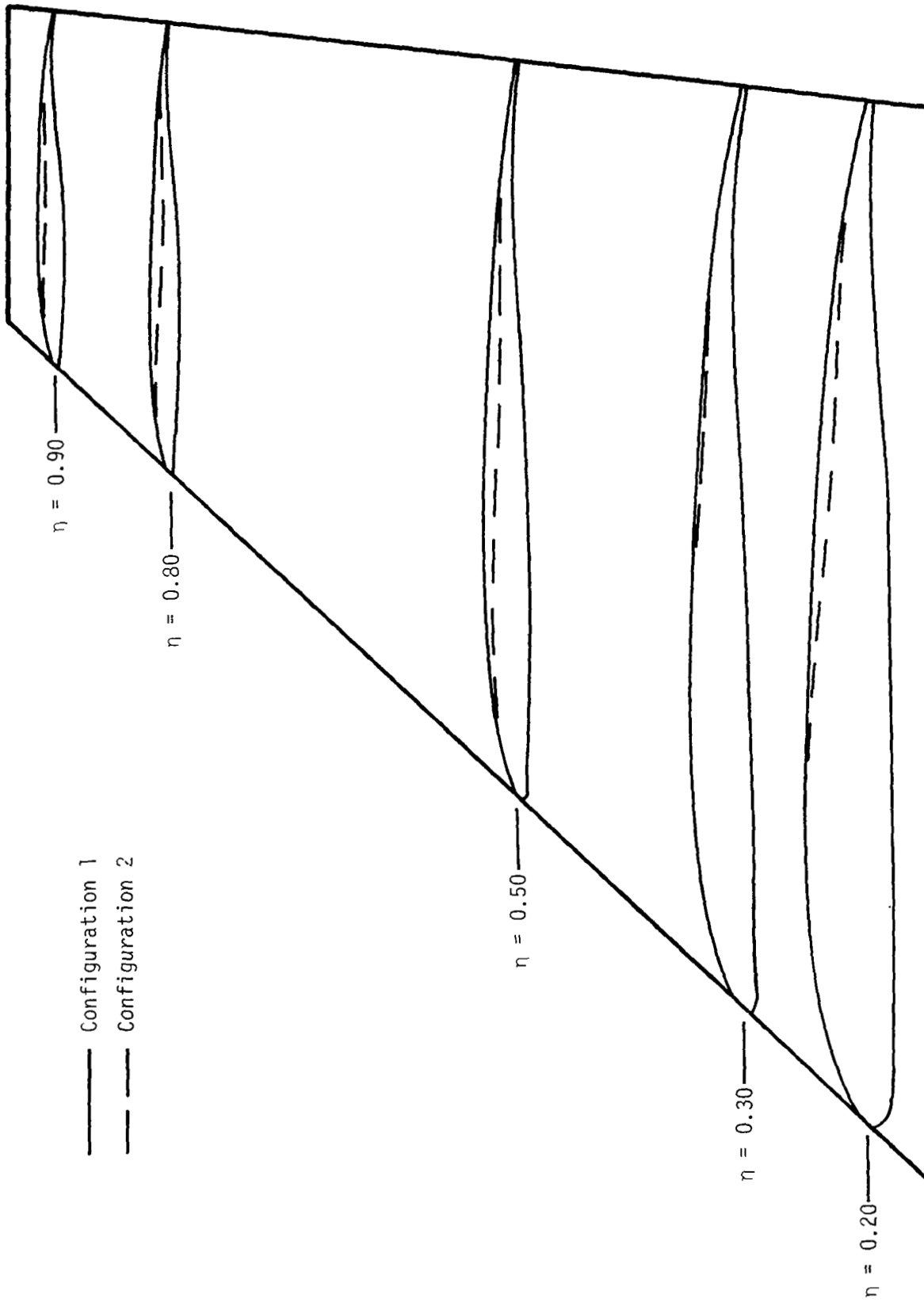
VG location and toe-in angles



Details of VG (section A-A)

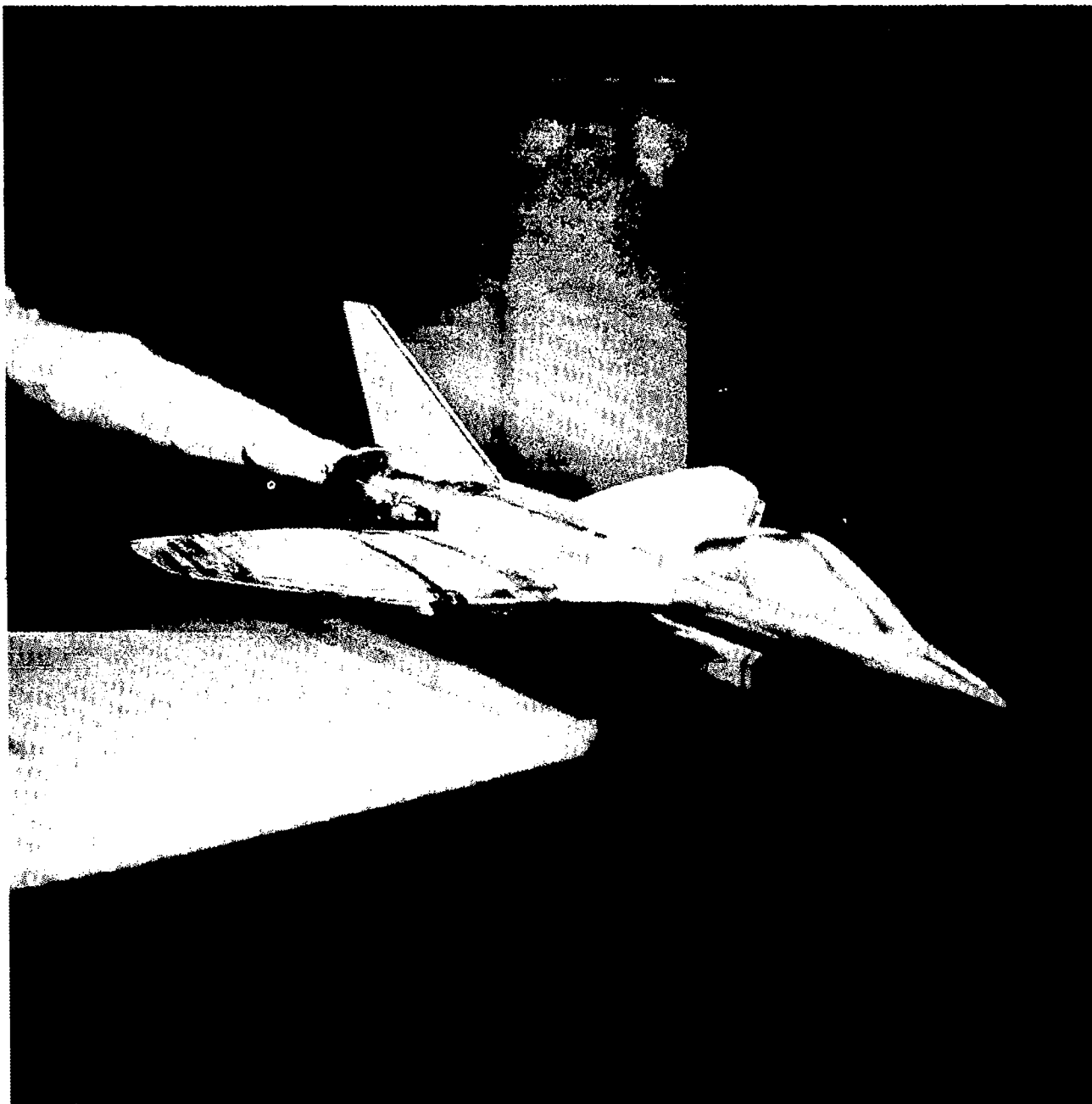
(e) Vortex generators.

Figure 1.- Continued.



(f) Comparison of wing airfoil sections for configurations 1 and 2. Twist is not shown.

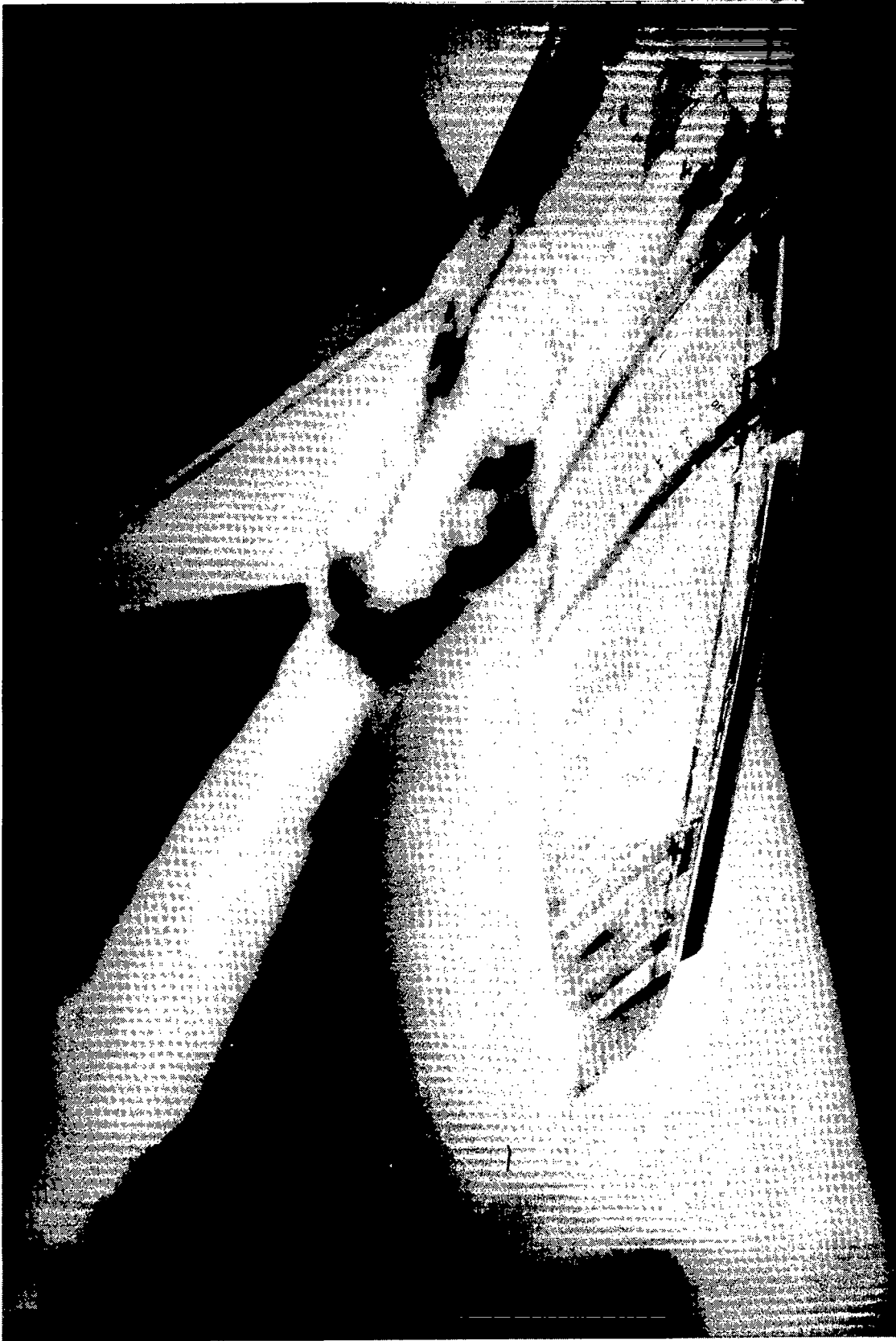
Figure 1.- Concluded.



L-83-10

(a) Large SLEF on configuration 2. Three-quarter front view;  $\delta_f = 10^\circ$ .

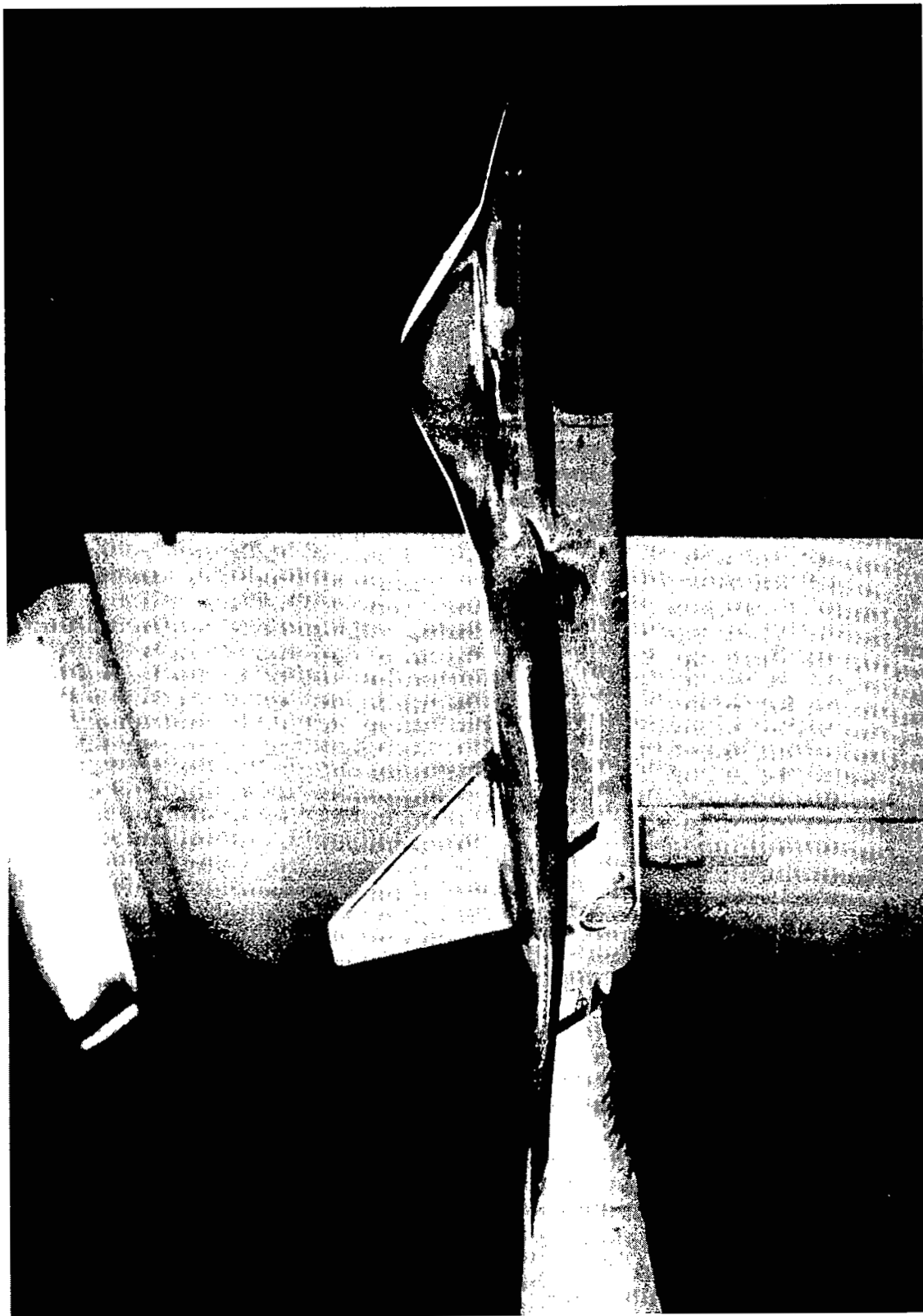
Figure 2.- Photographs of the SMF-2 model installed in the Langley 7- by 10-Foot High-Speed Tunnel.



L-83-11

(b) Large SLEF on configuration 2. Front view of right wing;  $\delta_f = 10^\circ$ .

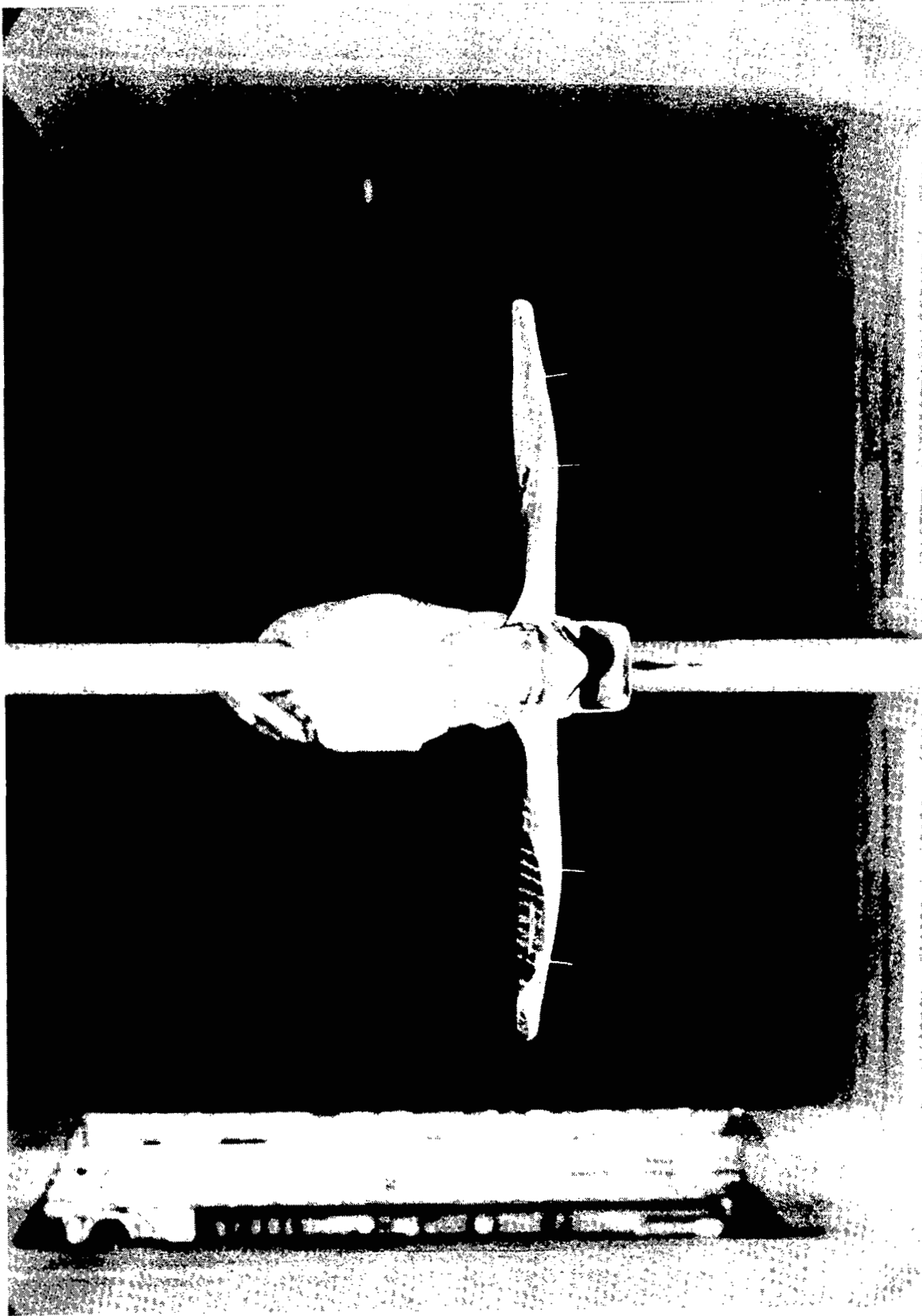
Figure 2.- Continued.



L-80-7551

(c) VG on configuration 1. Three-quarter front view; VG at  $\eta = 0.50$  and  $0.75$ ;  $\phi = 0^\circ$ .

Figure 2.- Continued.



L-80-7533

(d) VG on configuration 1. Front view; VG at  $\eta = 0.50$  and  $0.75$ ;  $\phi = 0^\circ$ .

Figure 2.- Concluded.

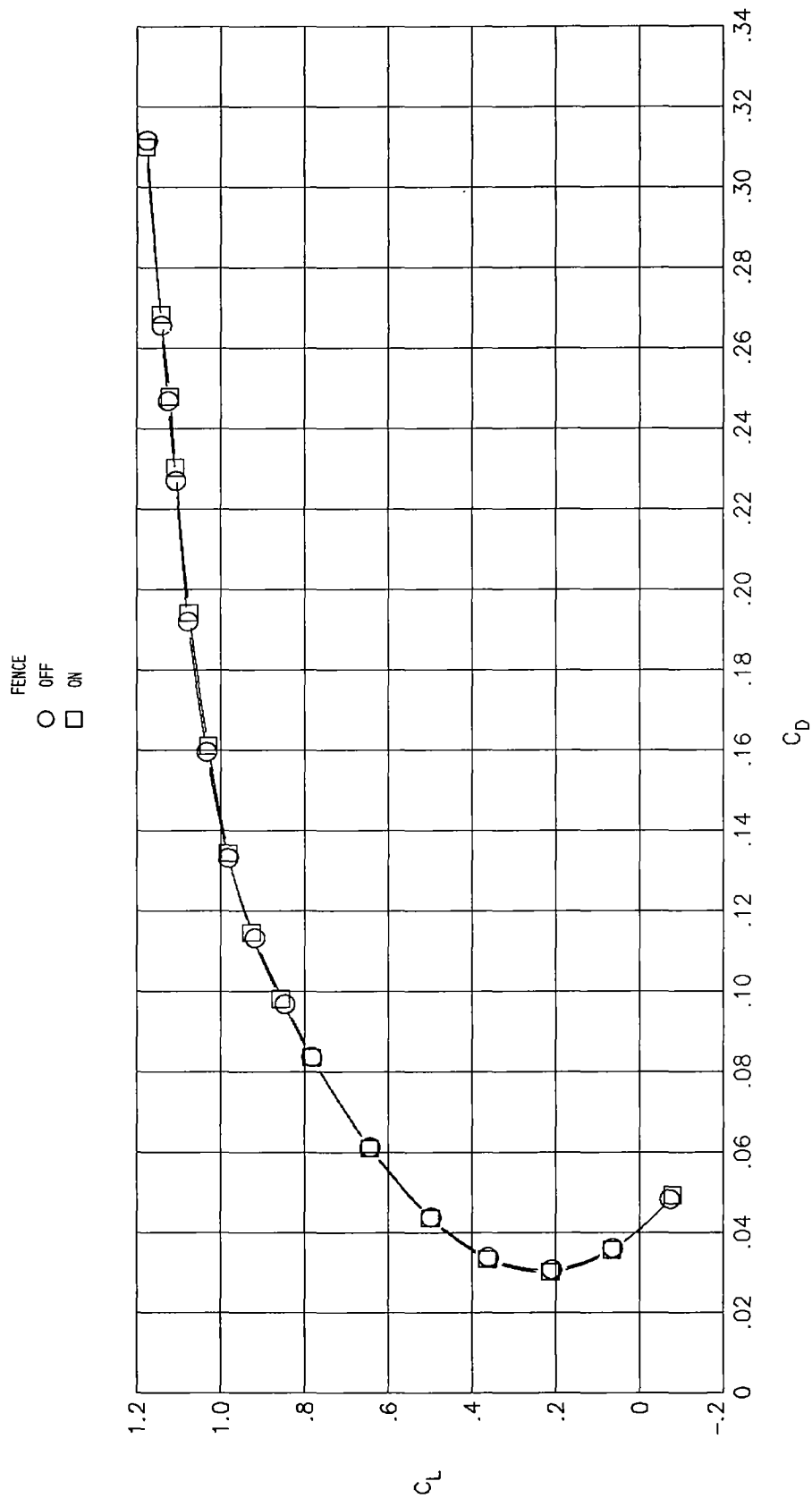


Figure 3.- Effect of fence on longitudinal aerodynamic characteristics at  $M = 0.60$ .  
Small SLEF;  $\delta_f = 20^\circ$ ; configuration 2.

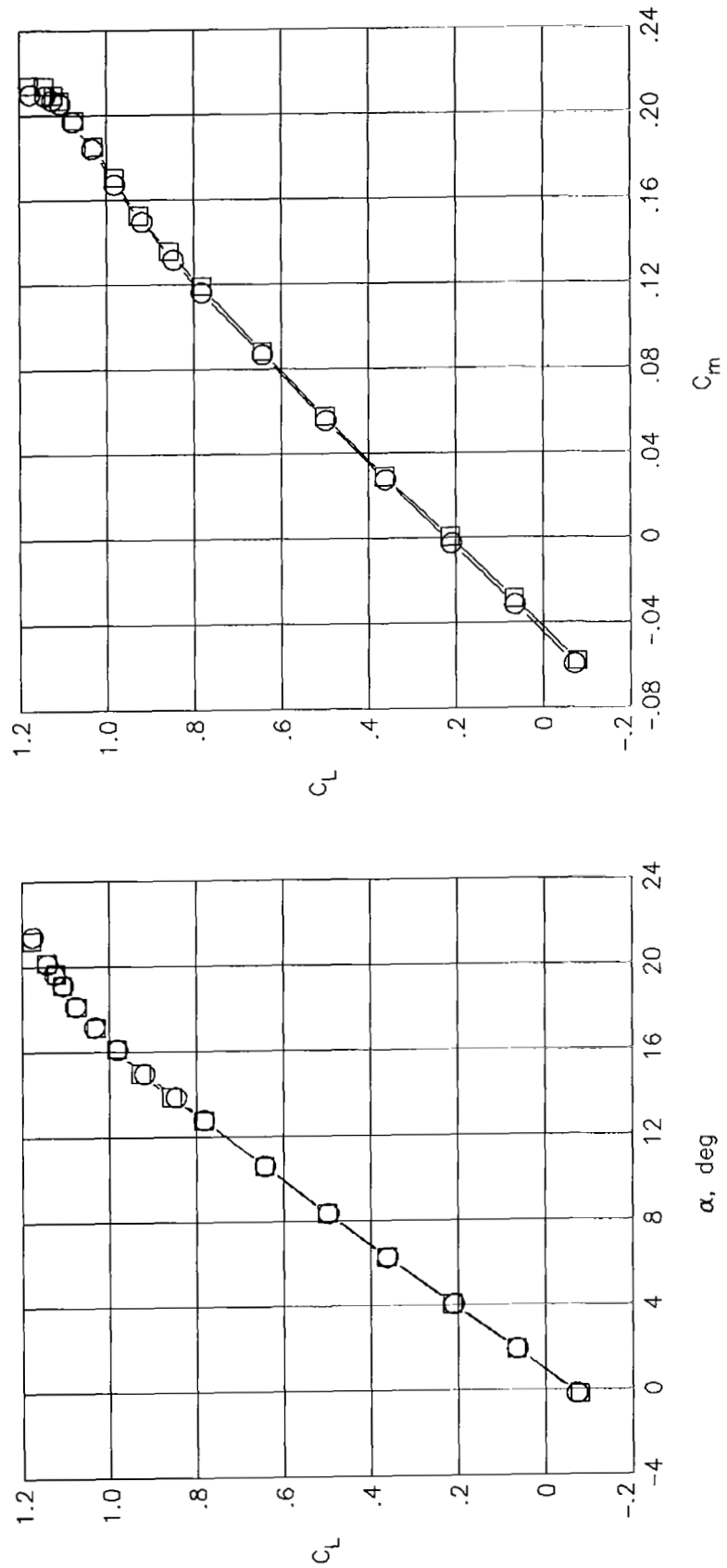
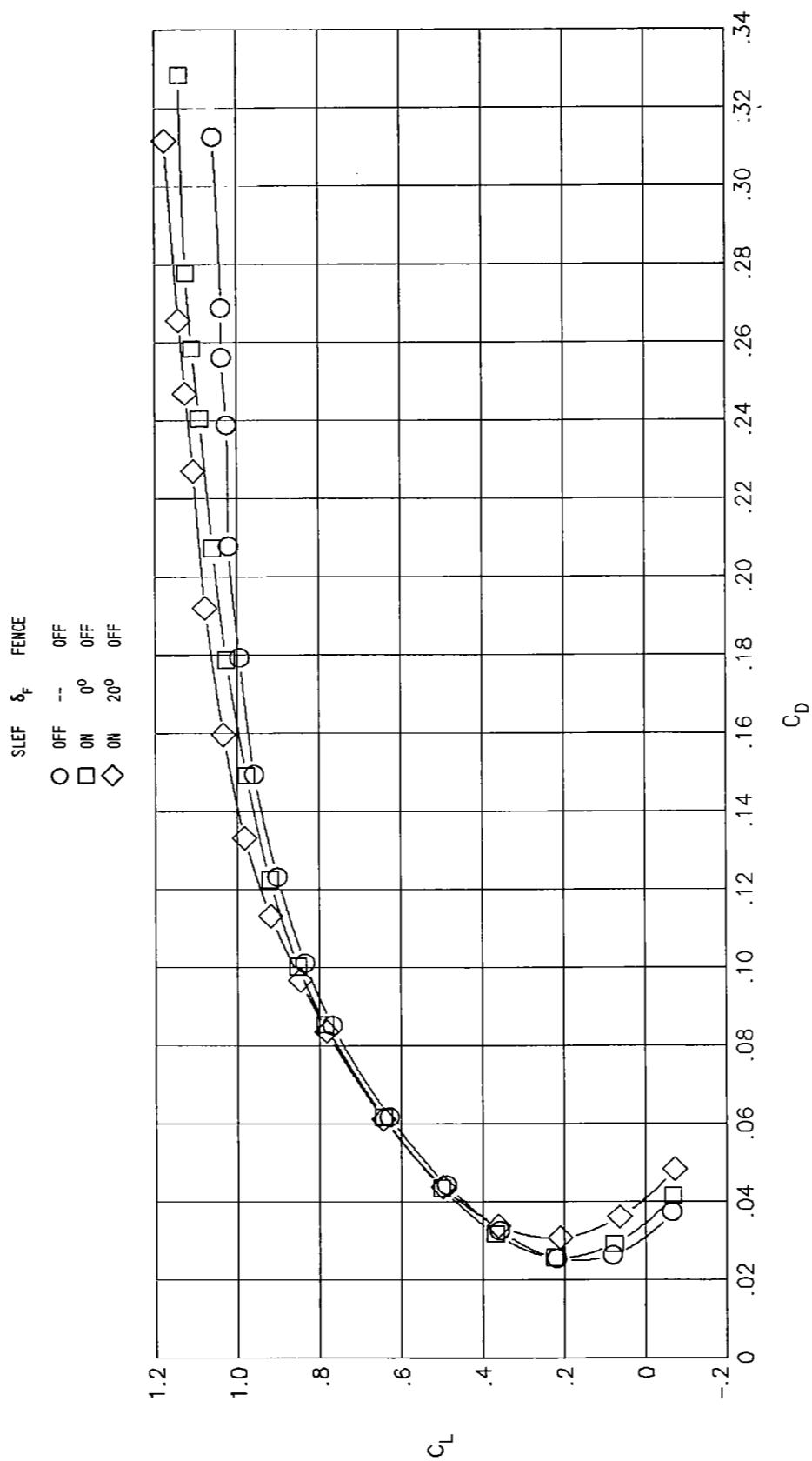
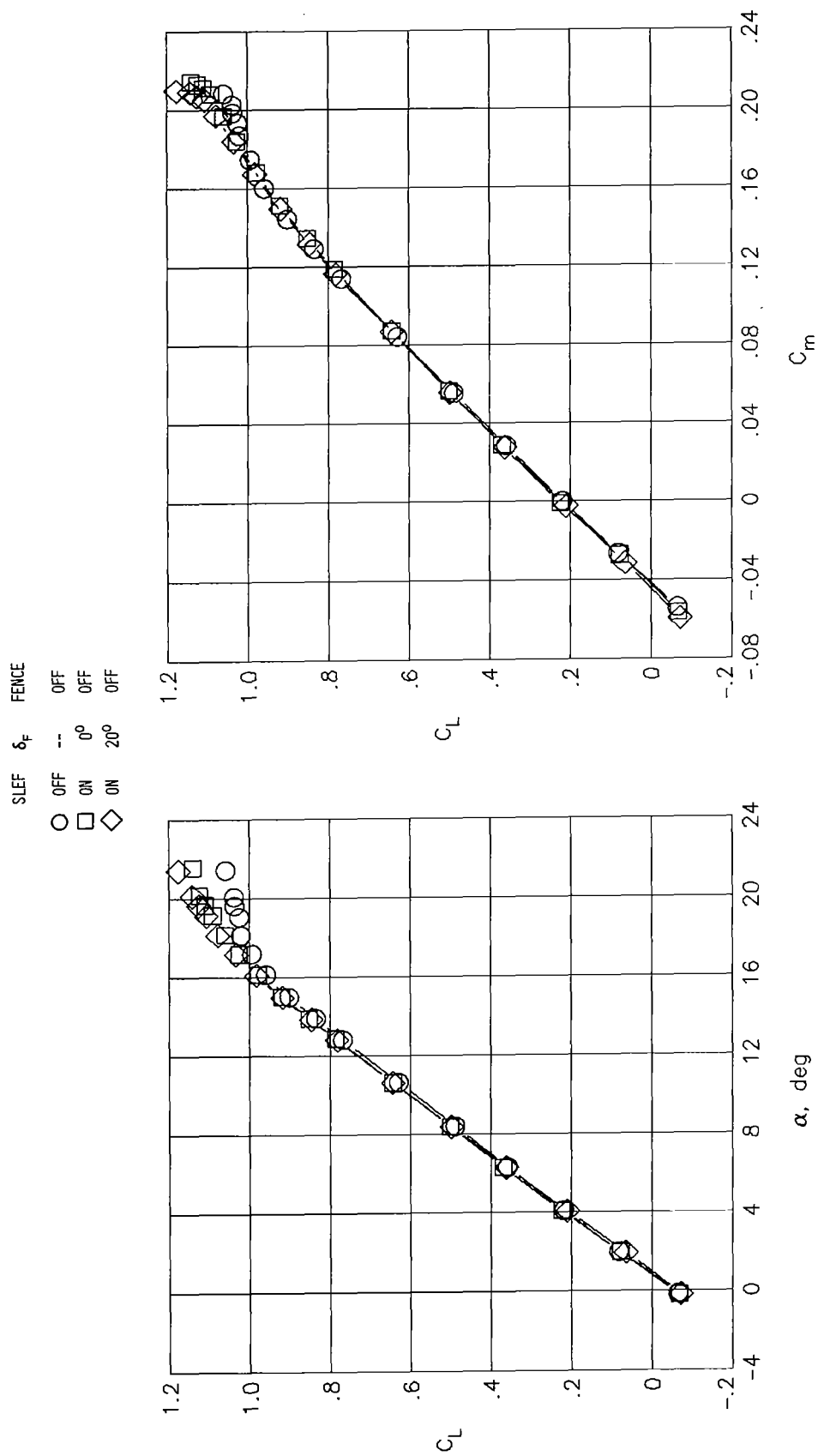


Figure 3.- Concluded.



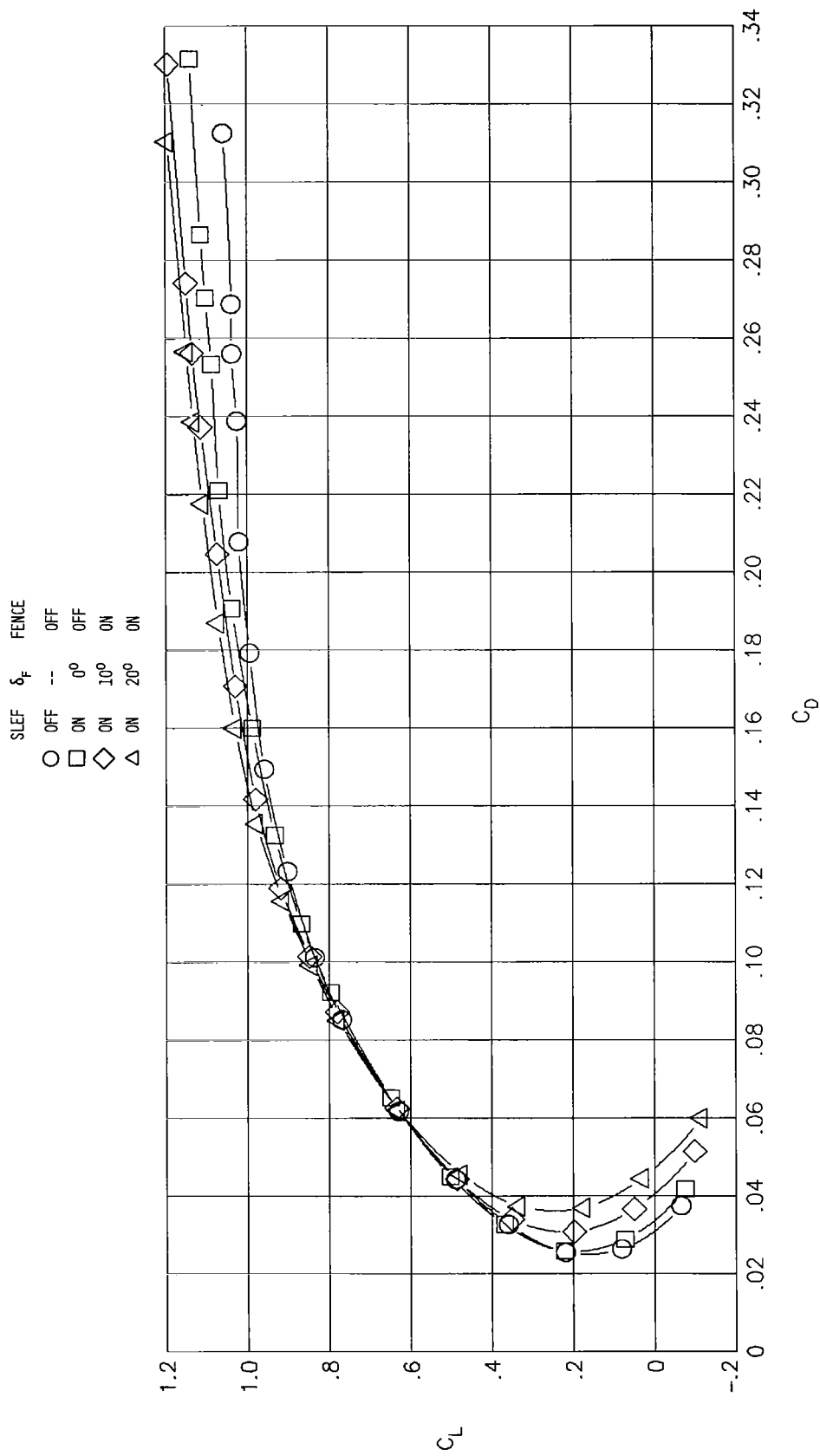
(a) Small SLEF.

Figure 4.- Effect of SLEF deflection angle on longitudinal aerodynamic characteristics at  $M = 0.60$ . Configuration 2.



(a) Concluded.

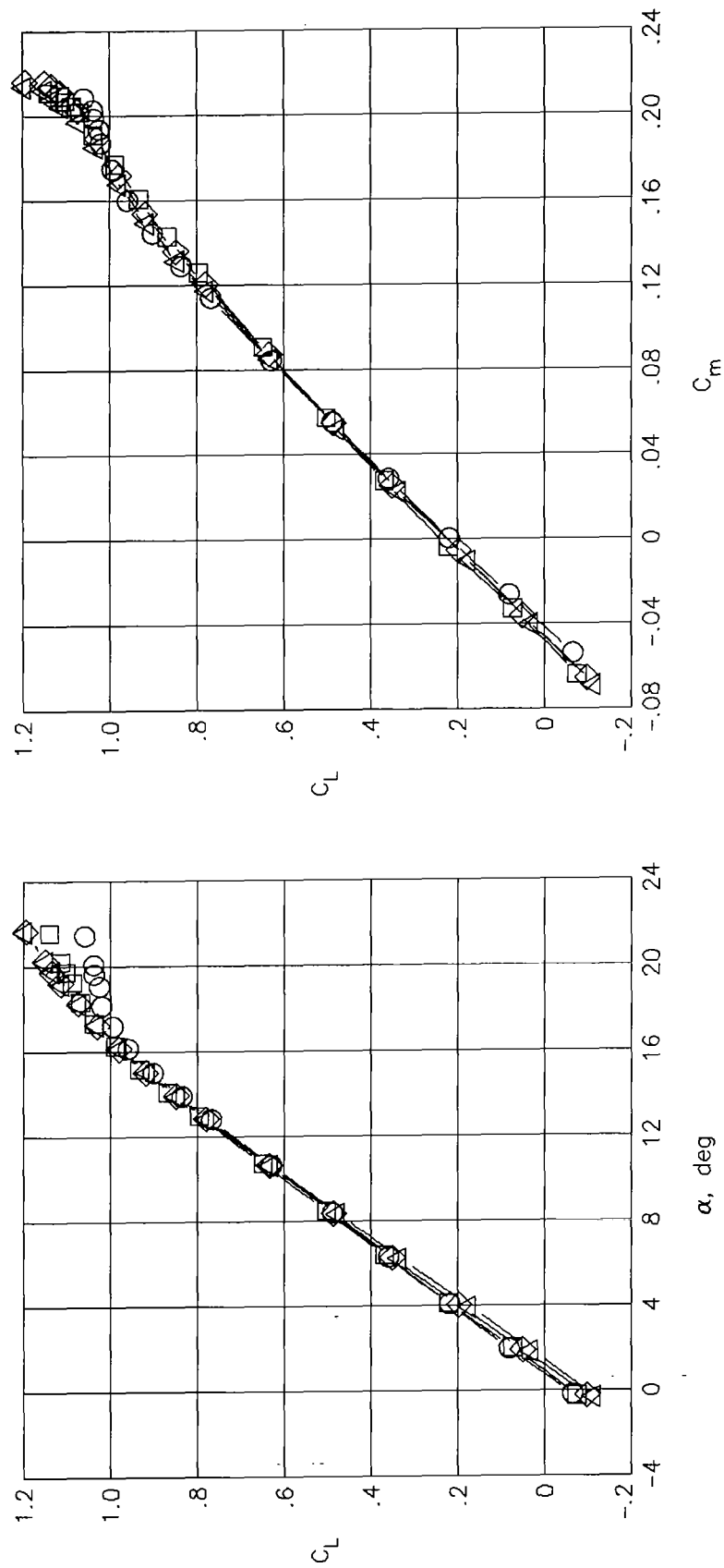
Figure 4.- Continued.



(b) Large SLEF.

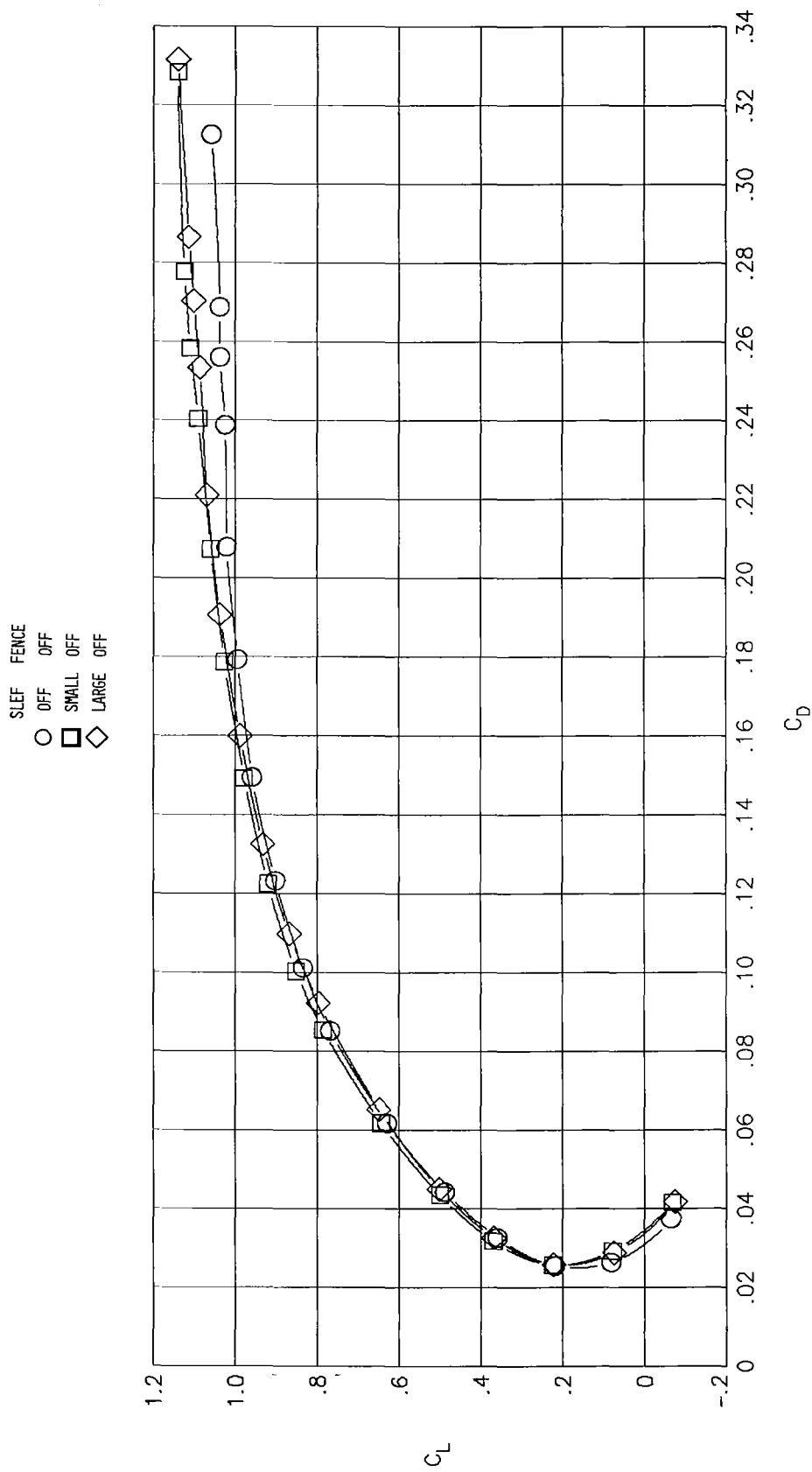
Figure 4.- Continued.

SLEF	$\delta_F$	FENCE
○	OFF	OFF
□	ON	OFF
◇	ON	ON
△	ON	ON



(b) Concluded.

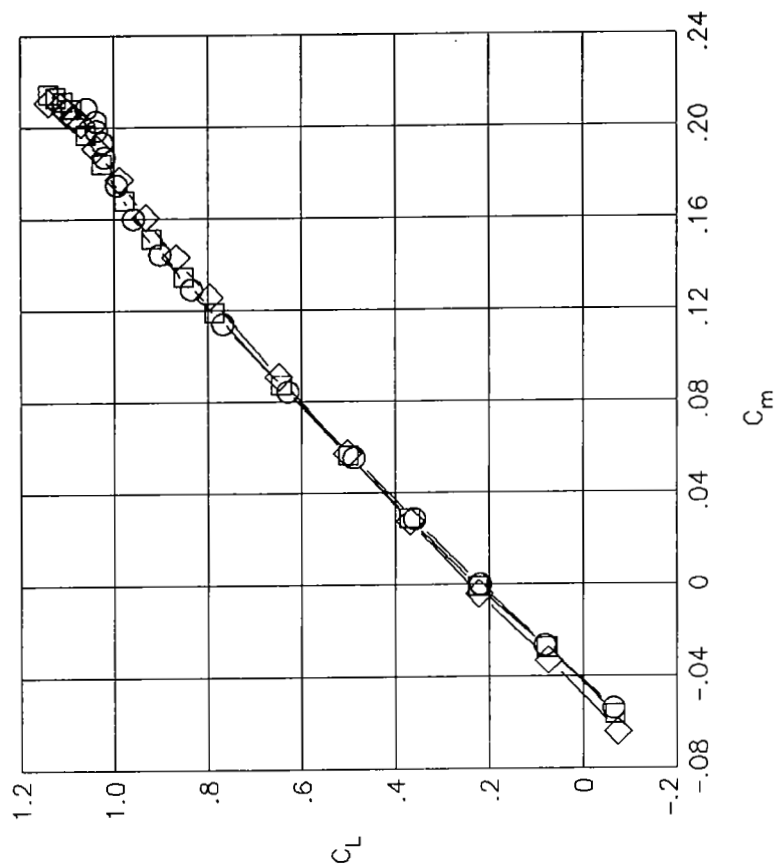
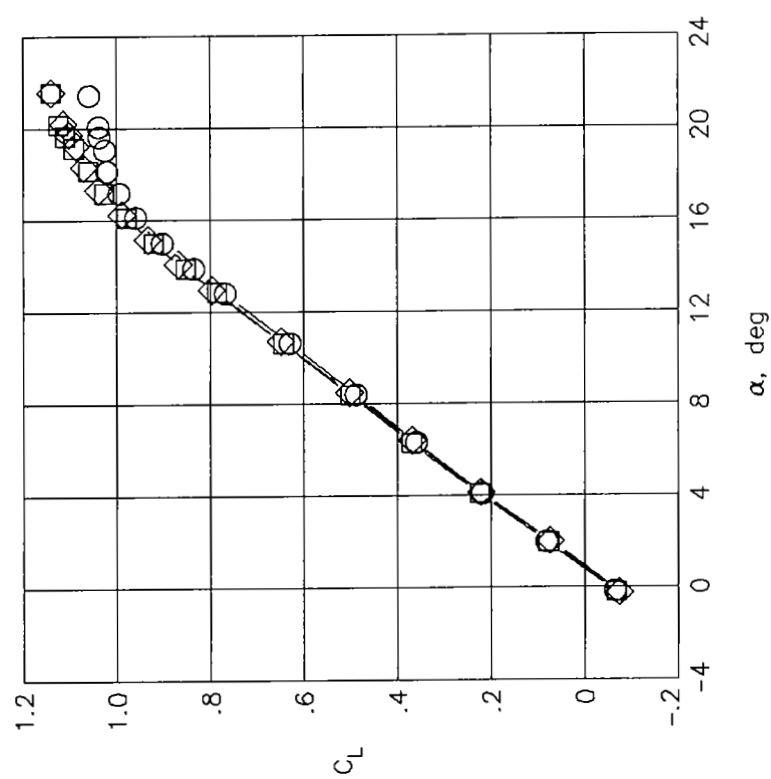
Figure 4.- Concluded.



(a)  $\delta_f = 0^\circ$ .

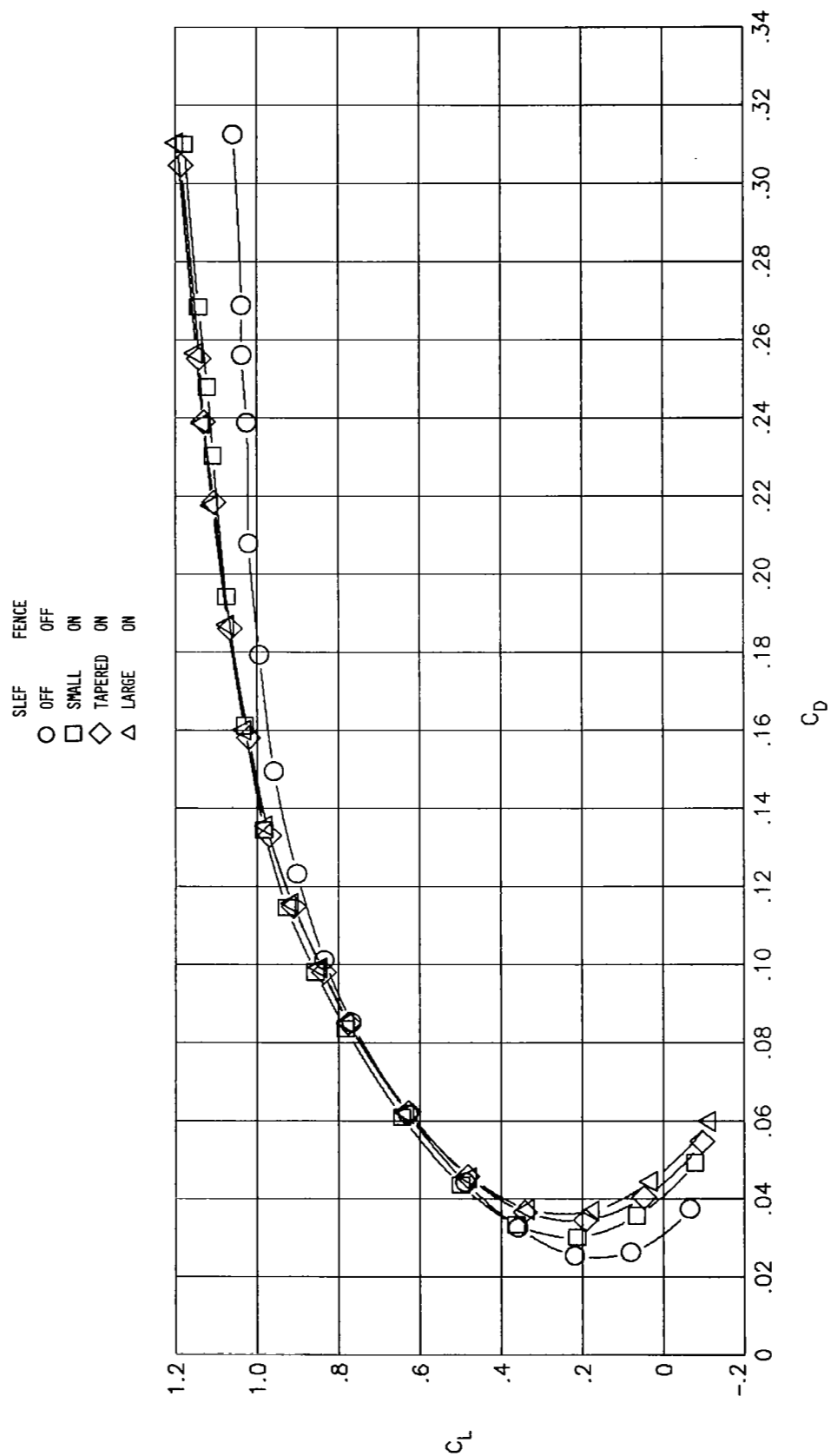
Figure 5.- Effect of SLEF chord length on longitudinal aerodynamic characteristics at  $M = 0.60$ . Configuration 2.

SLEF FENCE  
 ○ OFF OFF  
 □ SMALL OFF  
 ◇ LARGE OFF

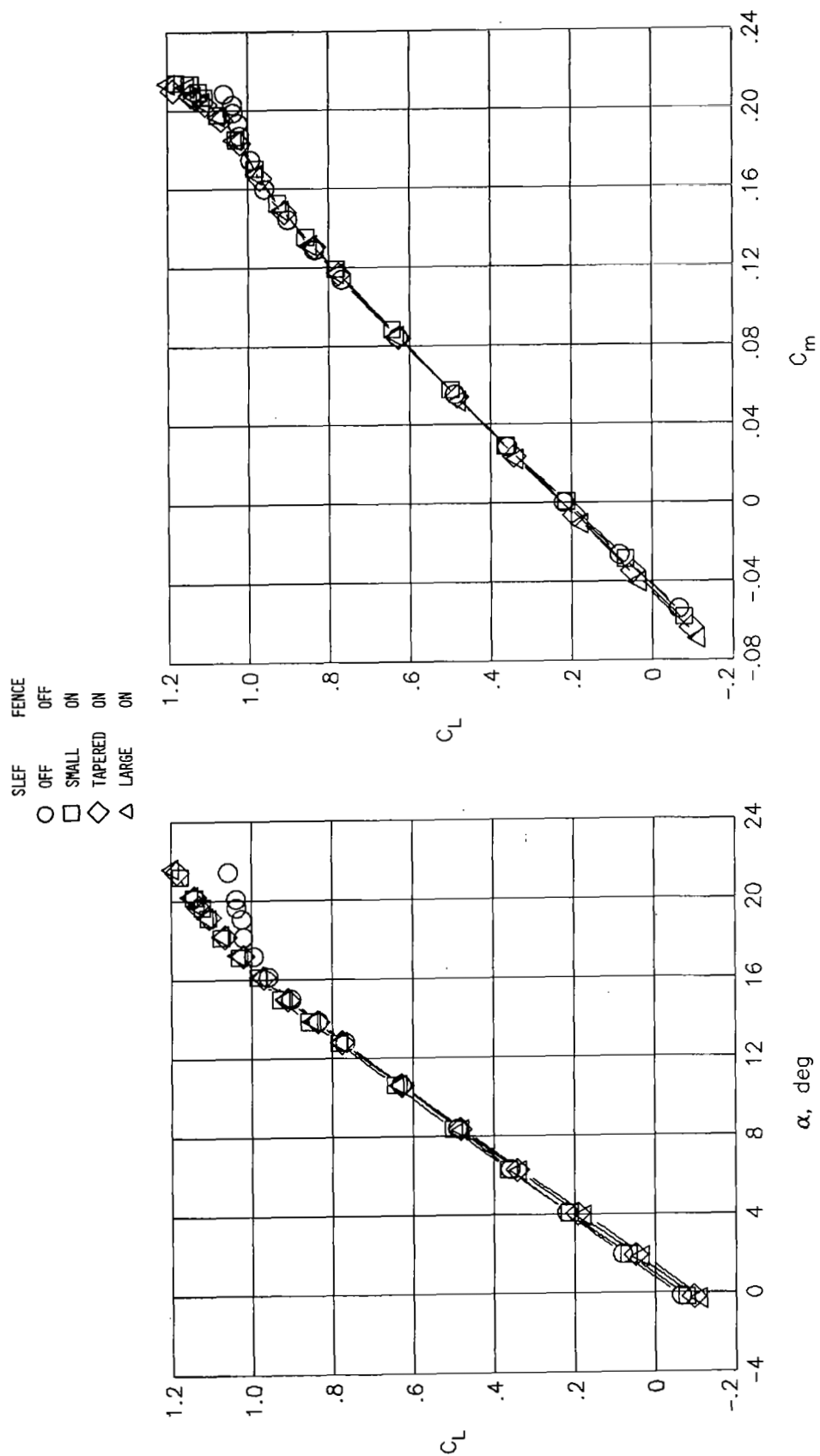


(a) Concluded.

Figure 5.- Continued.



(b)  $\delta_f = 20^\circ$ .  
Figure 5.- Continued.



(b) Concluded.

Figure 5.- Concluded.

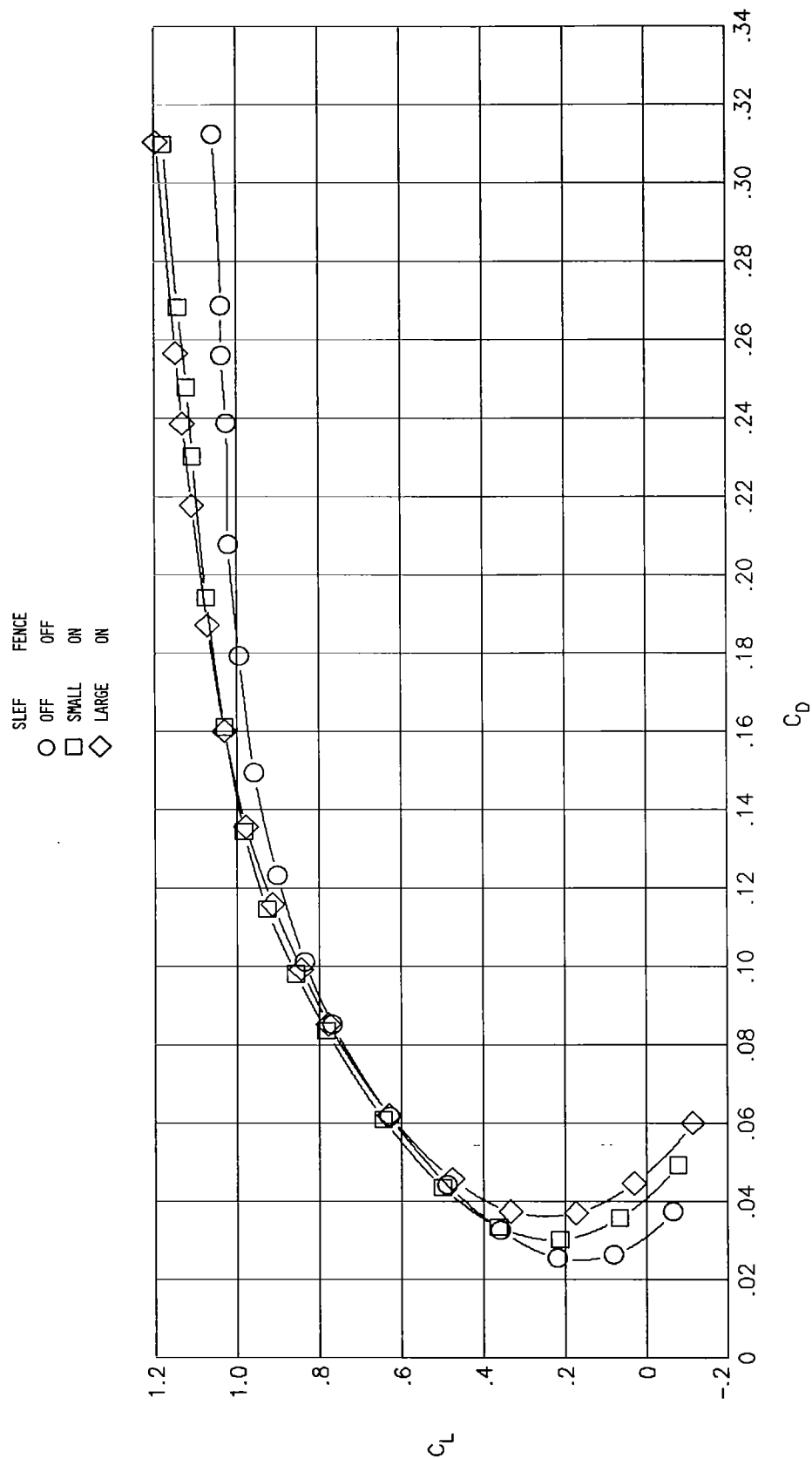


Figure 6.- Summary of longitudinal aerodynamic characteristics of constant-chord SLEF with  $\delta_f = 20^\circ$  at  $M = 0.60$ . Configuration 2.

SLEF      FENCE  
 ○   OFF   OFF  
 □   SMALL   ON  
 ◇   LARGE   ON

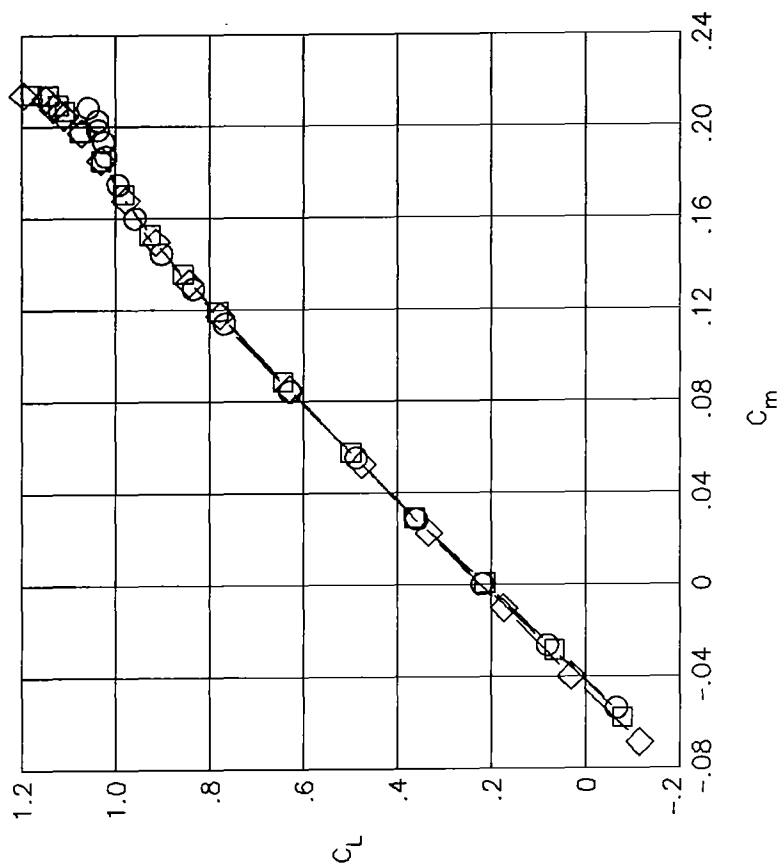
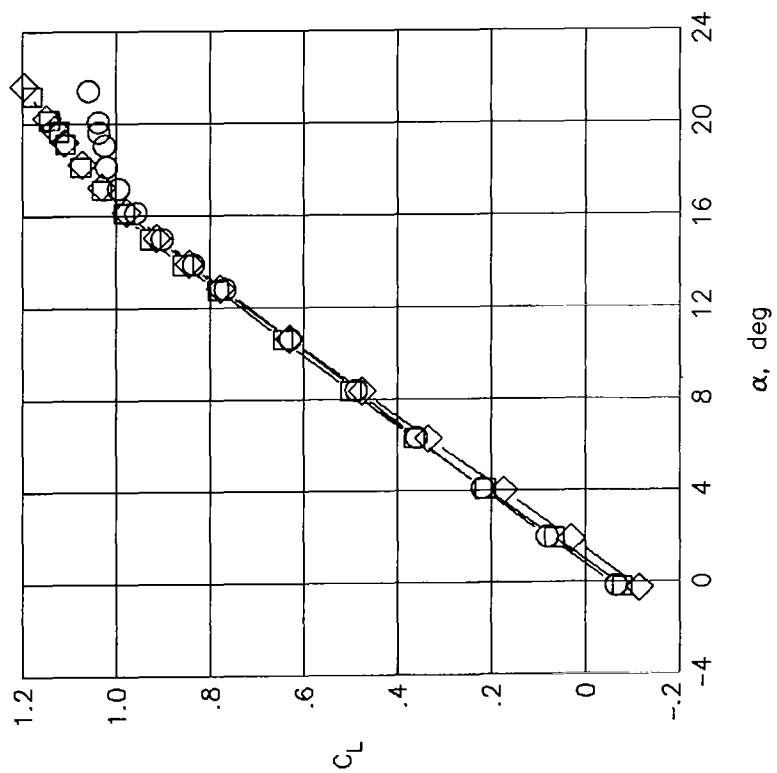


Figure 6.- Concluded.

SLEF      FENCE  
 ○   OFF   OFF  
 □   SMALL   ON  
 ◇   LARGE   ON

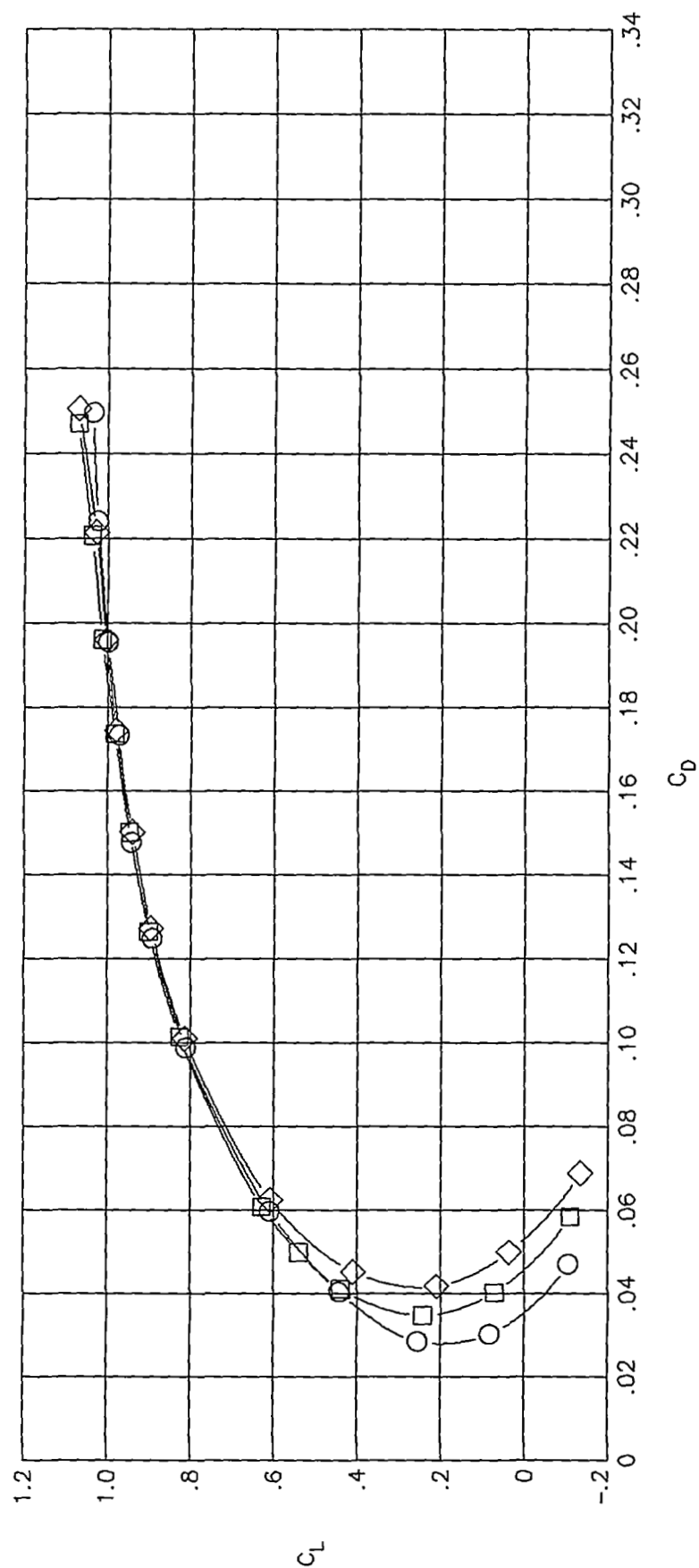


Figure 7.- Effect of SLEF chord length on longitudinal aerodynamic characteristics at  $M = 0.85$ .  $\delta_f = 20^\circ$ ; configuration 2.

ORIGINAL PAGE IS  
OF POOR QUALITY

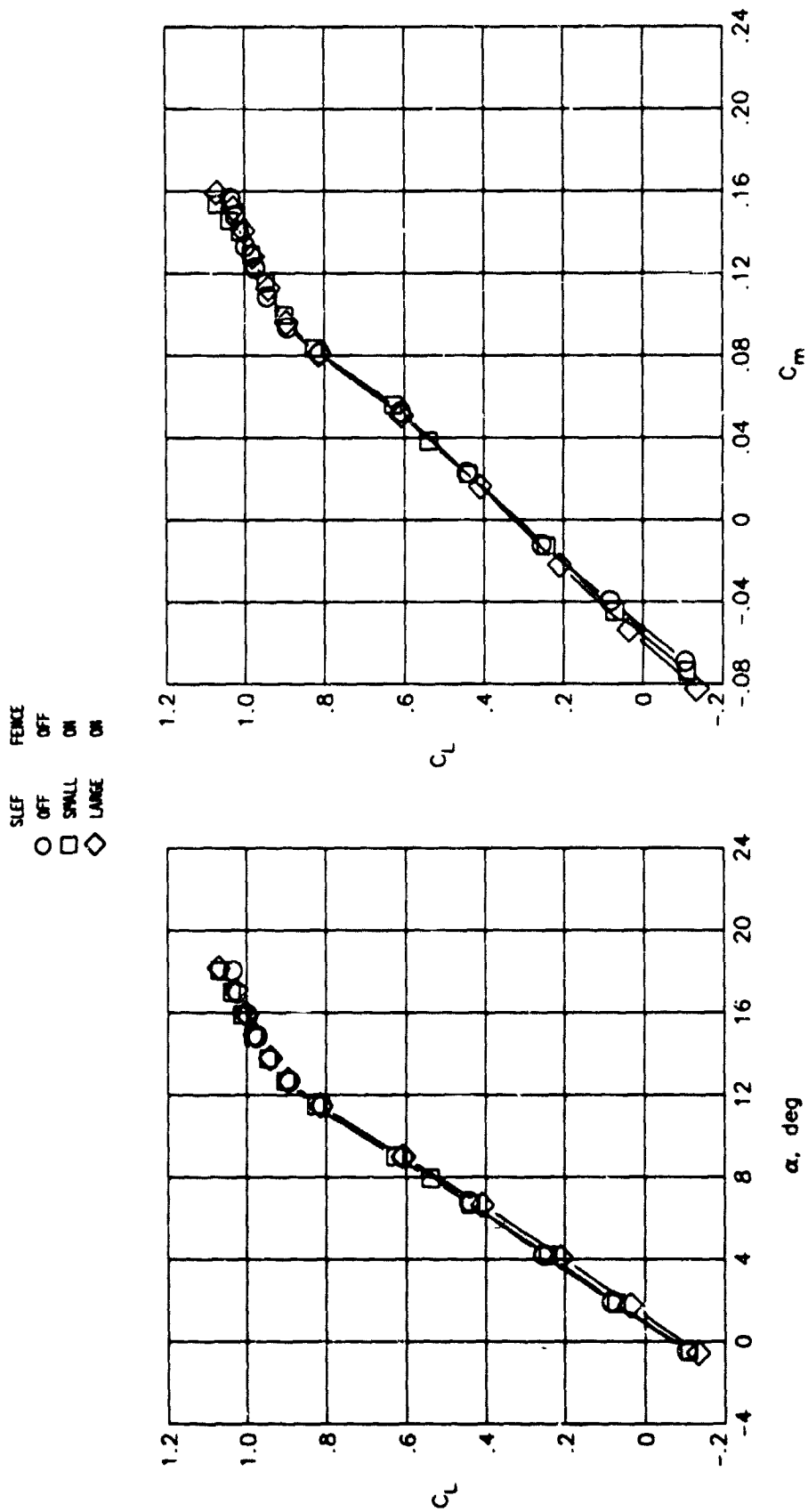


Figure 7.- Concluded.

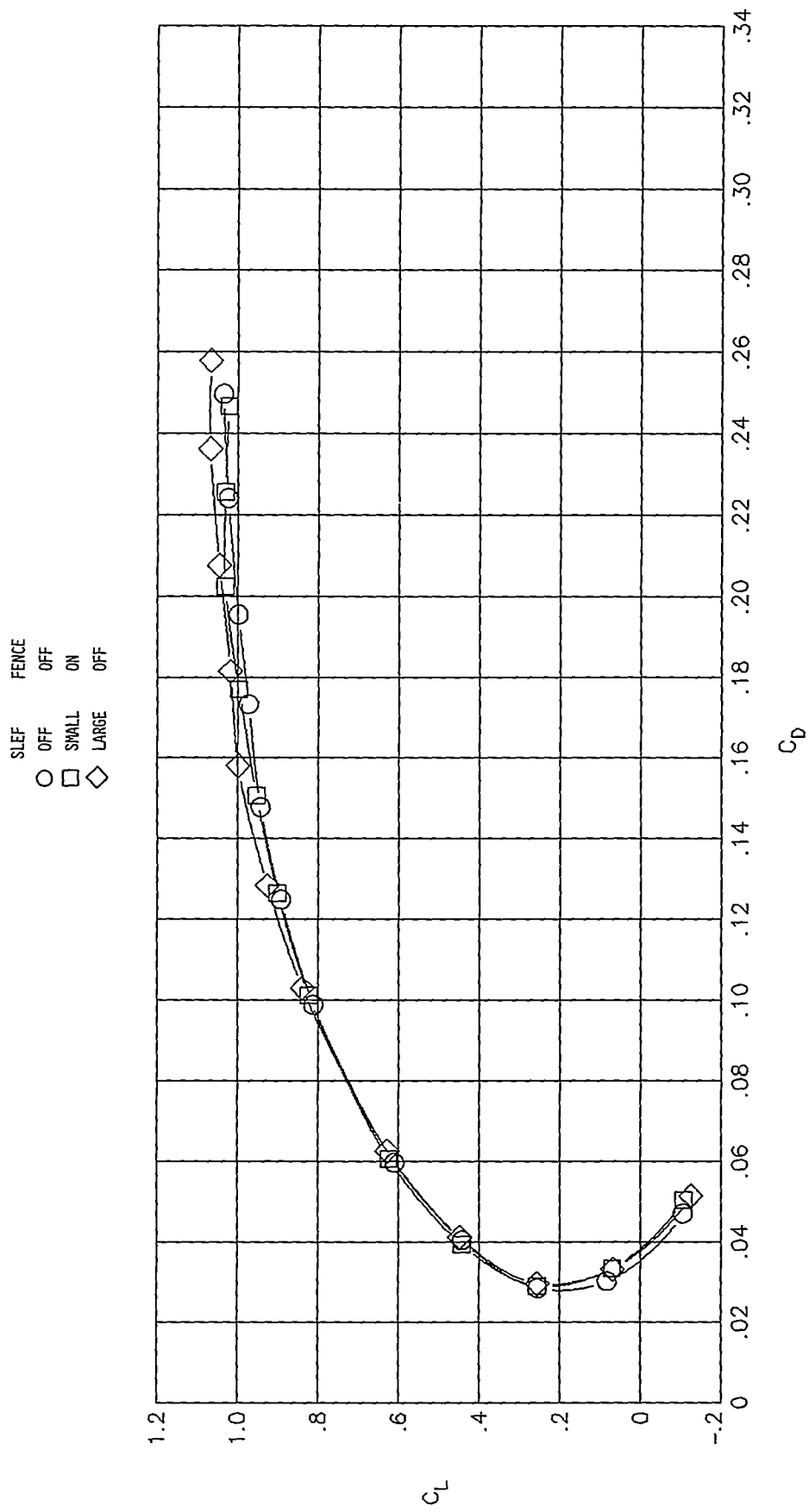


Figure 8.- Longitudinal aerodynamic characteristics of SLEF with  $\delta_f = 0^\circ$  at  $M = 0.85$ . Configuration 2.

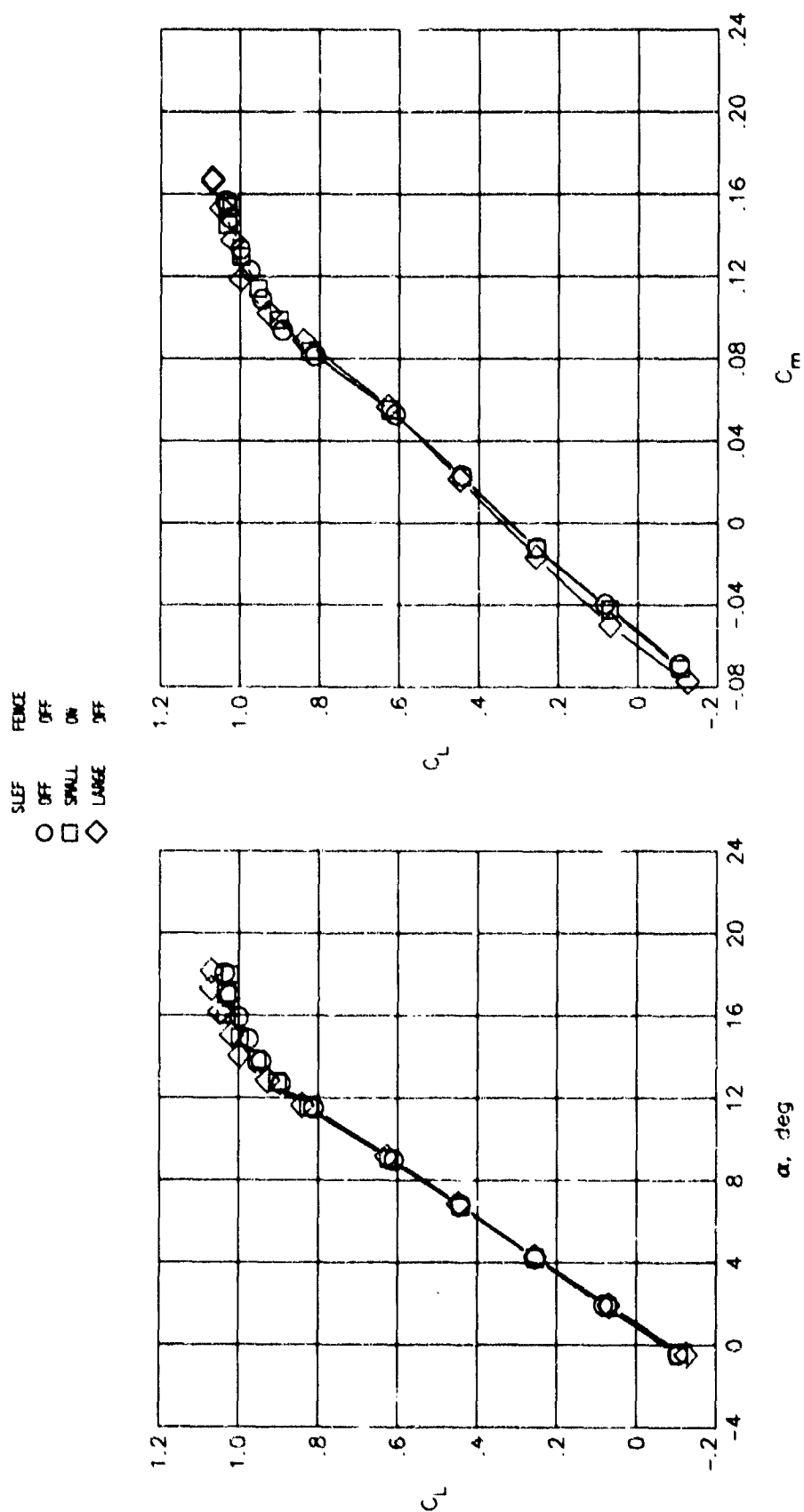
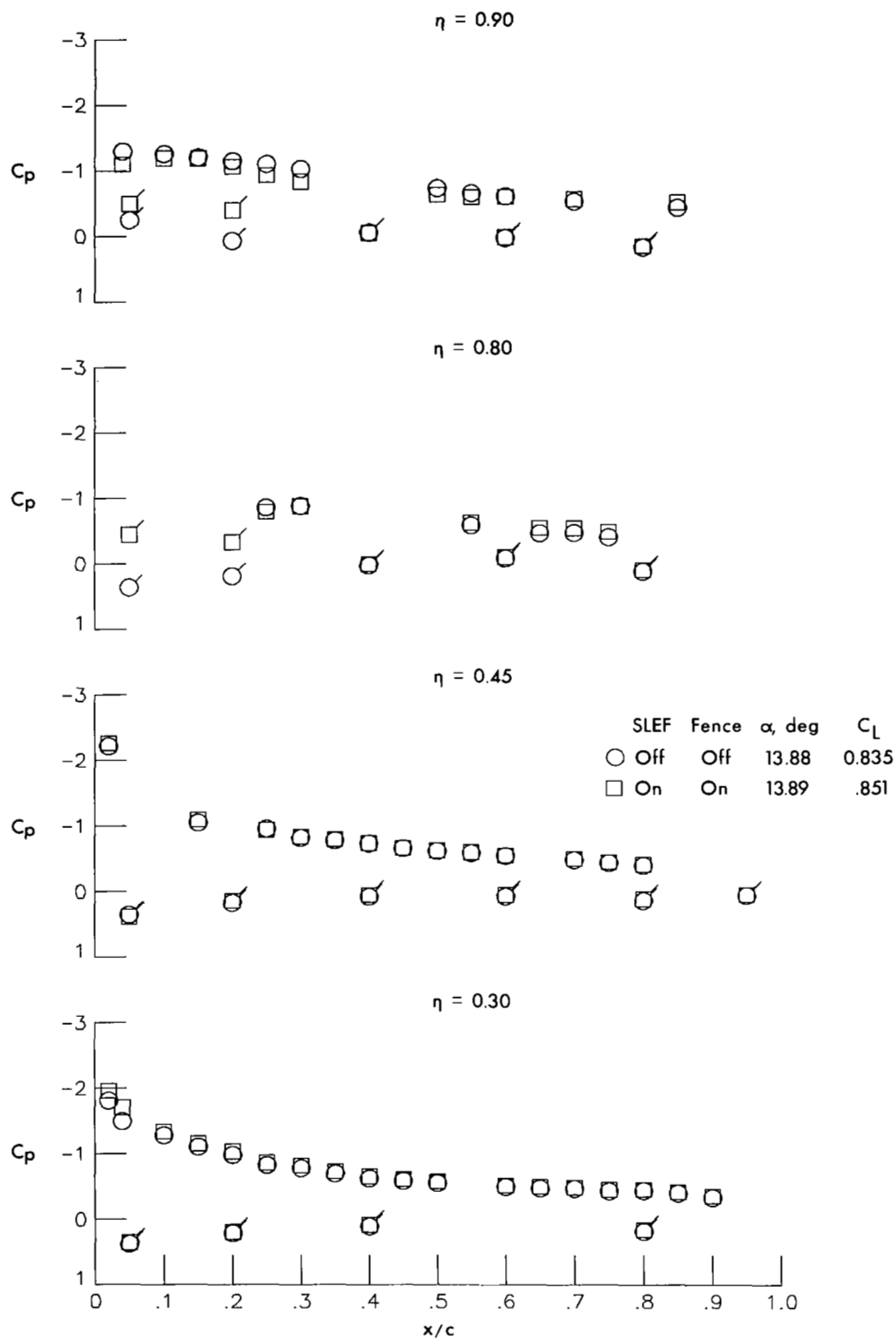
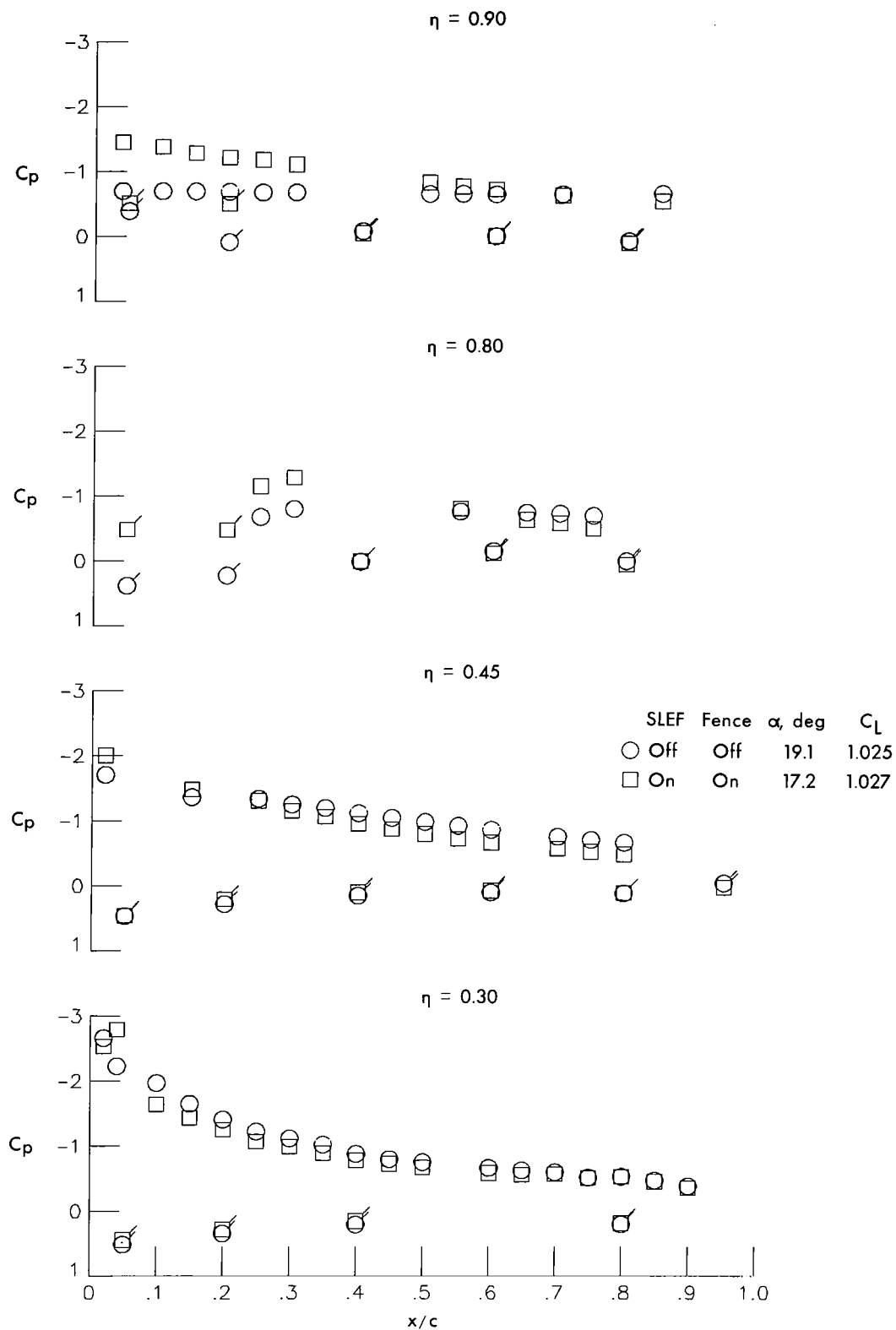


Figure 8.- Concluded.



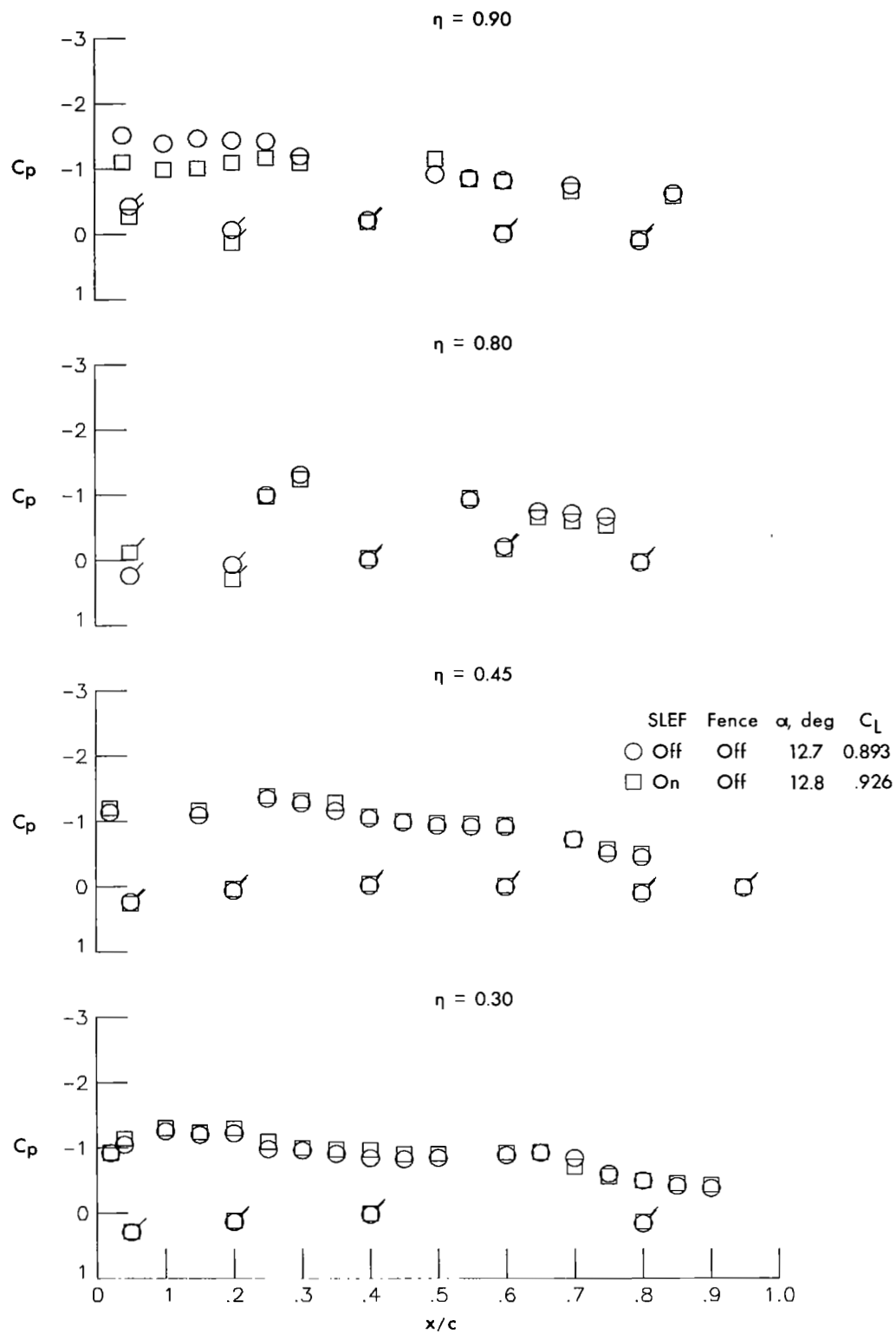
(a)  $M = 0.60$ . Small SLEF;  $\delta_f = 20^\circ$ ;  $C_L \approx 0.85$ .

Figure 9.- Effect of SLEF on wing upper- and lower-surface pressure coefficients. Configuration 2. Flagged symbols indicate lower surface.



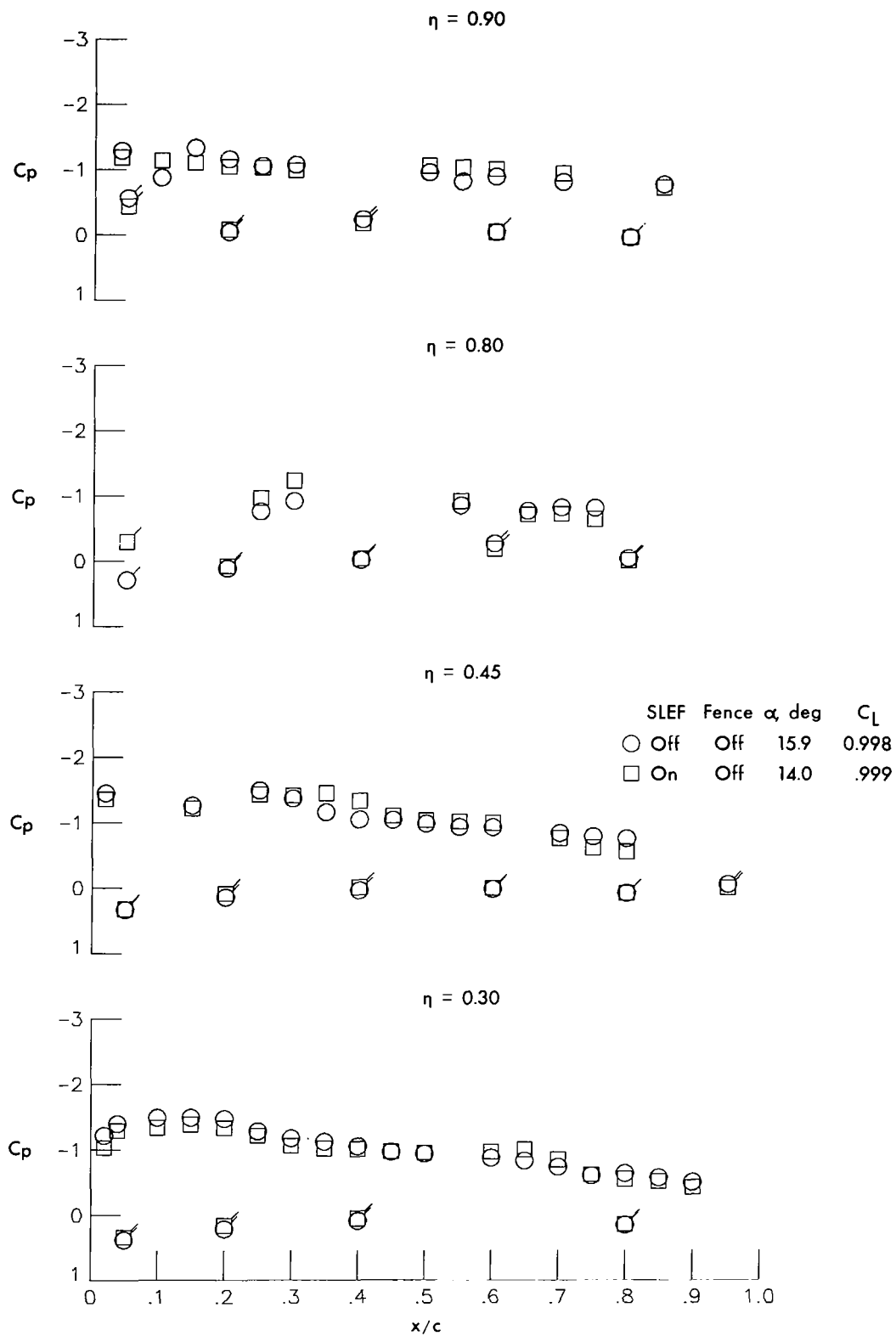
(b)  $M = 0.60$ . Small SLEF;  $\delta_f = 20^\circ$ ;  $C_L \approx 1.03$ .

Figure 9.- Continued.



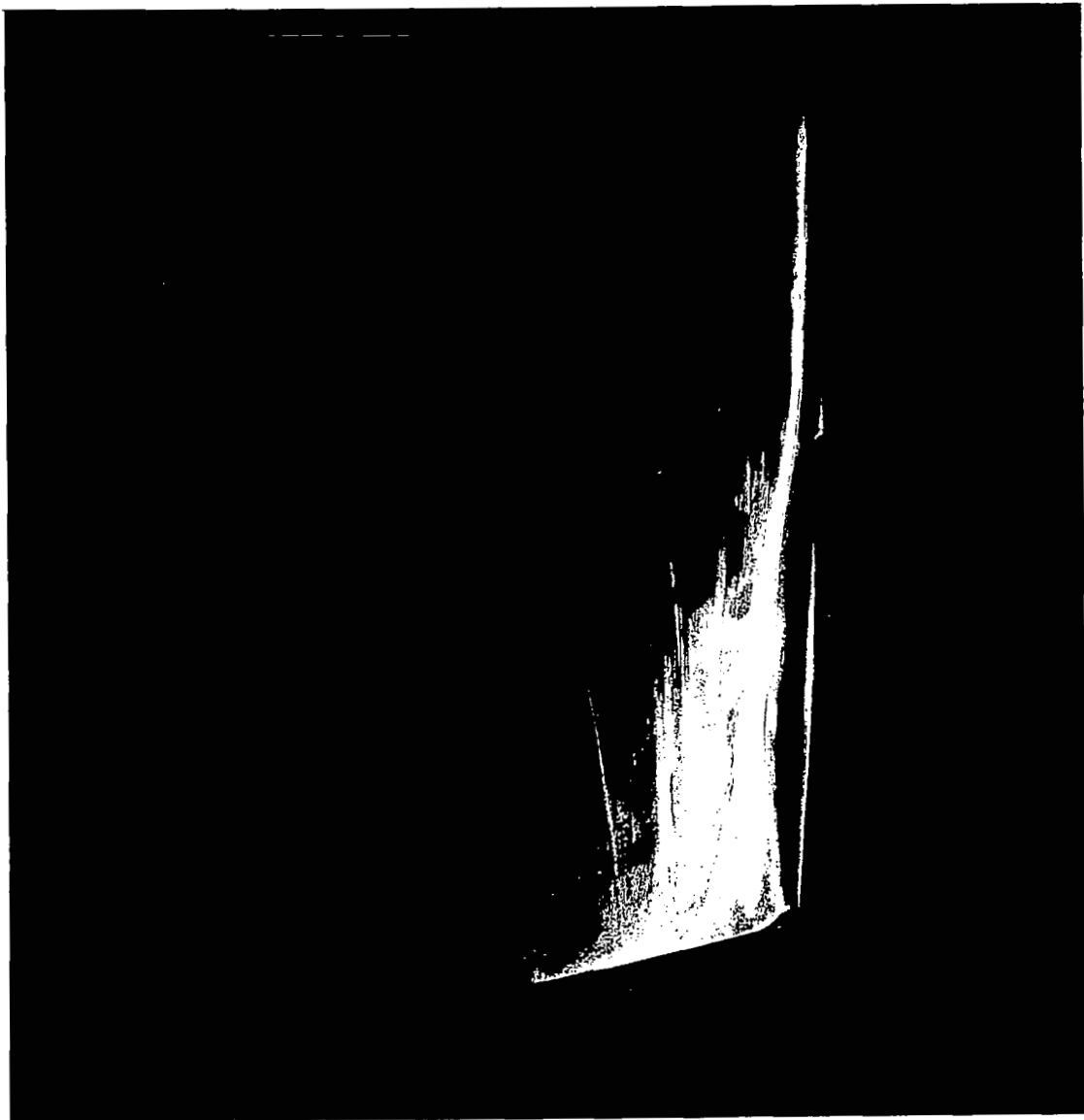
(c)  $M = 0.85$ . Large SLEF;  $\delta_f = 0^\circ$ ;  $C_L \approx 0.9$ .

Figure 9.- Continued.



(d)  $M = 0.85$ . Large SLEF;  $\delta = 0^\circ$ ;  $C_L \approx 1.0$ .

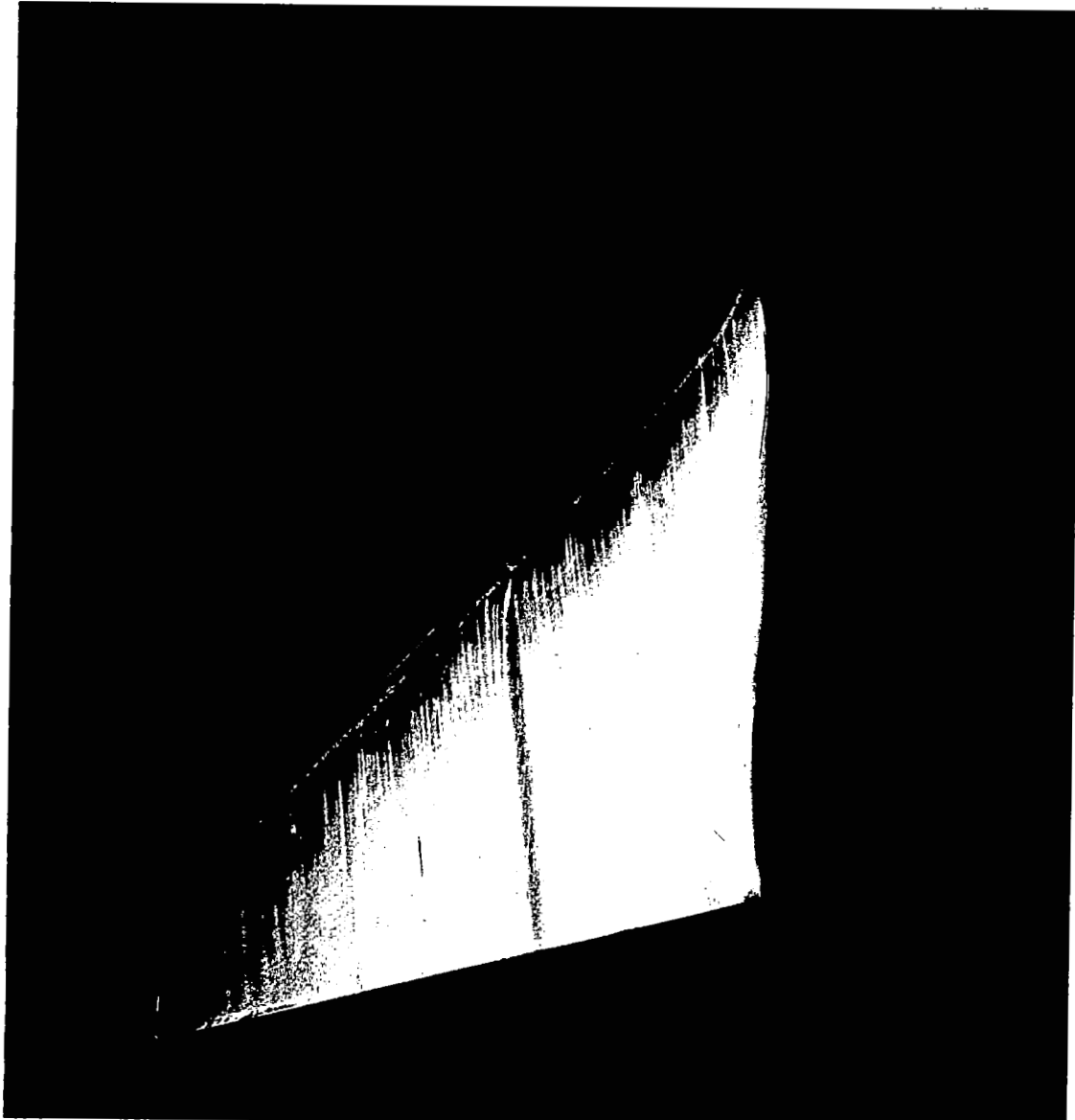
Figure 9.- Concluded.



L-83-12

(a) SLEF off; fence off;  $\alpha = 8.39^\circ$ .

Figure 10.- Photographs of oil-flow patterns on wing upper surface at  $M = 0.60$  with and without the small SLEF.  $\delta_f = 20^\circ$ ; configuration 2.



L-83-13

(b) SLEF on; fence on;  $\alpha = 8.39^\circ$ .

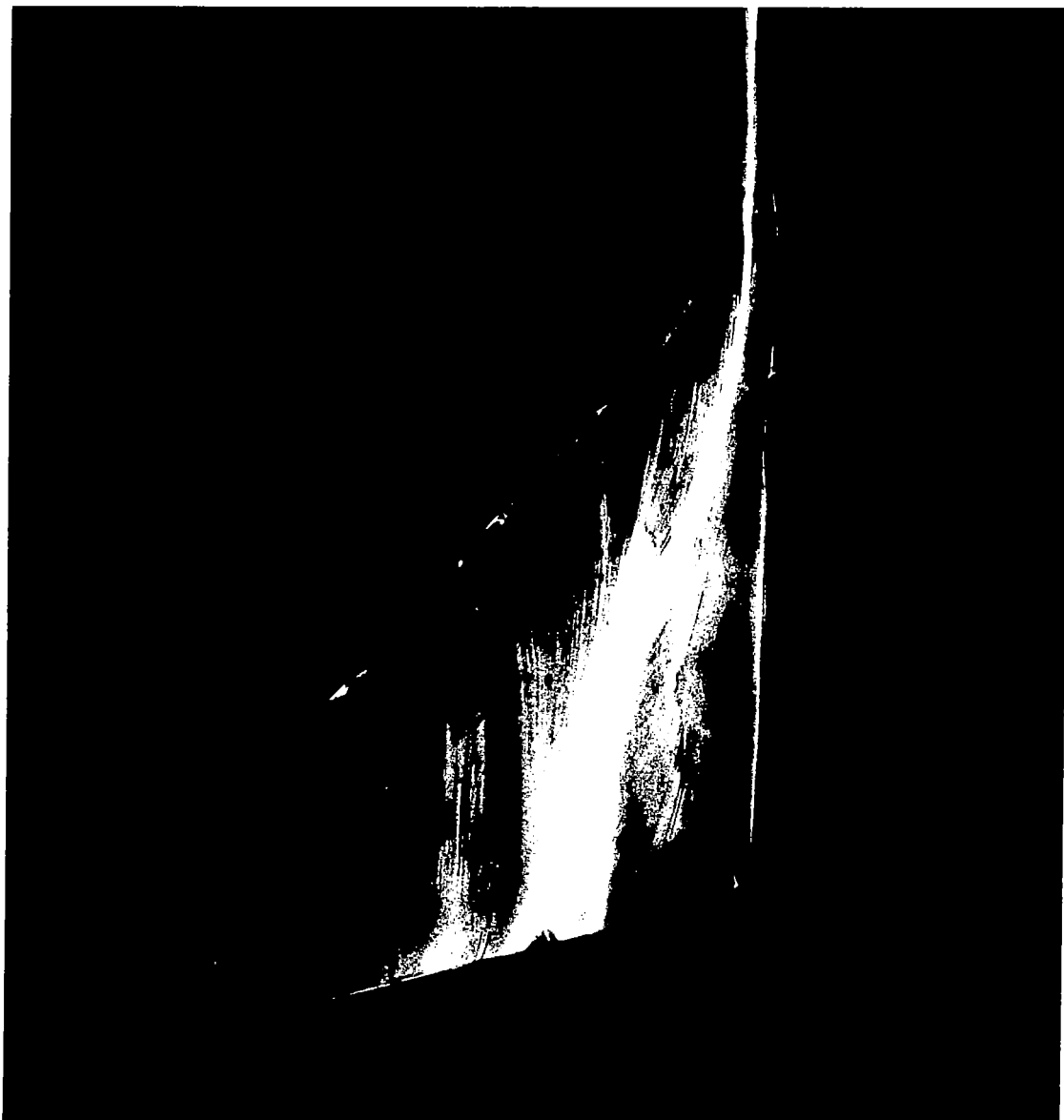
Figure 10.- Continued.



L-83-14

(c) SLEF on; fence off;  $\alpha = 8.39^\circ$ .

Figure 10.- Continued.



L-83-15

(d) SLEF off; fence off;  $\alpha = 13.88^\circ$ .

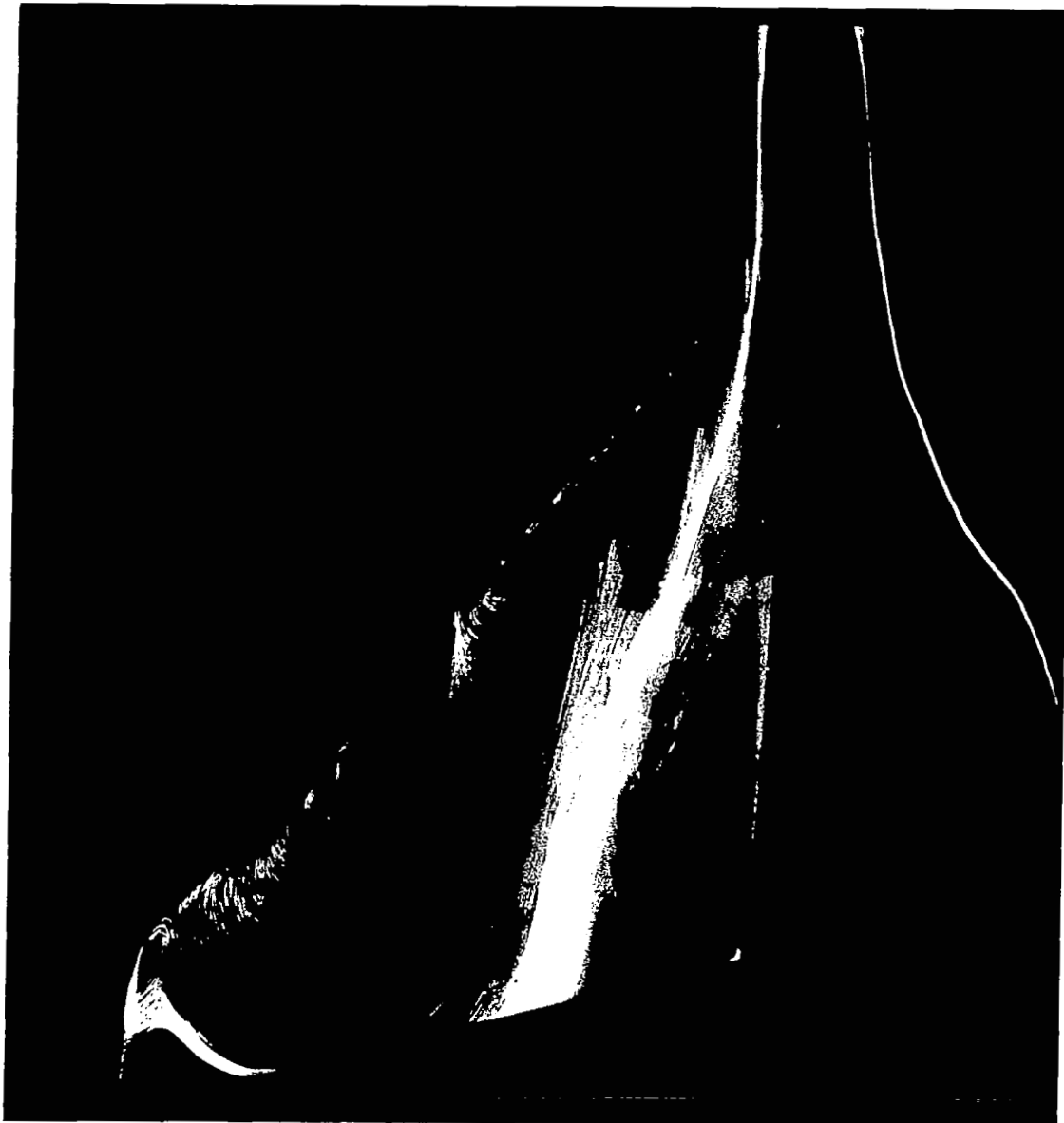
Figure 10.- Continued.



L-83-16

(e) SLEF on; fence on;  $\alpha = 13.88^\circ$ .

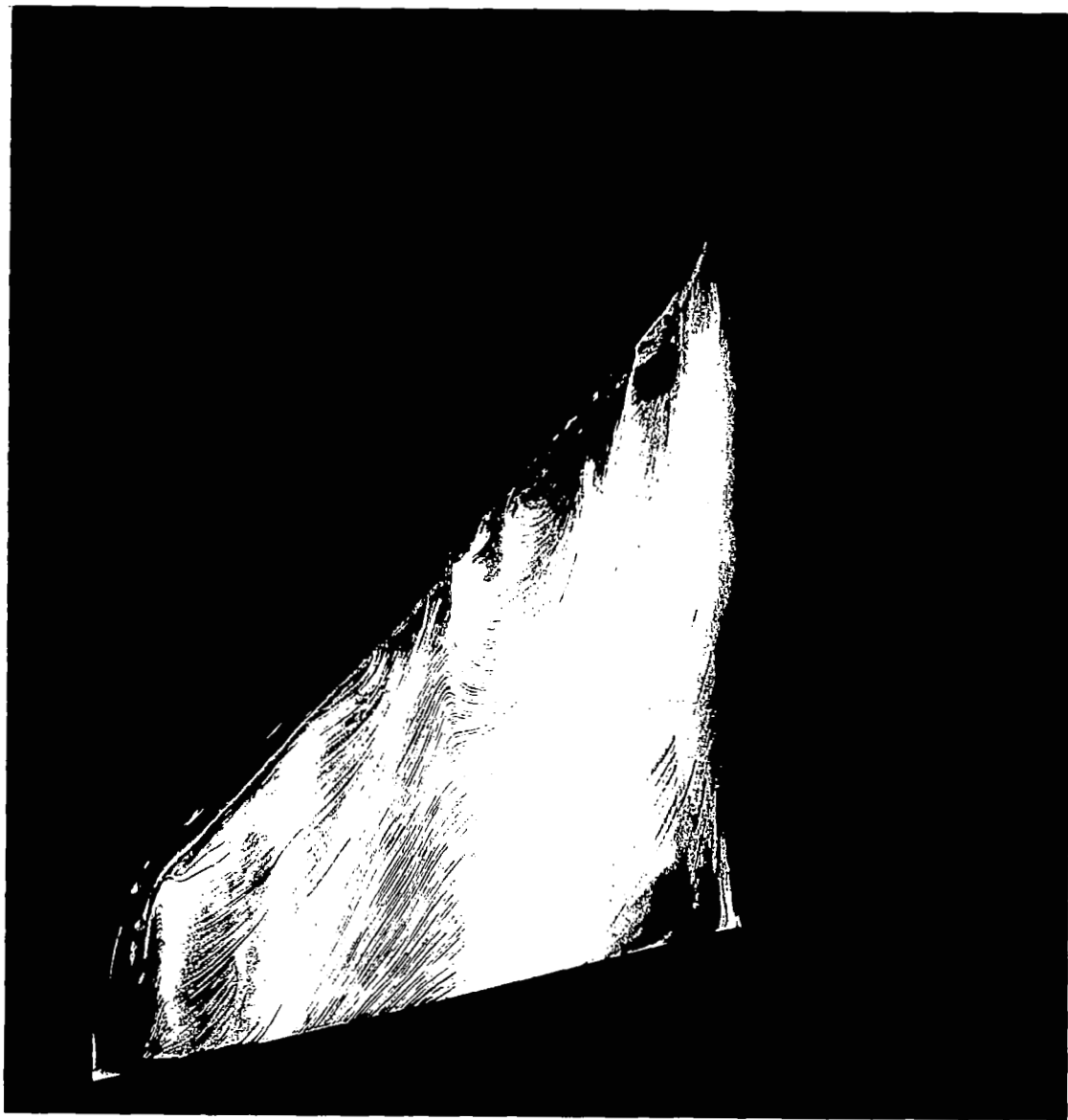
Figure 10.- Continued.



L-83-17

(f) SLEF off; fence off;  $\alpha = 17.18^\circ$ .

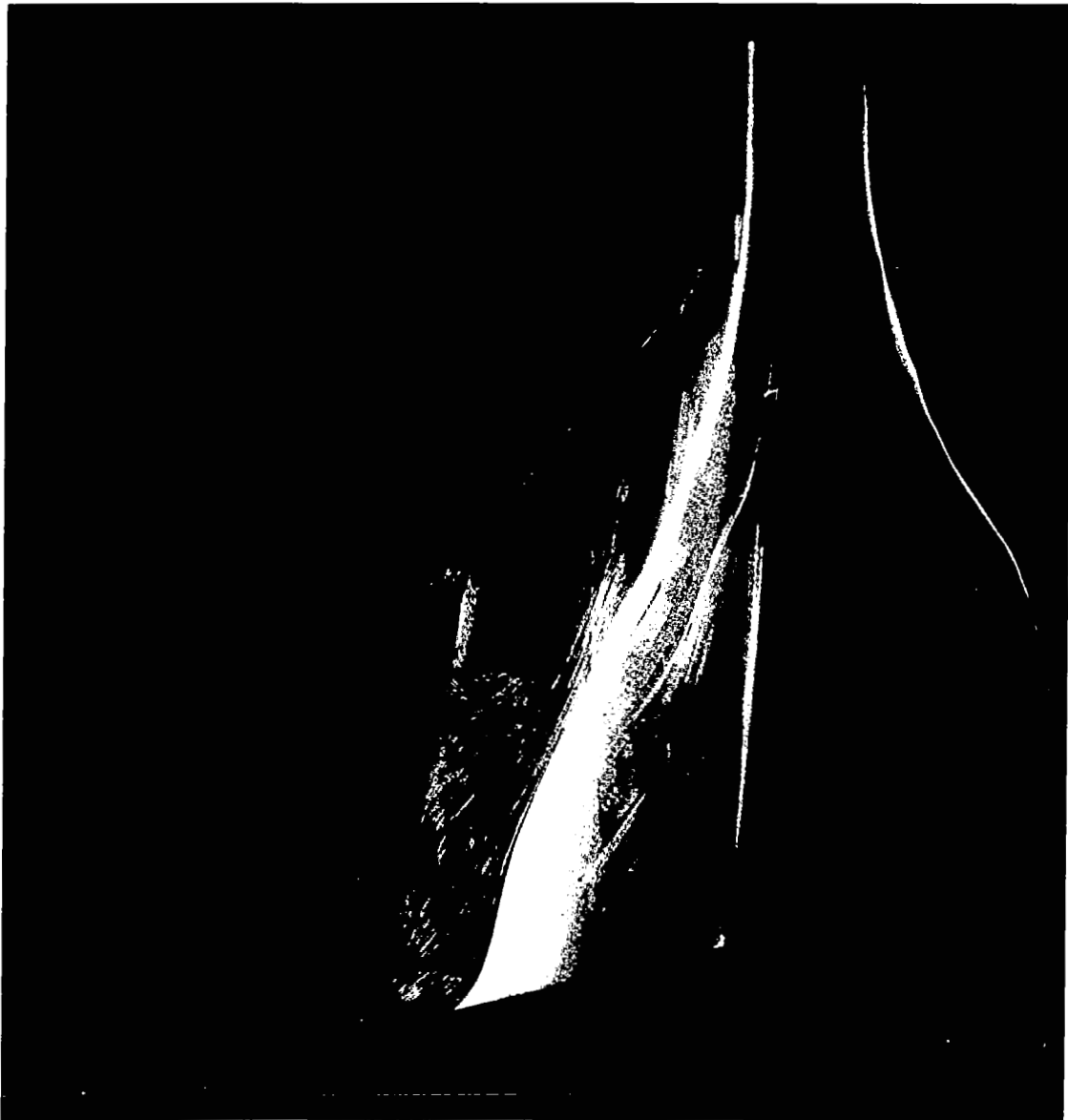
Figure 10.- Continued.



L-83-18

(g) SLEF on; fence on;  $\alpha = 17.18^\circ$ .

Figure 10.- Continued.



L-83-19

(h) SLEF on; fence off;  $\alpha = 17.18^\circ$ .

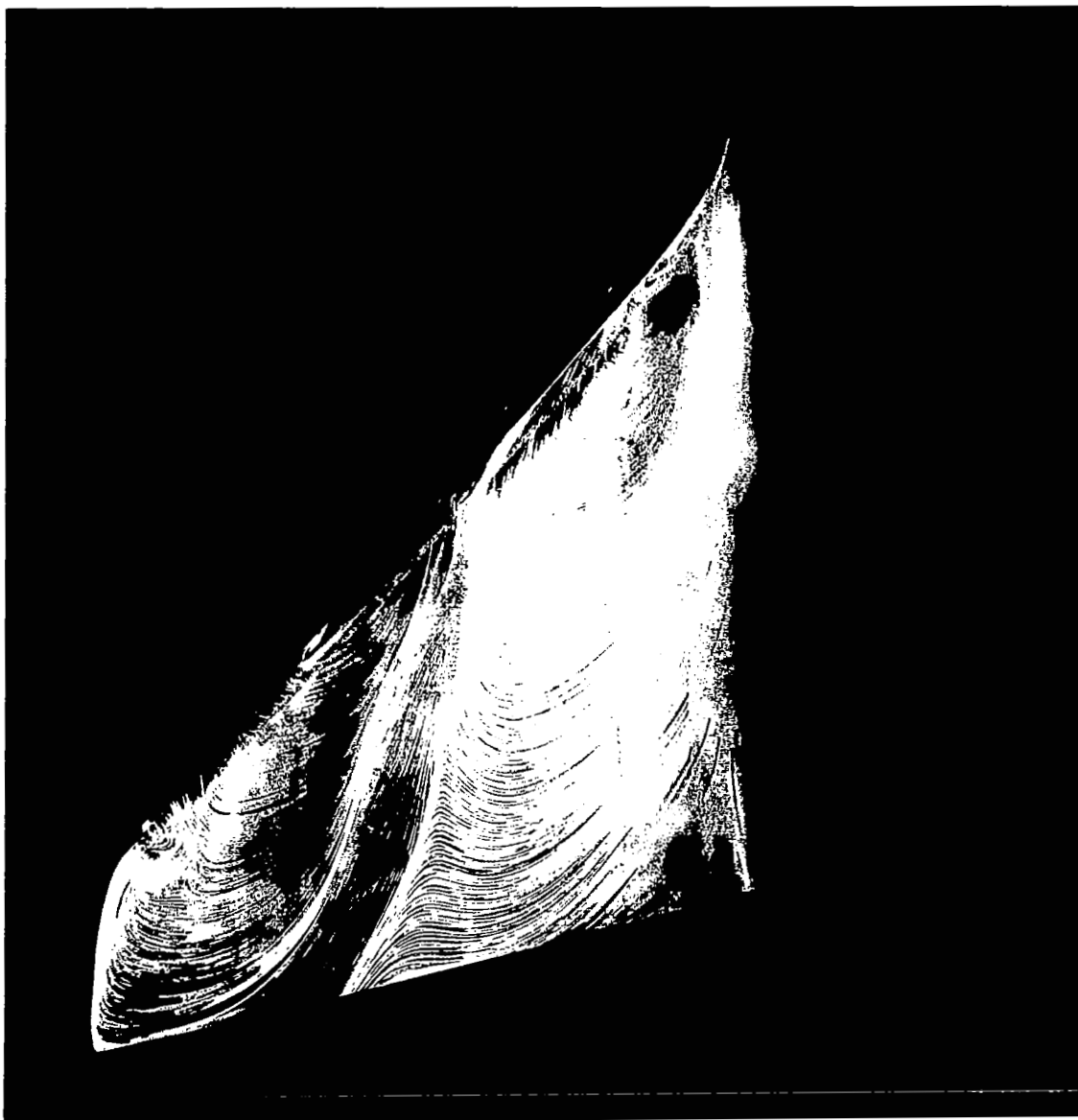
Figure 10.- Continued.



L-83-20

(i) SLEF off; fence off;  $\alpha = 20.07^\circ$ .

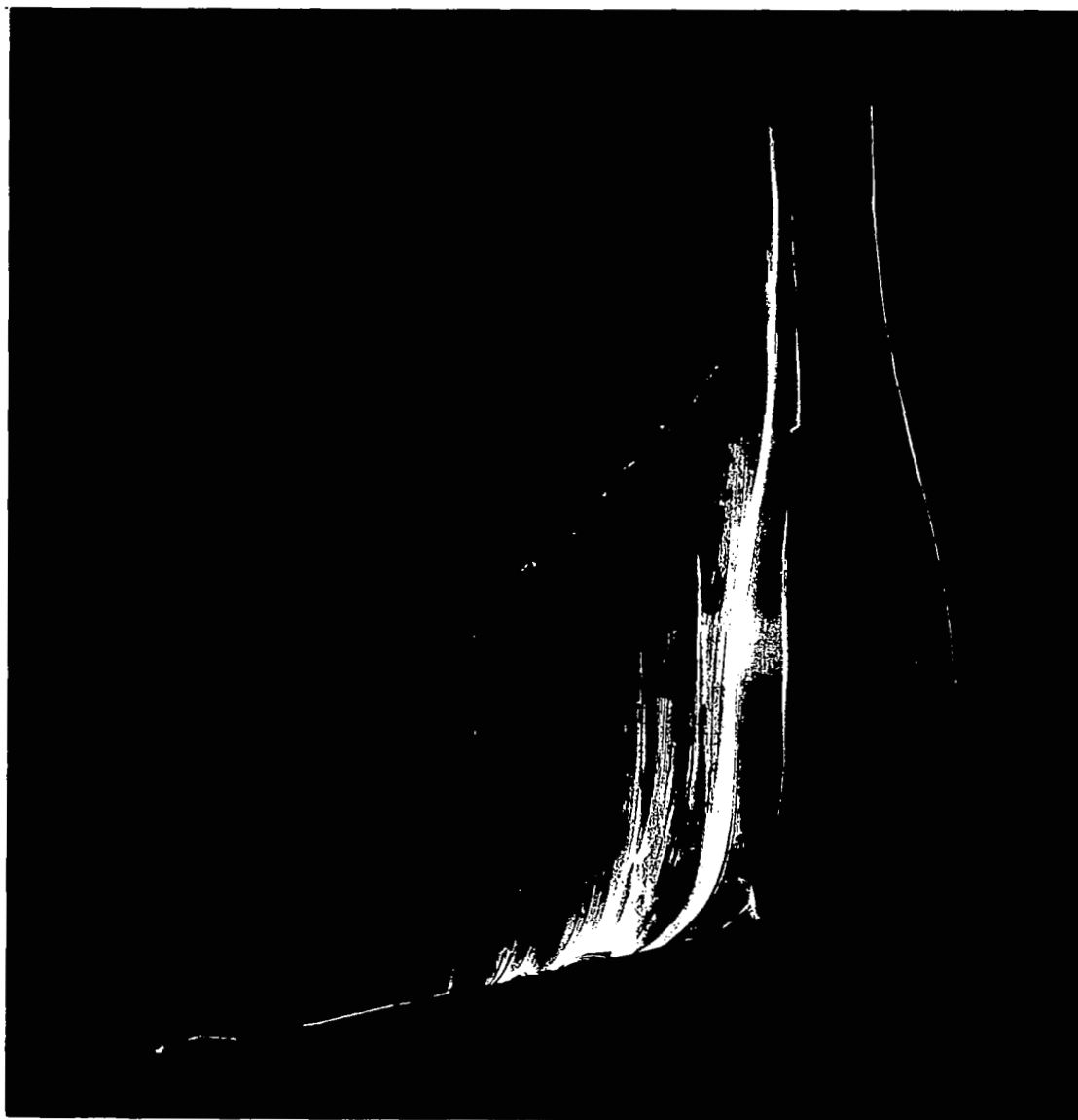
Figure 10.- Continued.



L-83-21

(j) SLEF on; fence on;  $\alpha = 20.07^\circ$ .

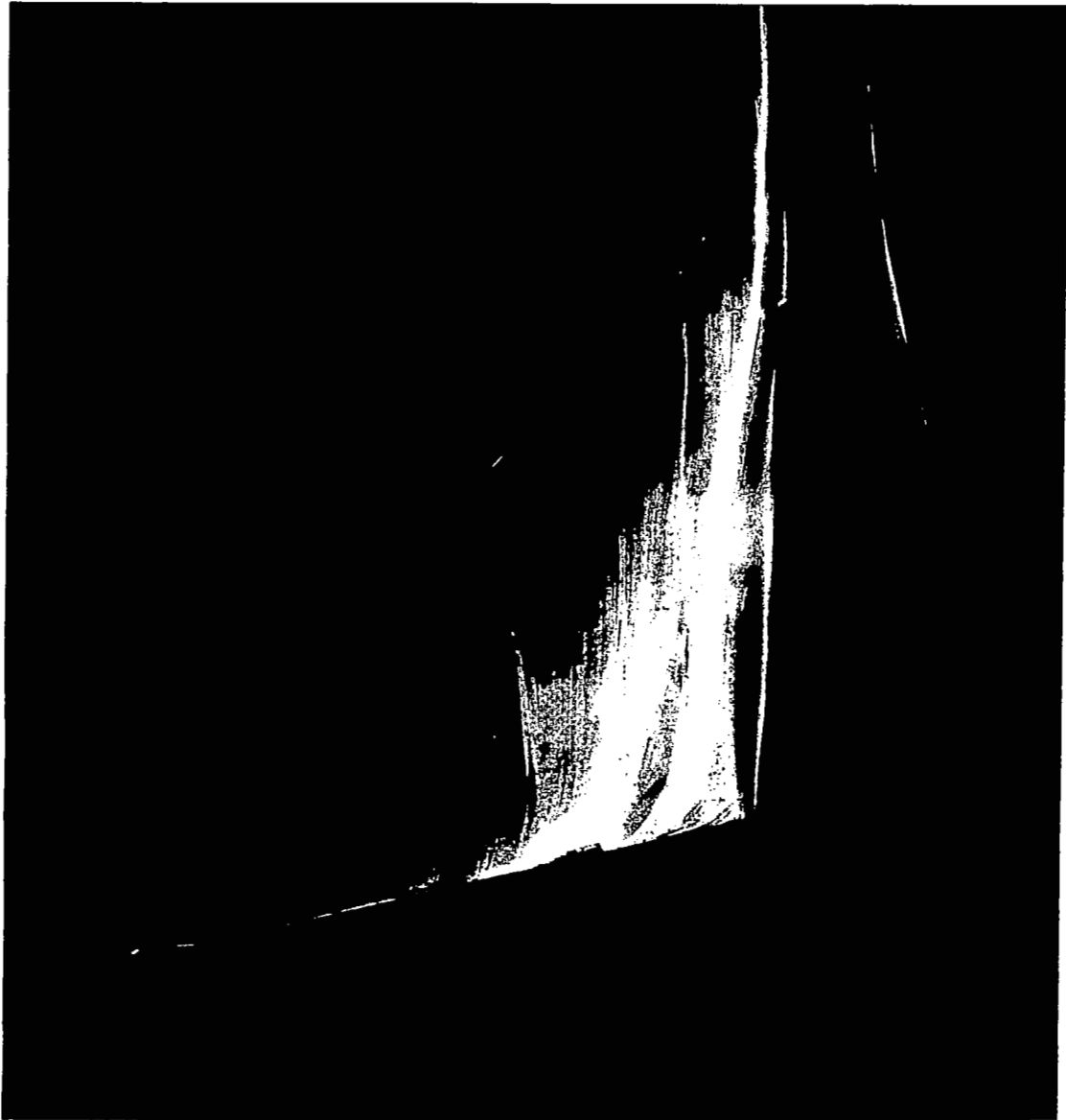
Figure 10.- Concluded.



L-83-22

(a) SLEF off;  $\alpha = 8.97^\circ$ .

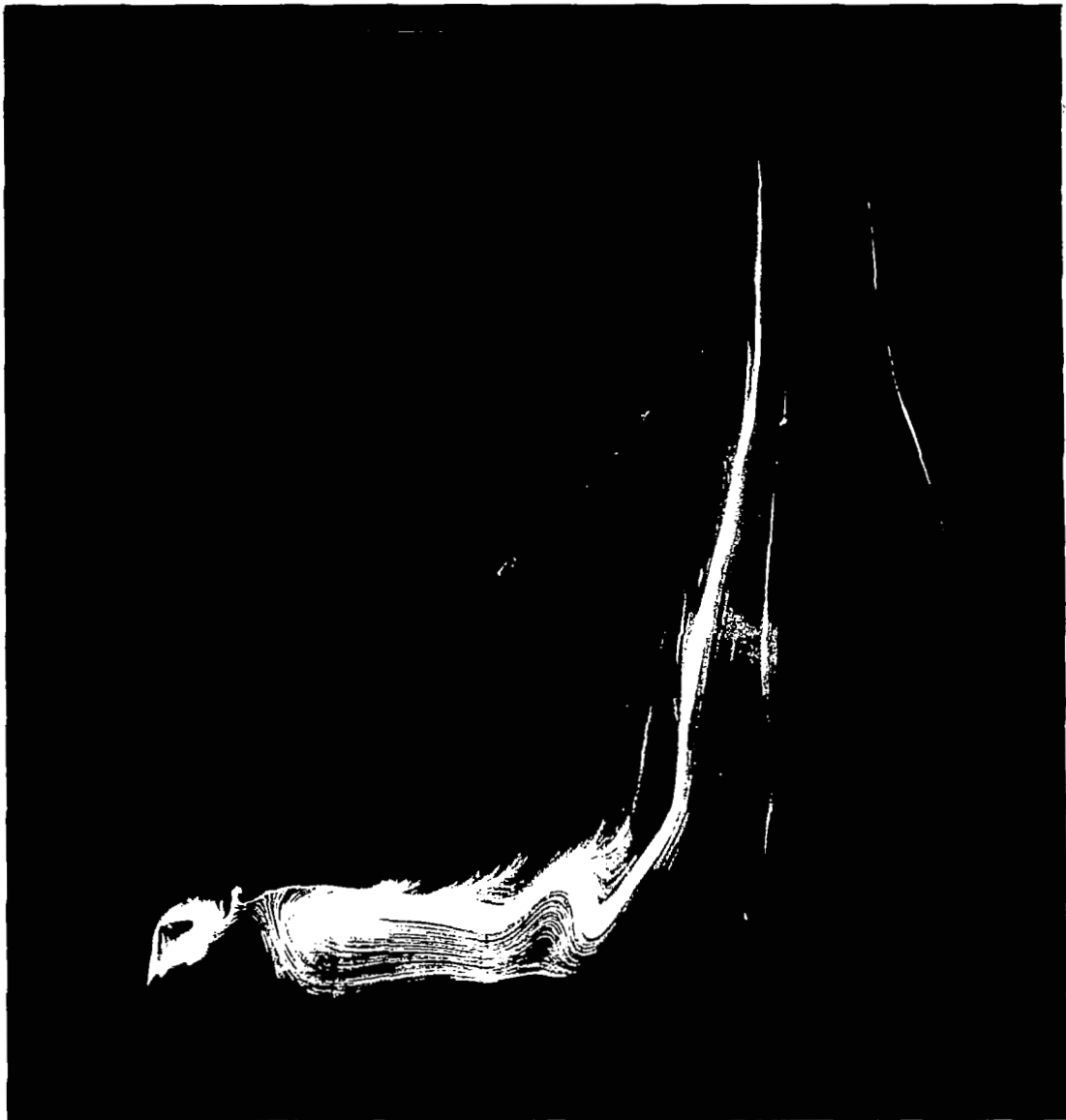
Figure 11.- Photographs of oil-flow patterns at  $M = 0.85$  with and without the large SLEF.  $\delta_f = 0^\circ$ ; fence off; configuration 2.



L-83-23

(b) SLEF on;  $\alpha = 8.97^\circ$ .

Figure 11.- Continued.



L-83-24

(c) SLEF off;  $\alpha = 12.67^\circ$ .

Figure 11.- Continued.



L-83-25

(d) SLEF on;  $\alpha = 12.67^\circ$ .

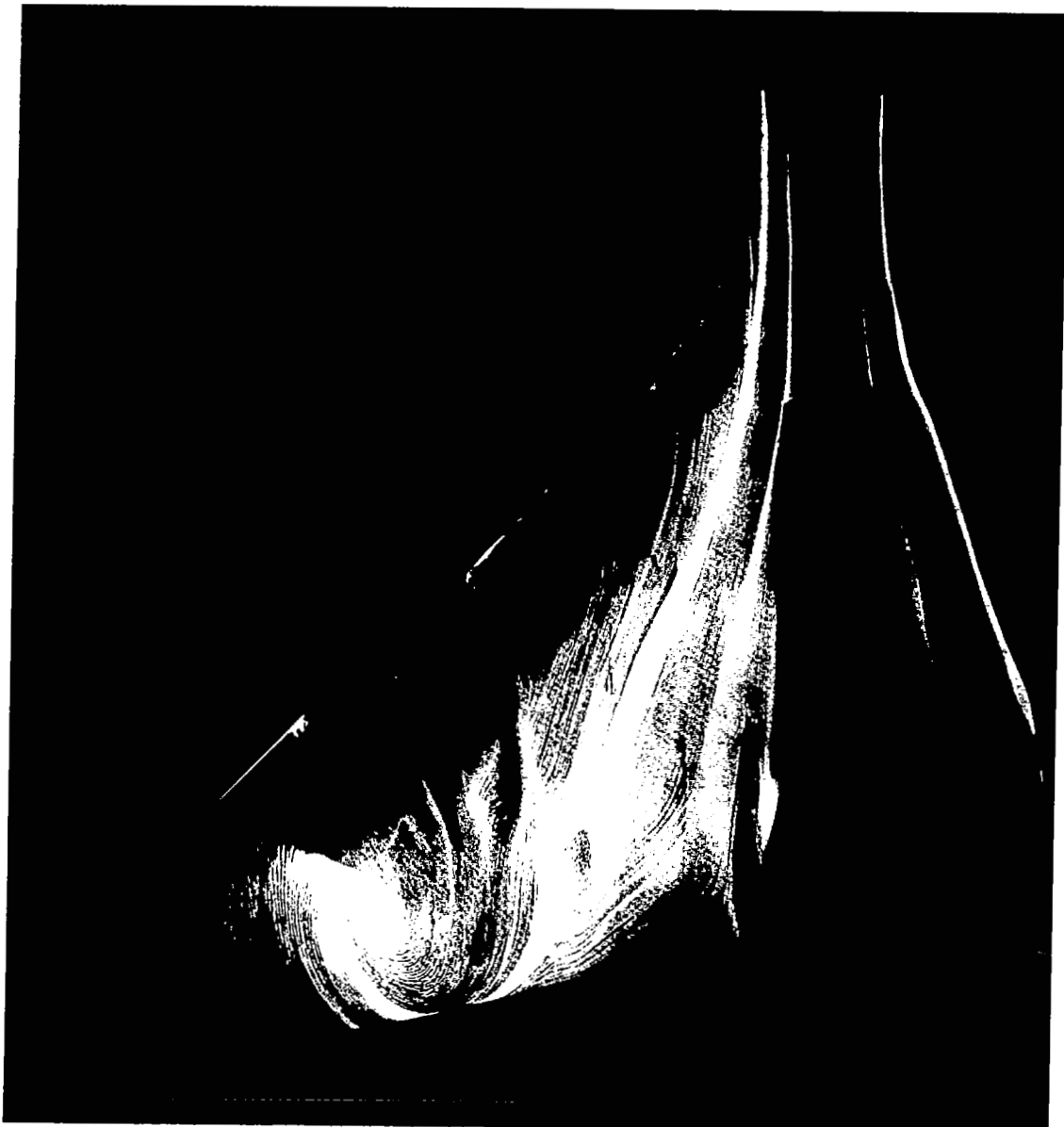
Figure 11.- Continued.



L-83-26

(e) SLEF off;  $\alpha = 14.83^\circ$ .

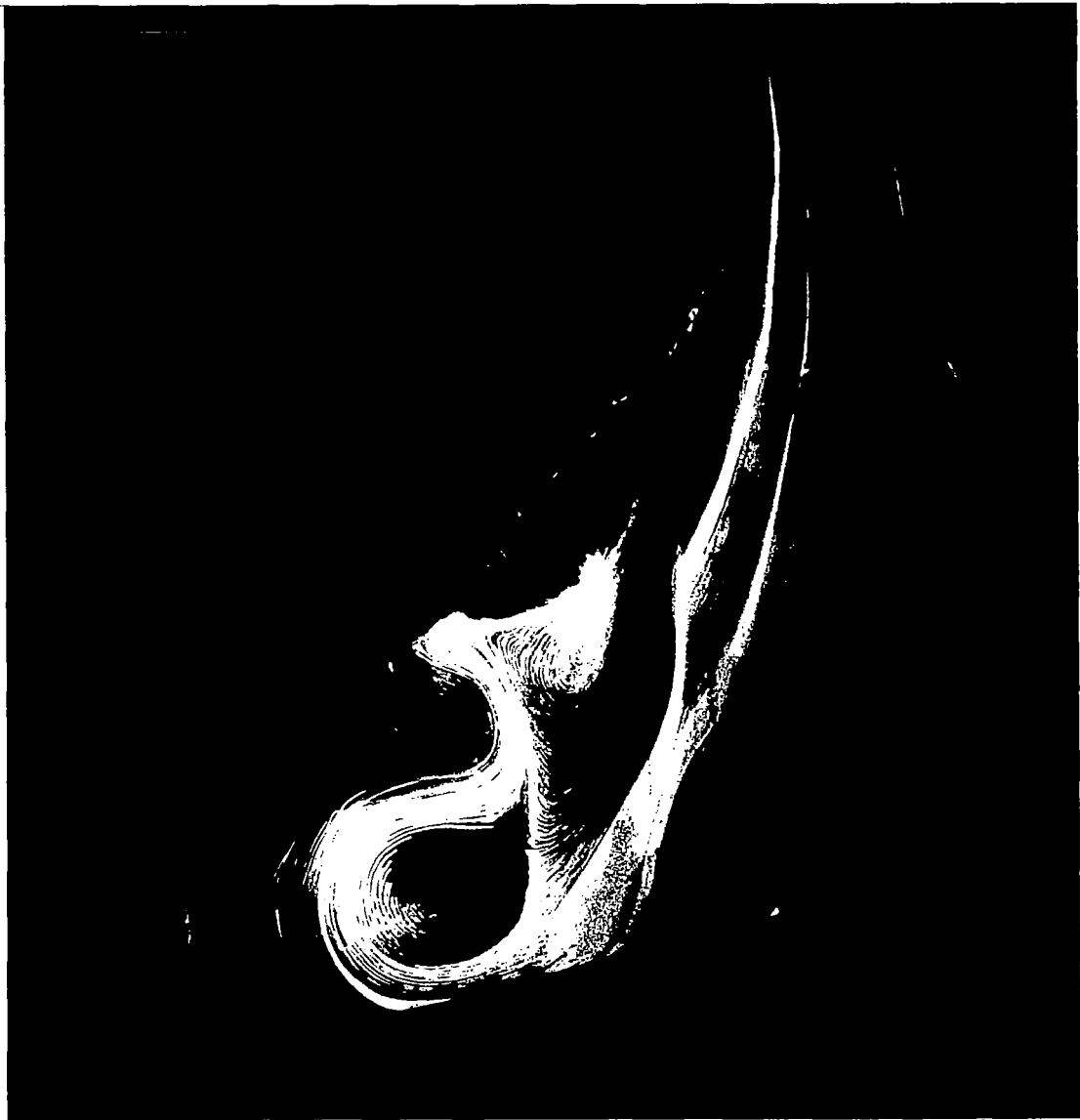
Figure 11.- Continued.



L-83-27

(f) SLEF on;  $\alpha = 14.83^\circ$ .

Figure 11.- Continued.



L-83-28

(g) SLEF off;  $\alpha = 18.03$ .

Figure 11.- Continued.



L-83-29

(h) SLEF on;  $\alpha = 18.03^\circ$ .

Figure 11.- Concluded.

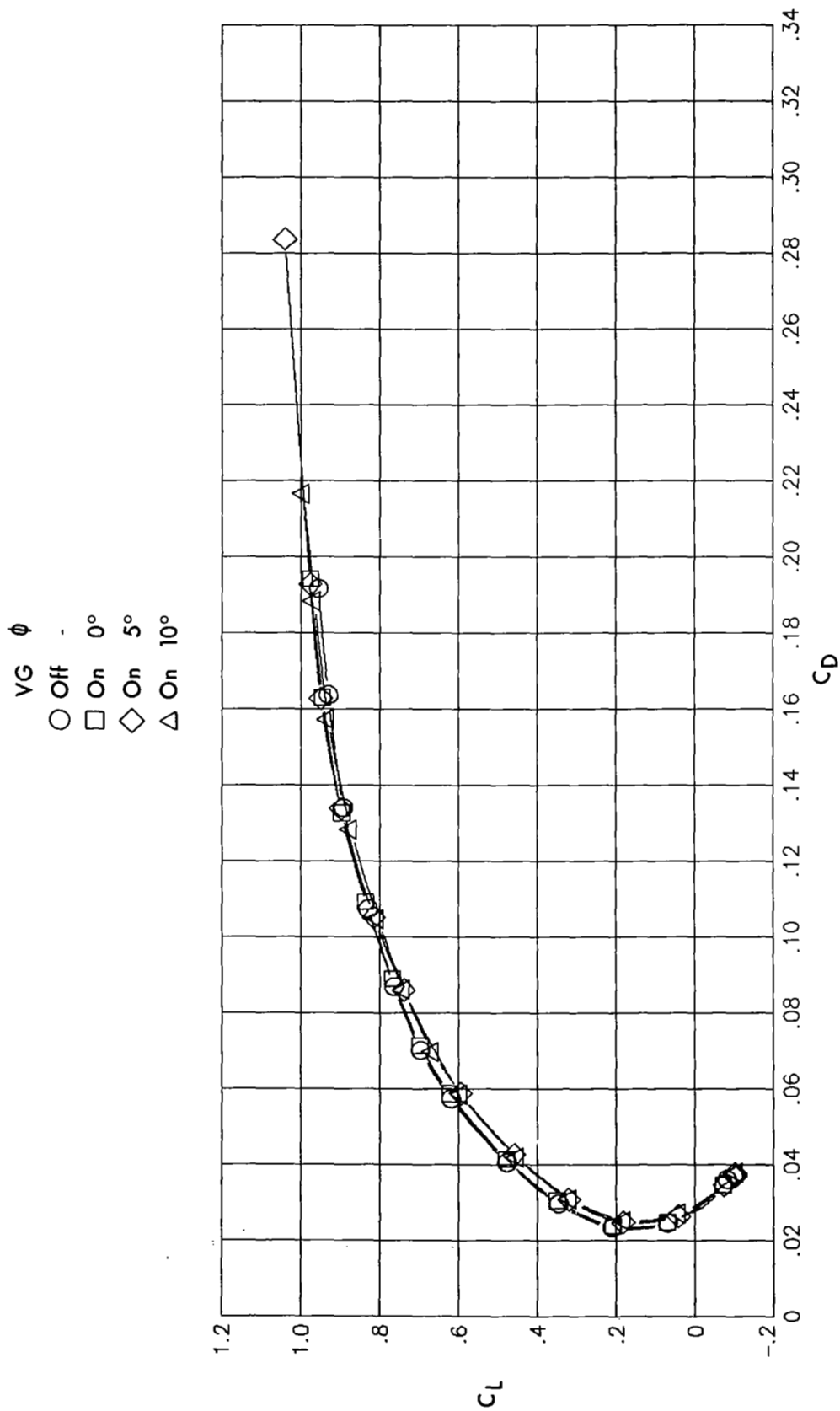


Figure 12.- Effect of VG toe-in angle on longitudinal aerodynamic characteristics at  $M = 0.60$ . VG at  $\eta = 0.50$  and  $0.75$ ; configuration 1.

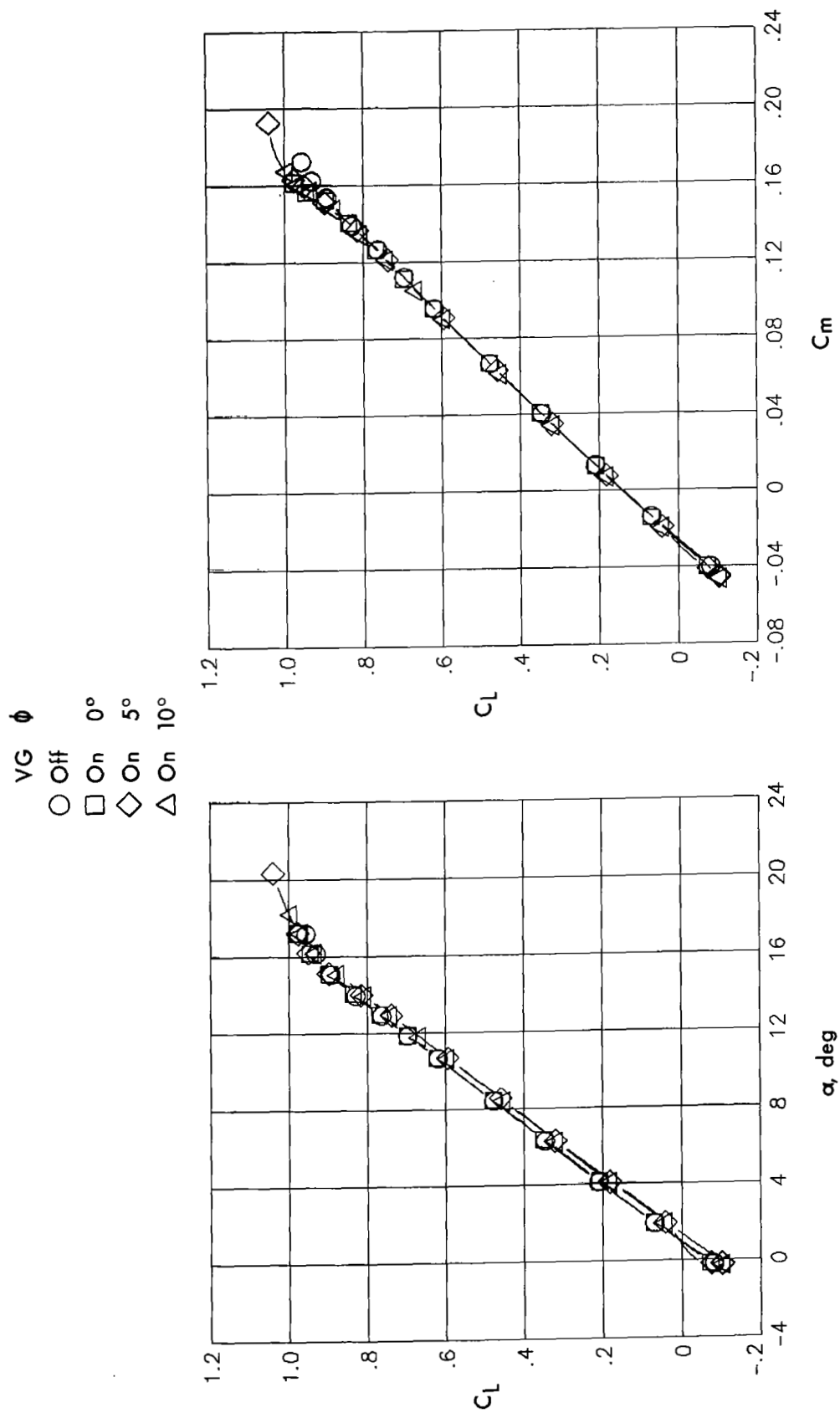


Figure 12.- Concluded.

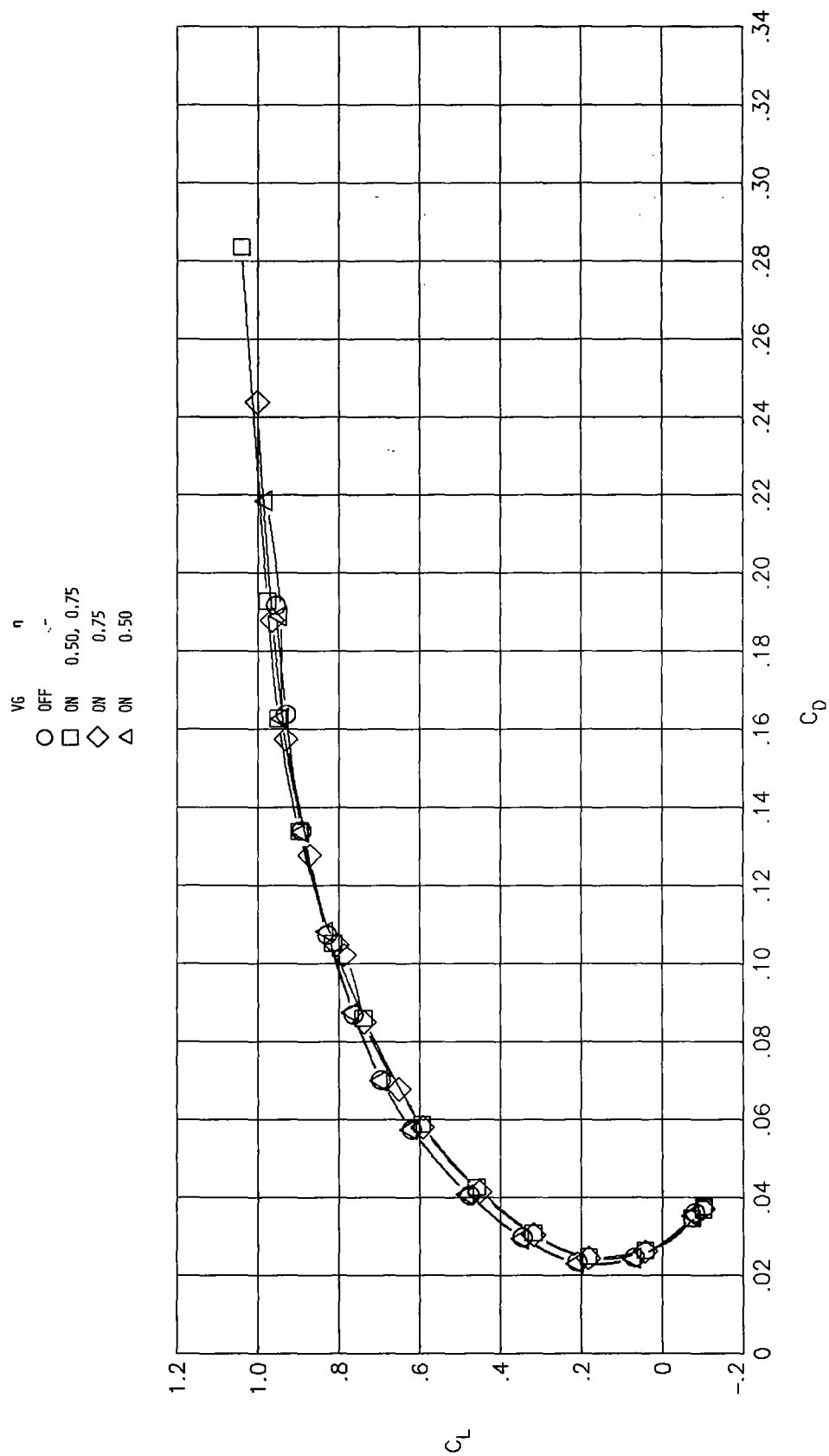


Figure 13.- Effect of spanwise location and number of VG on longitudinal aerodynamic characteristics at  $M = 0.60$ .  $\phi = 5^\circ$ ; configuration 1.

$V_G$     $\eta$   
 OFF   -  
 ON   0.50, 0.75  
 ON   0.75  
 ON   0.50

○   □   ◇   △

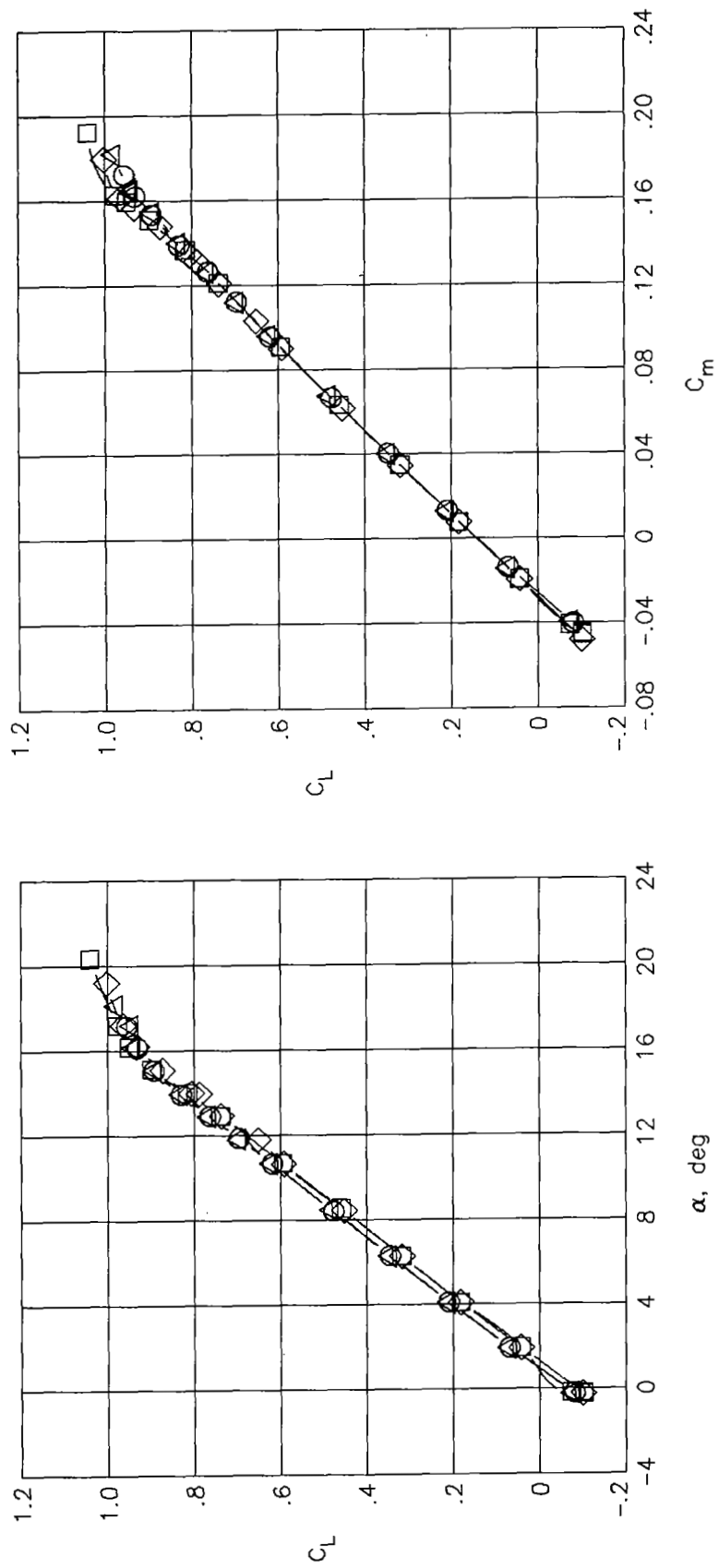


Figure 13.- Concluded.

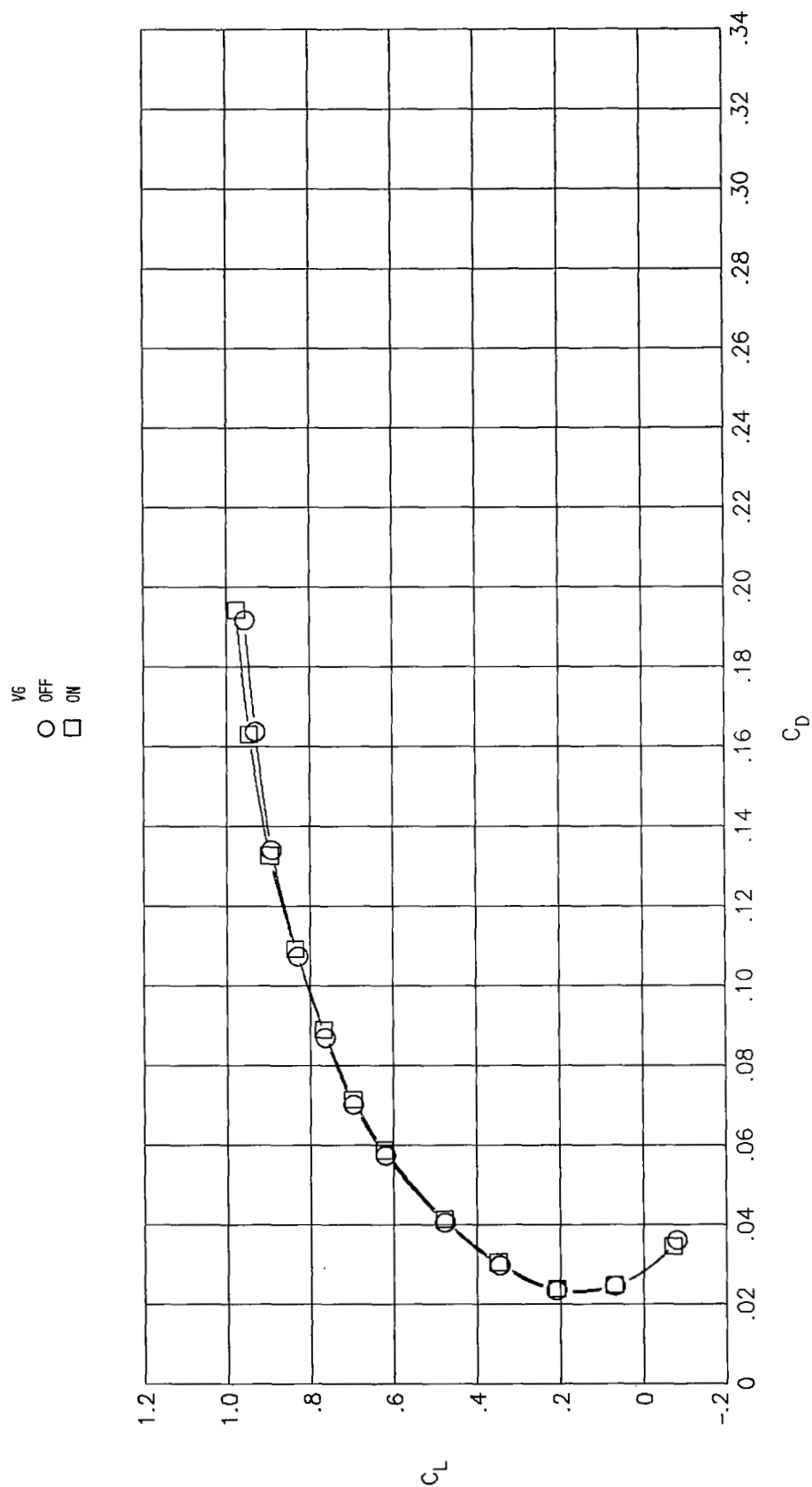


Figure 14.- Summary of longitudinal aerodynamic characteristics of VG with  $\phi = 0^\circ$   
 at  $M = 0.60$ . VG at  $\eta = 0.50$  and  $0.75$ ; configuration 1.

V6  
 ○ OFF  
 □ ON

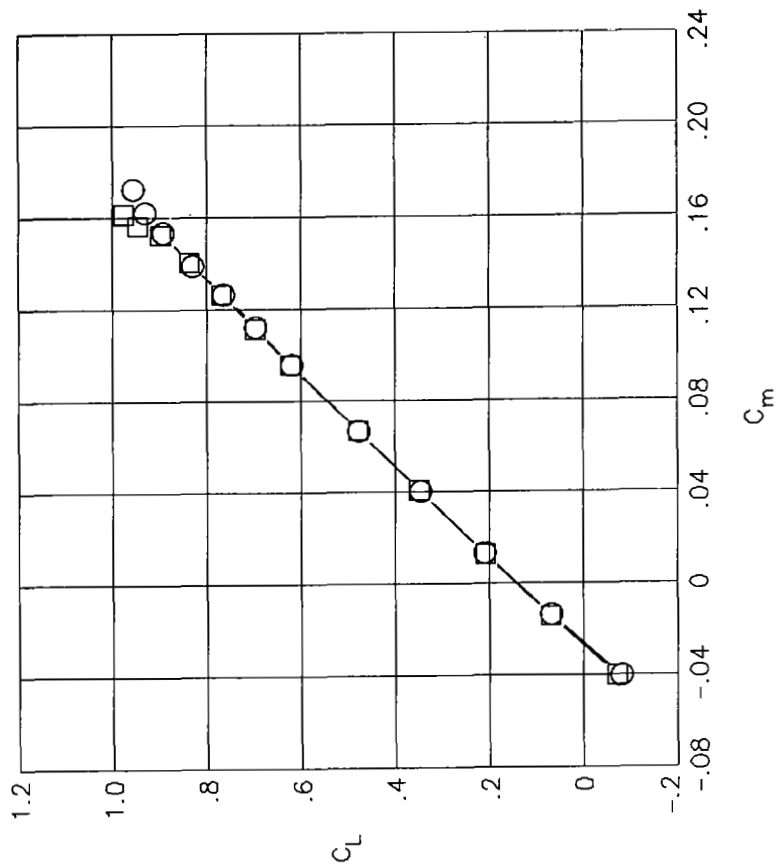
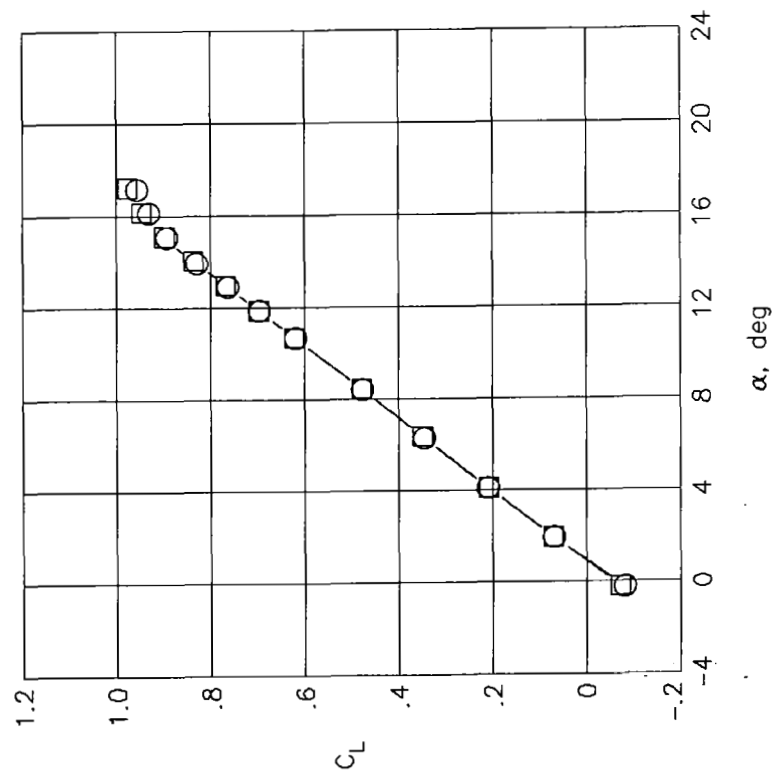


Figure 14.- Concluded.

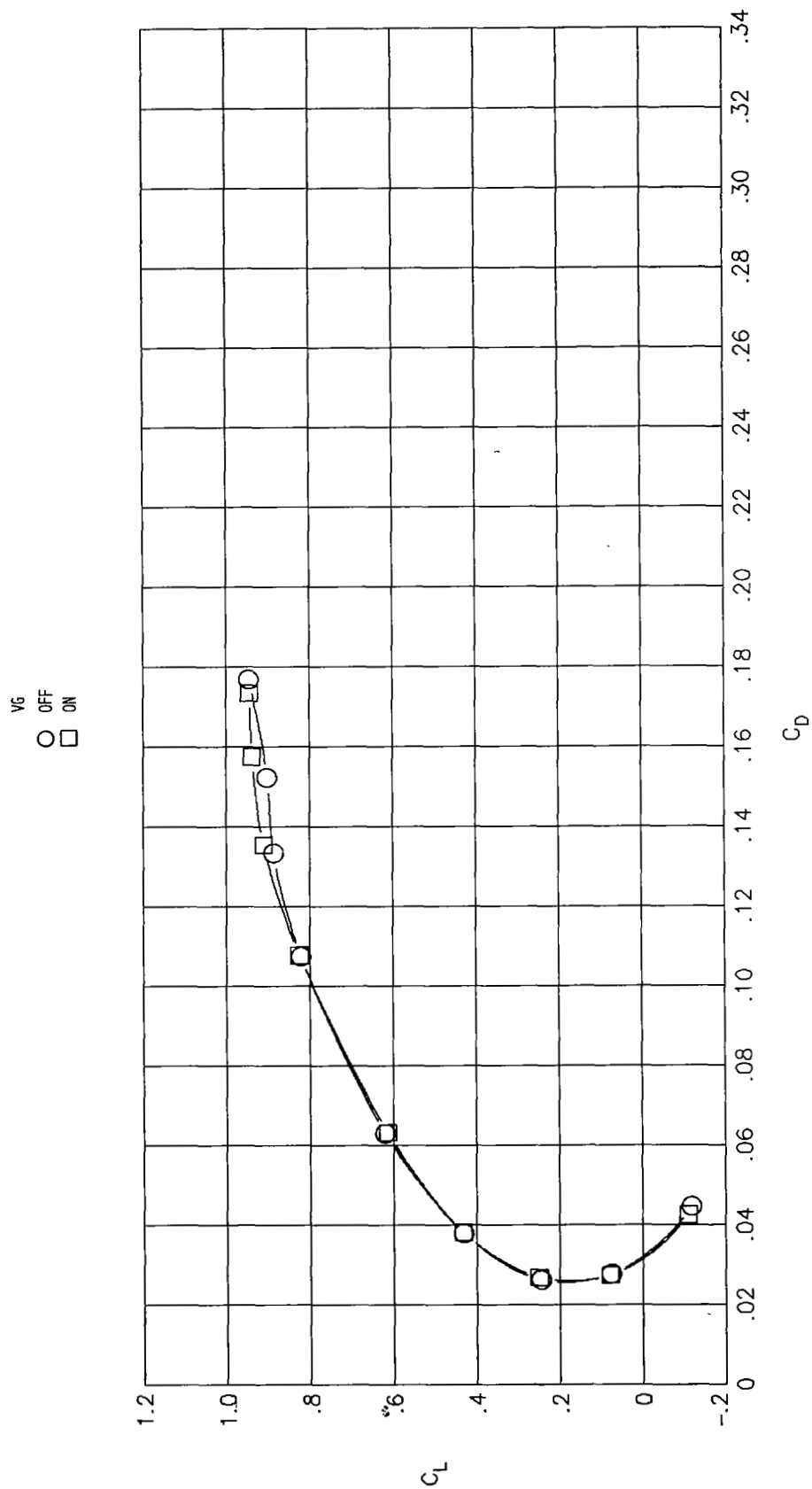


Figure 15.- Effect of VG on longitudinal aerodynamic characteristics at  $M = 0.85$ .  
 VG at  $\eta = 0.50$  and  $0.75$ ;  $\phi = 0^\circ$ ; configuration 1.

$V_G$   
 OFF  $\circ$   
 ON  $\square$

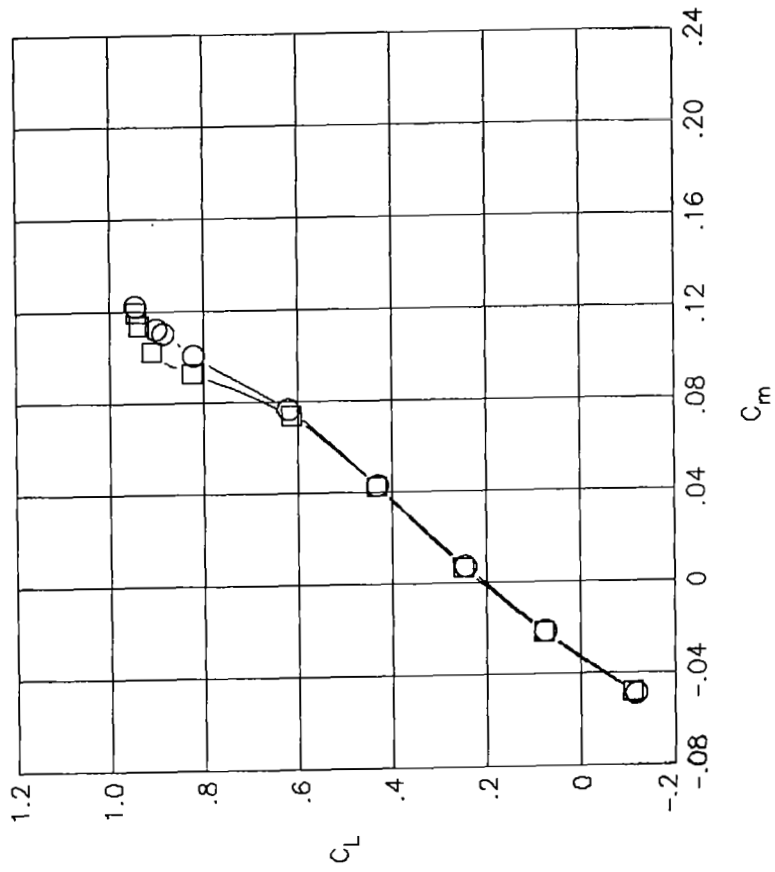
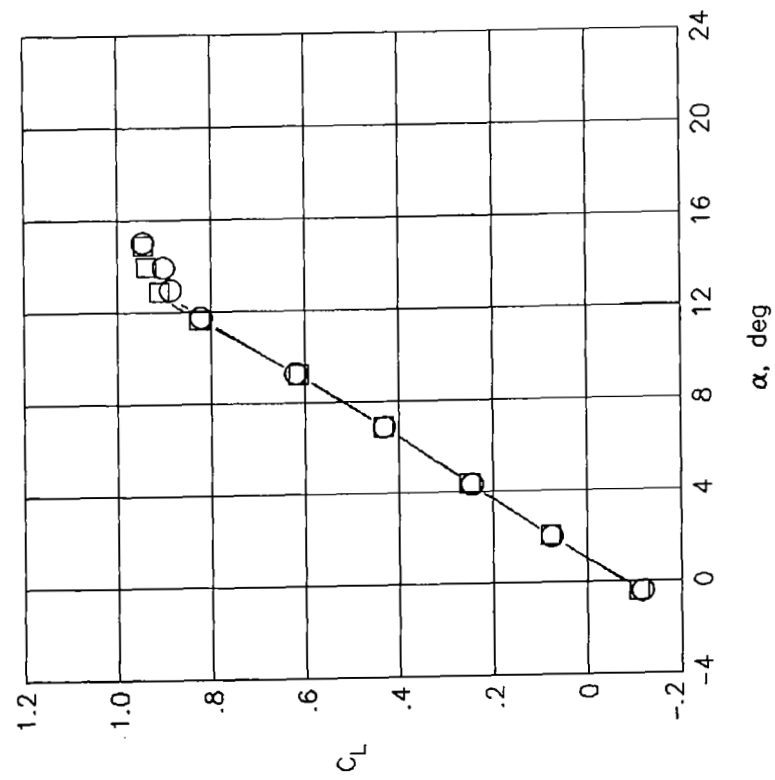
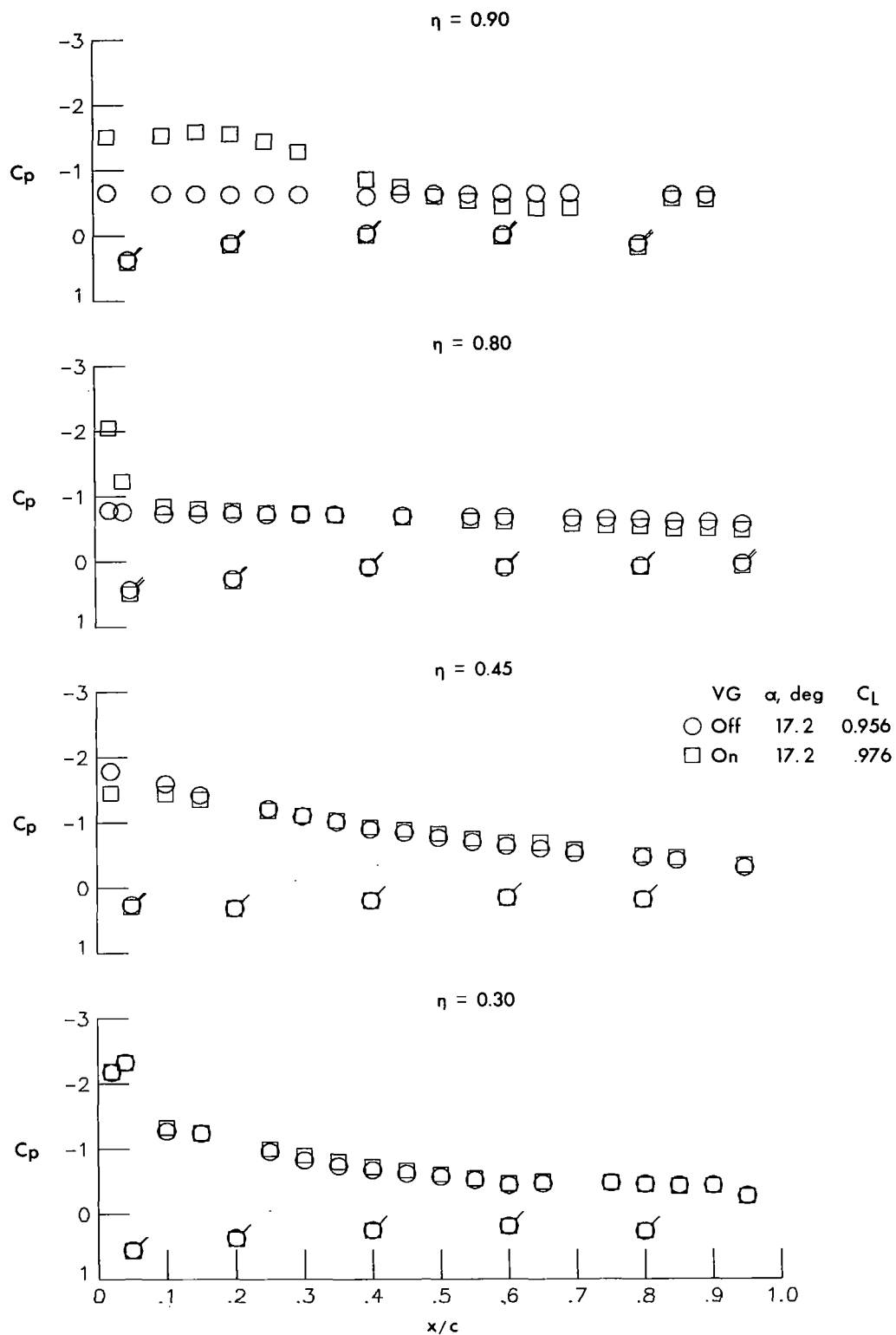
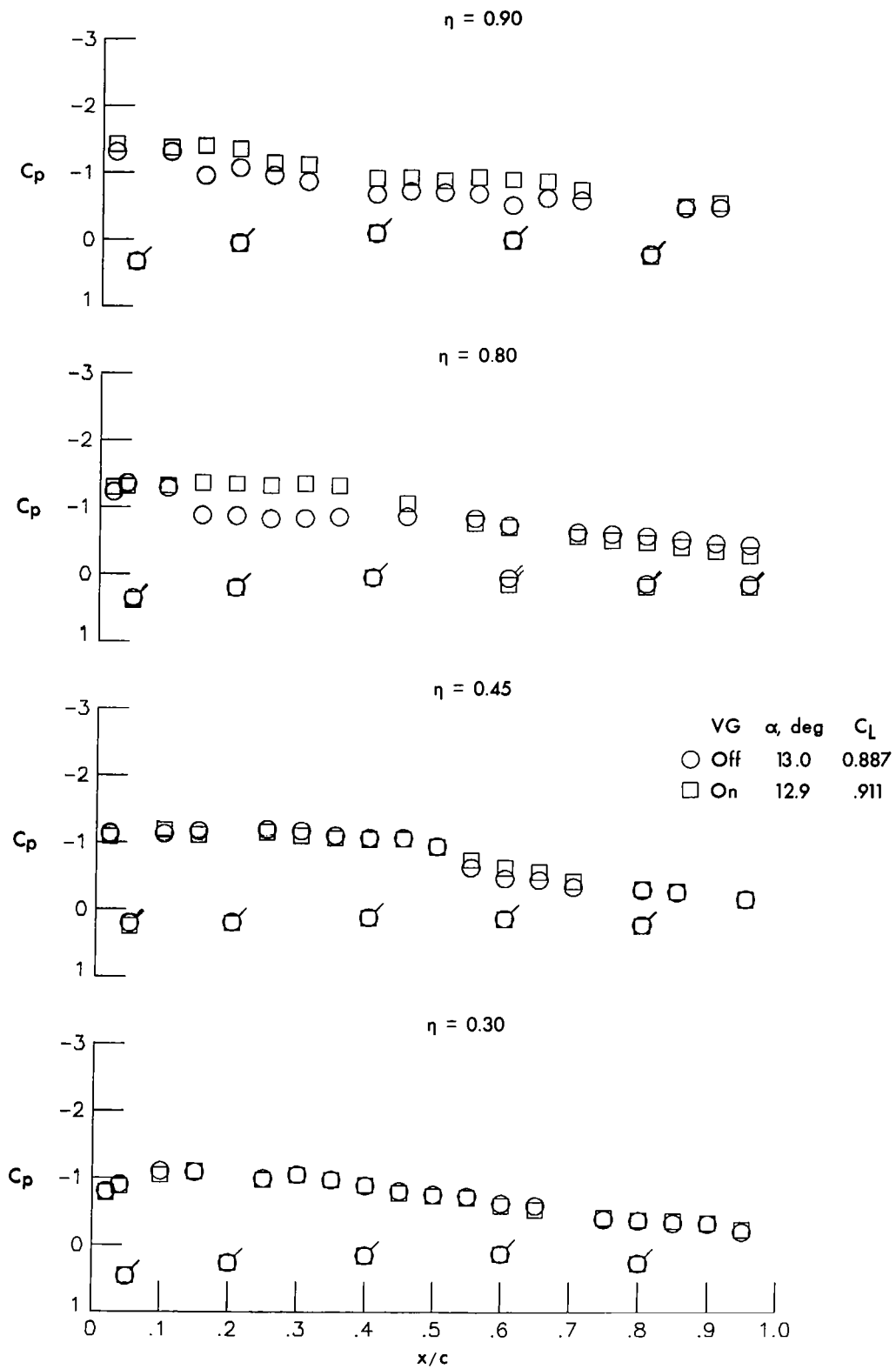


Figure 15.- Concluded.



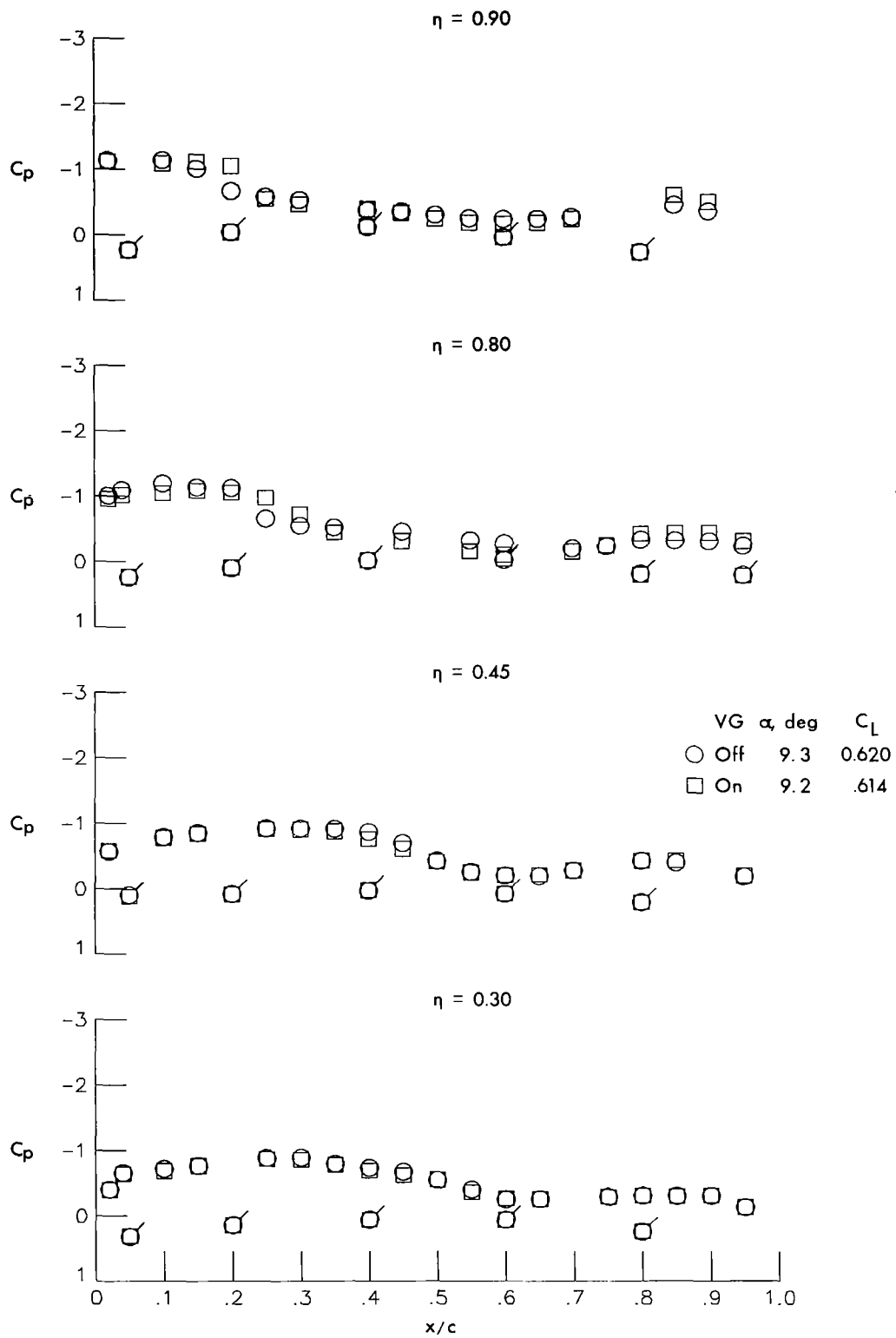
(a)  $M = 0.60$ ;  $C_L \approx 0.97$ .

Figure 16.- Effect of VG on wing upper- and lower-surface pressure coefficients. VG at  $\eta = 0.50$  and  $0.75$ ;  $\phi = 0^\circ$ ; configuration 1. Flagged symbols indicate lower surface.



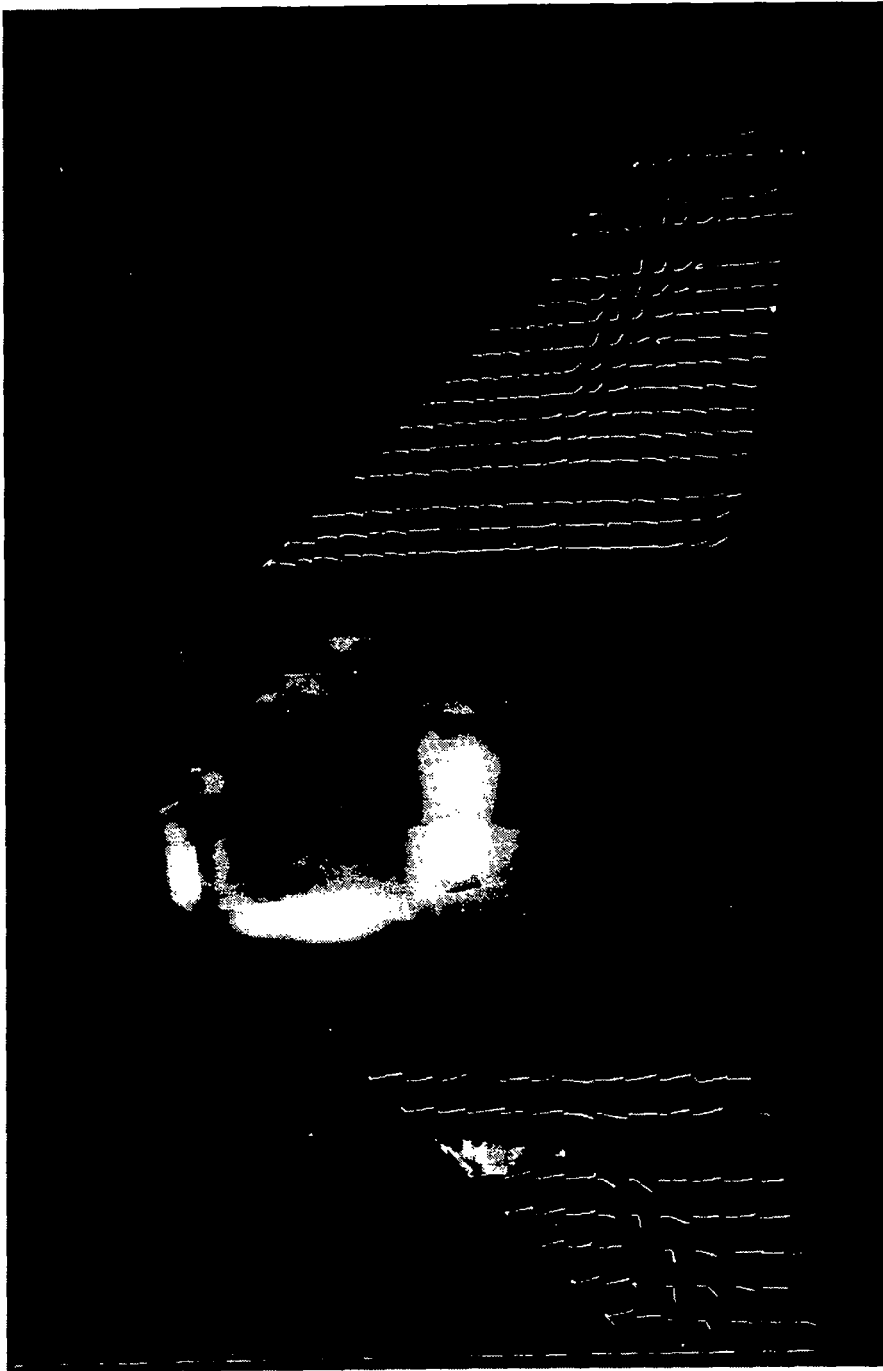
(b)  $M = 0.85$ ;  $C_L \approx 0.9$ .

Figure 16.- Continued.



(c)  $M = 0.85$ ;  $C_L \approx 0.6$ .

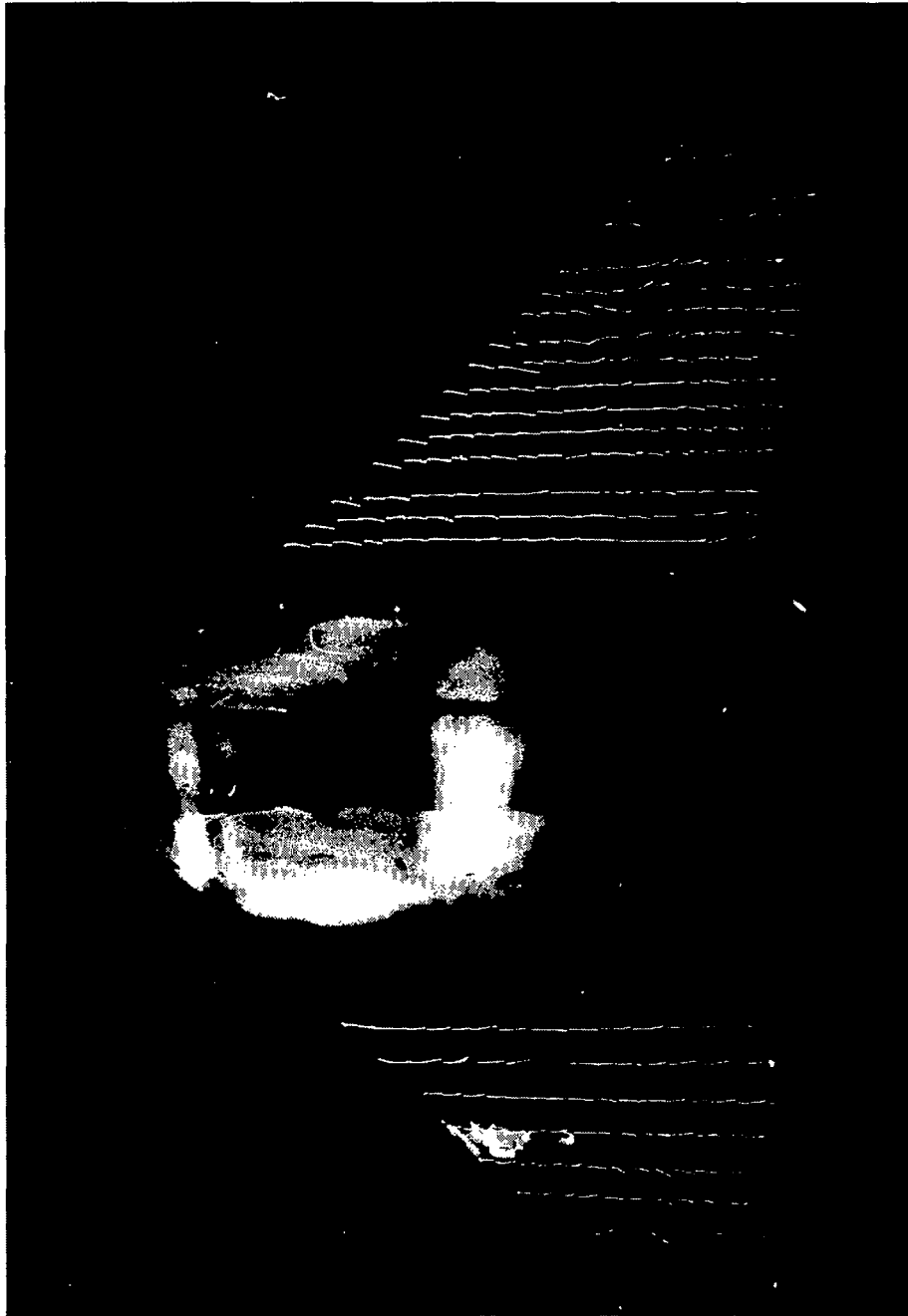
Figure 16.- Concluded.



L-83-30

(a) VG off;  $\alpha = 9.10^\circ$ ;  $C_L = 0.609$ .

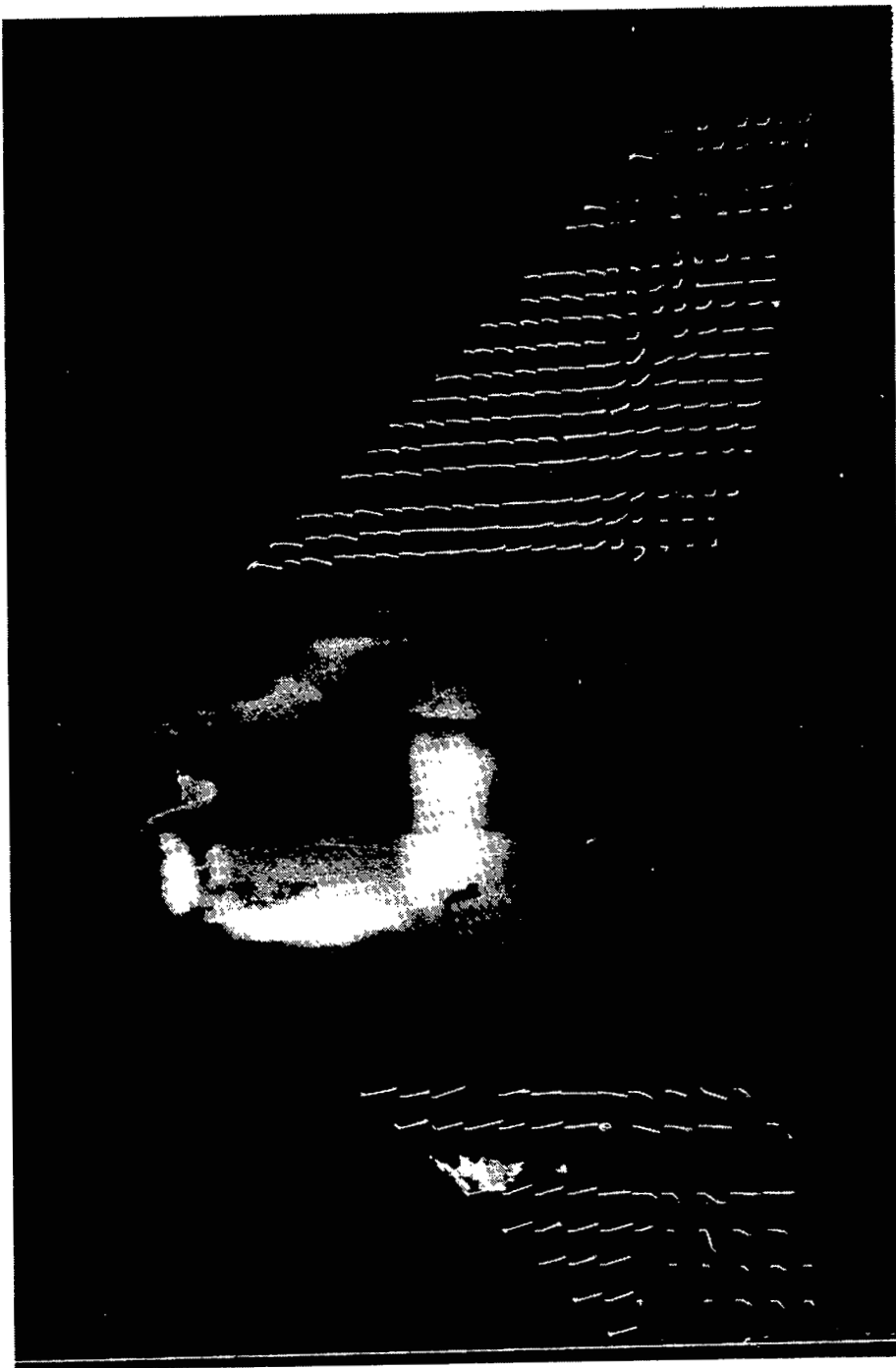
Figure 17.- Photographs of minituft patterns at  $M = 0.85$  with and without VG. VG at  $\eta = 0.50$  and  $0.75$ ;  $\phi = 0^\circ$ ; configuration 1.



L-83-31

(b) VG on;  $\alpha = 9.35^\circ$ ;  $C_L = 0.616$ .

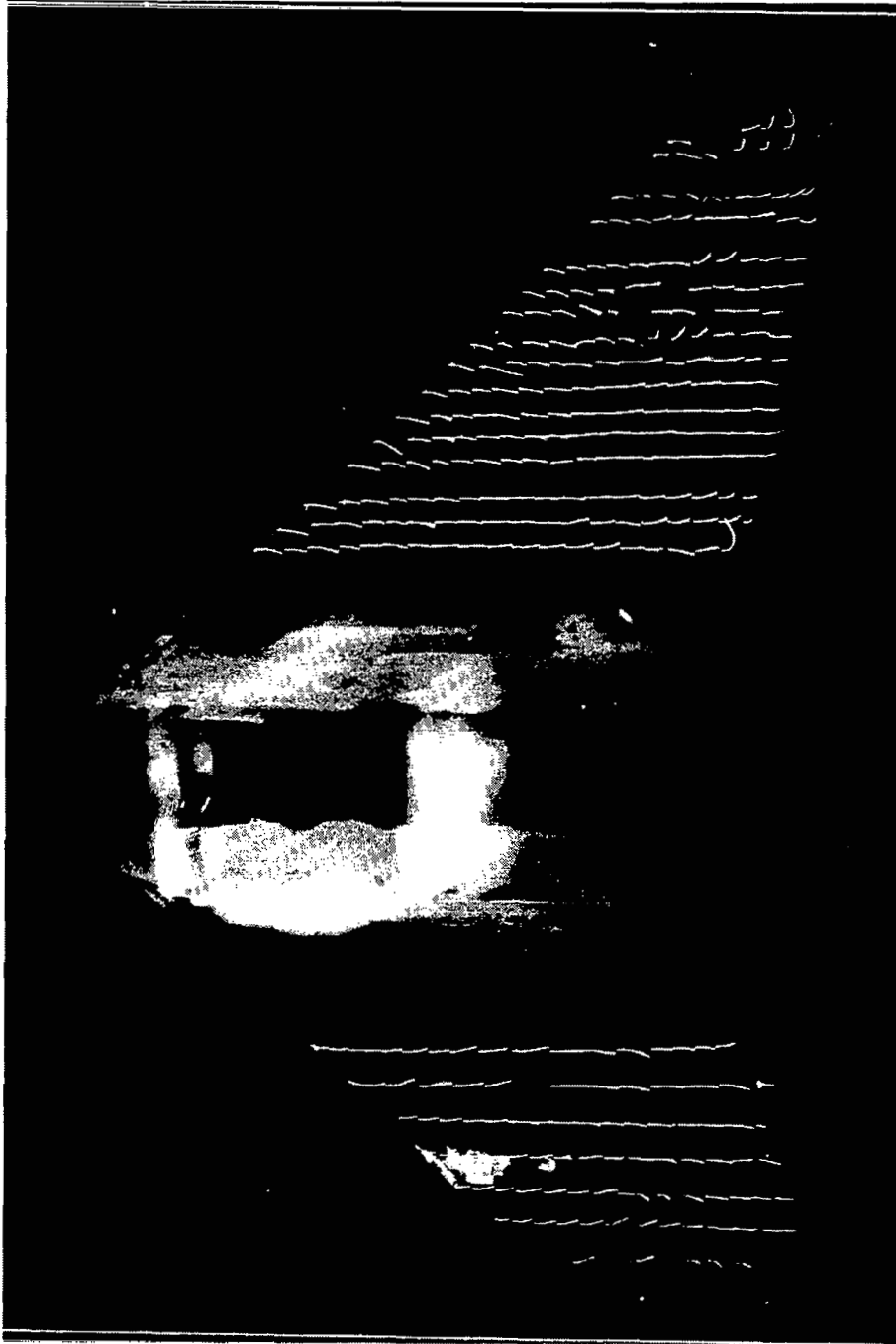
Figure 17.- Continued.



L-83-32

(c) VG off;  $\alpha = 12.84^\circ$ ;  $C_L = 0.900$ .

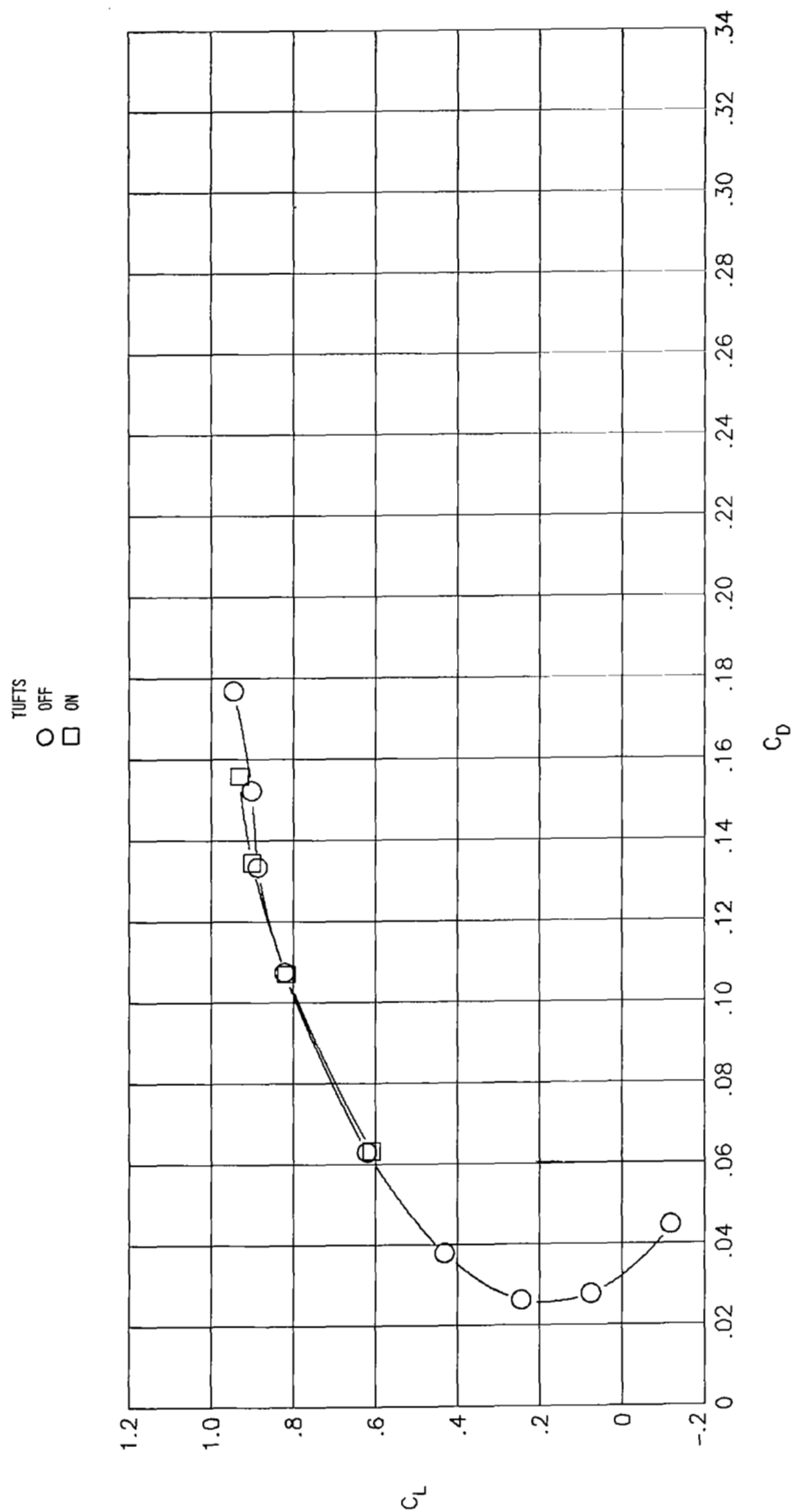
Figure 17.- Continued.



L-83-33

(d) VG on;  $\alpha = 13.12^\circ$ ;  $C_L = 0.917$ .

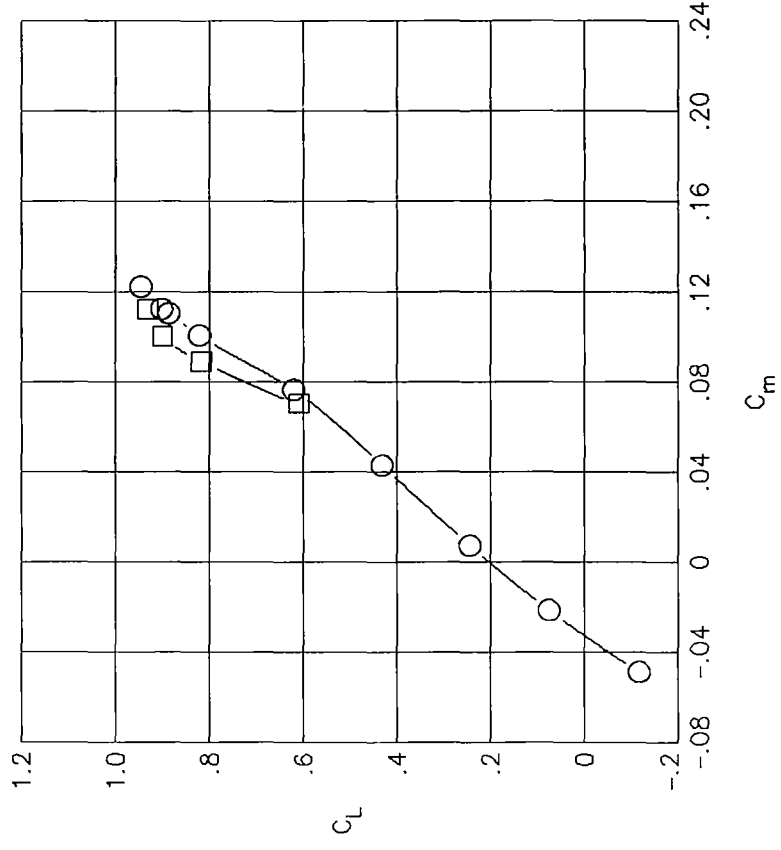
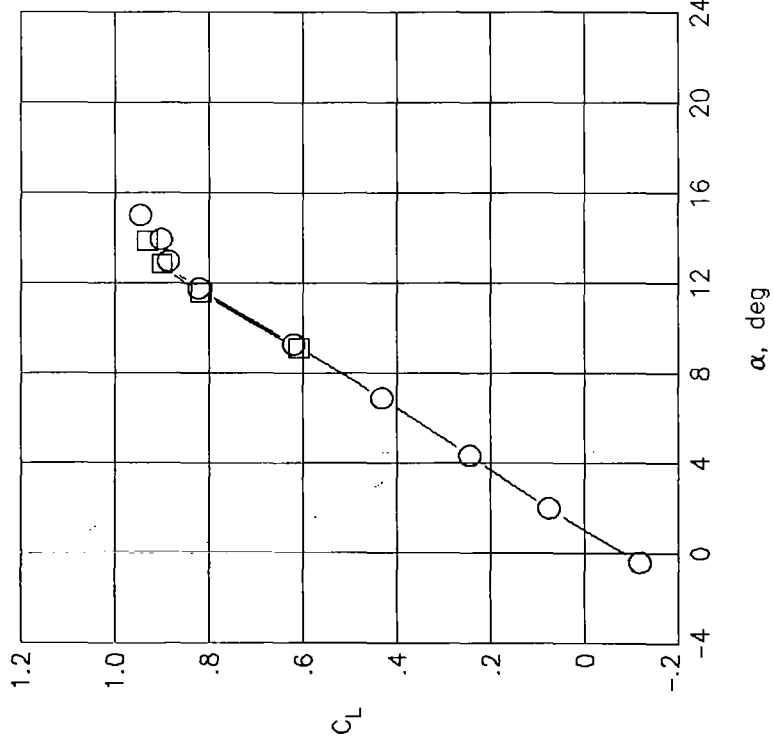
Figure 17.- Concluded.



(a) VG off.

Figure 18.- Effect of minitufts on longitudinal aerodynamic characteristics for  $M = 0.85$ . Configuration 1.

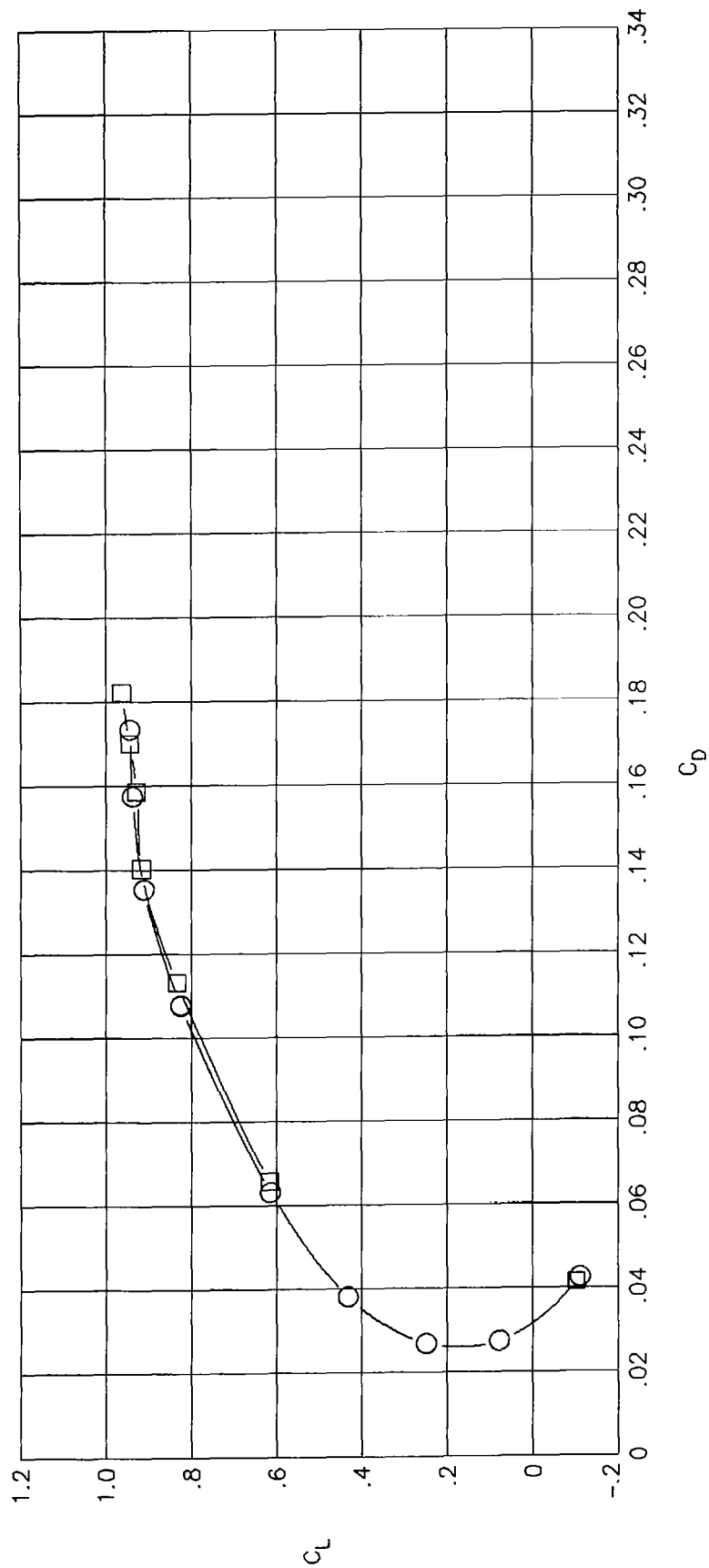
TUFTS  
 ○ OFF  
 □ ON



(a) Concluded.

Figure 18.- Continued.

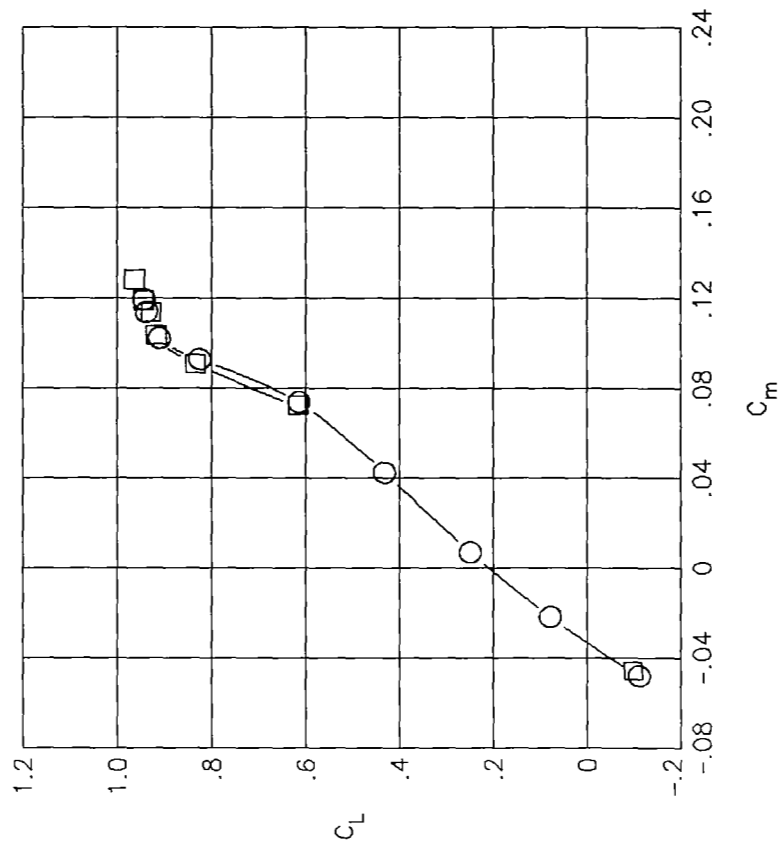
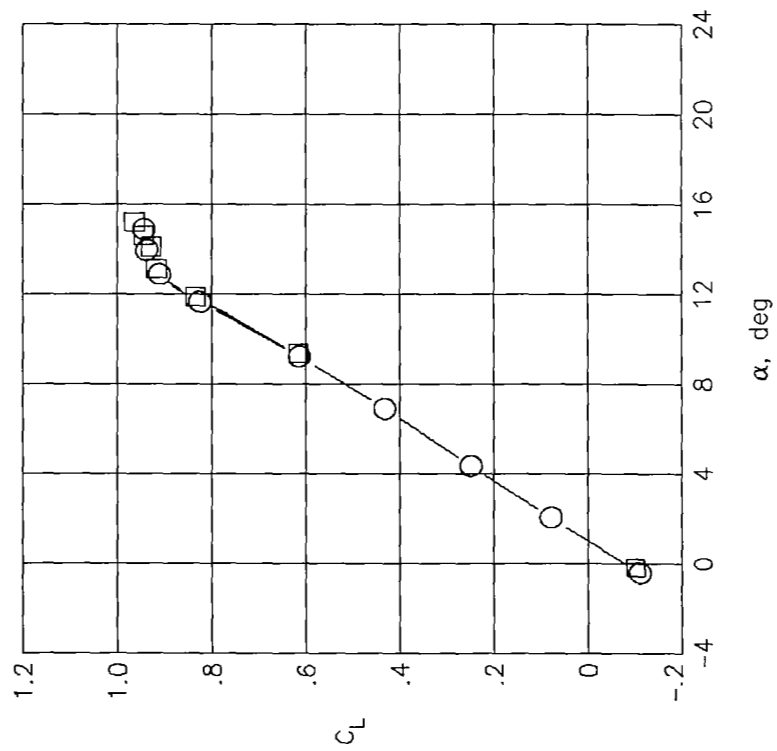
TUFTS  
 ○ OFF  
 □ ON



(b) VG at  $\eta = 0.50$  and  $0.75$ .  $\phi = 0^\circ$ .

Figure 18.- Continued.

TUFTS  
 ○ OFF  
 □ ON



(b) Concluded.

Figure 18.- Concluded.

1. Report No. NASA TP-2125		2. Government Accession No.		3. Recipient's Catalog No.	
4. Title and Subtitle EXPERIMENTAL STUDY OF WING LEADING-EDGE DEVICES FOR IMPROVED MANEUVER PERFORMANCE OF A SUPERCRITICAL MANEUVERING FIGHTER CONFIGURATION				5. Report Date March 1983	
				6. Performing Organization Code 505-31-03-01	
7. Author(s) Michael J. Mann, Jarrett K. Huffman, Charles H. Fox, Jr., and Richard L. Campbell				8. Performing Organization Report No. L-15539	
				10. Work Unit No.	
9. Performing Organization Name and Address  NASA Langley Research Center Hampton, VA 23665				11. Contract or Grant No.	
				13. Type of Report and Period Covered Technical Paper	
12. Sponsoring Agency Name and Address  National Aeronautics and Space Administration Washington, DC 20546				14. Sponsoring Agency Code	
15. Supplementary Notes					
16. Abstract  Wind-tunnel tests have been conducted to examine the use of wing leading-edge devices for improved subsonic and transonic maneuver performance. These devices were tested on a fighter configuration which utilized supercritical-wing technology. The configuration had a leading-edge sweep of 45° and an aspect ratio of 3.28. The tests were conducted at Mach numbers of 0.60 and 0.85 with angles of attack from -0.5° to 22°. At both Mach numbers, sharp leading-edge flaps produced vortices which greatly altered the flow pattern on the wing and resulted in substantial reductions in drag at high lift. Underwing or pylon-type vortex generators also reduced drag at high lift. The vortex generators worked better at a Mach number of 0.60. The vortex generators gave the best overall results with zero toe-in angle and when mounted on either the outboard part of the wing or at both an outboard location and halfway out the semispan. Both the flaps and the vortex generators had a minor effect on the pitching moment. Fluorescent minitufts were found to be useful for flow visualization at transonic maneuver conditions.					
17. Key Words (Suggested by Author(s))  Transonic aerodynamics Leading-edge devices Fighter aircraft Maneuvering aerodynamics Transonic wing design			18. Distribution Statement  Unclassified - Unlimited  Subject Category 02		
19. Security Classif. (of this report)  Unclassified	20. Security Classif. (of this page)  Unclassified	21. No. of Pages  82	22. Price  A05		